

DEVELOPMENT OF A COMPREHENSIVE ANALYSIS FOR ROTORCRAFT—I. ROTOR MODEL AND WAKE ANALYSIS

WAYNE JOHNSON

NASA Ames Research Center and Aeromechanics Laboratory, AVRADCOM
Research and Technology Laboratories, Moffett Field, CA U.S.A.

(Received 30 September 1980)

Abstract—The development of a comprehensive analytical model of rotorcraft aerodynamics and dynamics is described. Particular emphasis is given to describing the reasons behind the choices and decisions involved in constructing the model. The analysis is designed to calculate rotor performance, loads and noise; helicopter vibration and gust response; flight dynamics and handling qualities; and system aeroelastic stability. It is intended for use in the design, testing and evaluation of a wide class of rotors and rotorcraft, and to be the basis for further development of rotary wing theories. The general characteristics of the geometric, structural, inertial, and aerodynamic models used for the rotorcraft components are described, including the assumptions introduced by the chosen models and the resulting capabilities and limitations. Finally, some examples from recent applications of the analysis are given.

1. INTRODUCTION

For the design, testing and evaluation of rotors and rotorcraft, a reliable and efficient analysis of the aircraft aerodynamics and dynamics is required. It is necessary to predict and explain the rotor performance, loads, and noise; helicopter vibration and gust response; flight dynamics and handling qualities; and system aeroelastic stability. Such capability is also required as a basis for further development of rotary wing theory. A number of powerful analyses have been developed by industry and the government. However, upon review [1], these analyses exhibit a number of generic limitations. Typically rotary wing analyses have been developed or verified for only a particular type of helicopter or a particular technical problem, that reflects the specific interest of the originating organization. Most of the existing codes are fairly old, originating in investigations conducted ten or fifteen years ago. Some have been continuously updated, but eventually that mode of development produces its own limitations. Hence much of the presently available technology is not well utilized in the existing analyses. Moreover, with separate analyses for the various problems of interest, it is inevitable that the technology is not uniformly utilized.

Therefore the development of a new rotorcraft analysis was initiated. The intention was to produce an analysis that utilizes recently developed technology, and one that is applicable to a wide range of problems and a wide class of vehicles. Of course, the assumptions made about the rotor geometry and aircraft configuration ultimately introduce limits on the application of all such analyses. The present analysis is applicable to general two rotor aircraft, including single main-rotor and tandem helicopter configurations and side-by-side or tilting proprotor aircraft configurations. The case of a rotor or helicopter in a wind tunnel is also covered. The rotor model is applicable to articulated, hingeless, gimballed and teetering rotors with an arbitrary number of blades. Furthermore a single, consistent analysis is provided for all of the tasks enumerated in the beginning of the preceding paragraph.

The development of a comprehensive analysis centers on the combination of appropriate elements from the relevant technology. The key concern is to obtain a consistent, balanced choice of elements, that will provide a high level of capability in a practical

raft

le

Issues

times are
film and
lable on
ition and
ex at the

h Barton,
58; Telex

Itaneously
ransferred
m authors
duce and
ature, and
or by any
in writing

le U.S.A.,
107 or 108
age of the
ies of the
t does not
sion must

tool. The result goes beyond the state-of-the-art however. The analysis implements the results from investigations of specific aspects of helicopter aerodynamics or dynamics technology. Normally what is learned and therefore available for implementation in a comprehensive analysis, goes beyond what was actually produced and used in such investigations. In addition, comprehensive helicopter analyses are characterized by strong coupling between the modelling elements, so by combining elements a model is produced that is greater than the sum of its parts.

The development of this rotorcraft analysis has been completed. The mathematical description of the analysis is given in detail elsewhere [2]. The present paper describes the analysis in more general terms, and in addition discusses the reasons behind the choices and decisions involved in constructing the model. The assumptions and limitations introduced by the chosen modelling elements will be described. Such an exposition also serves to define the current status of the technology available for comprehensive helicopter analyses. The development of the analysis involves two tasks: the formulation of the mathematical problem and its solution. The elements of the analysis to be described are the rotor structural, inertial and aerodynamic models; the blade mode calculation; the rotor nonuniform induced velocity calculation; the aircraft model; and the drive train model. The solution procedures will be described for the rotor motion and airframe vibration calculation; for the rotor performance and loads calculation; and for the trim, transient, flight dynamics and flutter analyses.

An overview of the problem to be solved is appropriate before beginning the description of the rotor model. The first task is the trim analysis, in which the control positions and aircraft orientation are determined for the specified operating condition. The periodic blade motion is calculated, and then the rotor performance, loads and noise can be evaluated. The rotor model in the trim solution can use uniform inflow, nonuniform inflow with a rigid wake geometry, or nonuniform inflow with a free wake geometry. The aeroelastic stability, flight dynamics, and transient analyses begin from the trim solution. The flight dynamics analysis calculates the rotor and airframe stability derivatives, and constructs linear differential equations for the aircraft rigid body motions; the poles, zeros, and eigenvectors of these equations define the aircraft flying qualities. The transient analysis numerically integrates the rigid body equations of motion for a prescribed control or gust input. The aeroelastic stability analysis constructs a set of linear differential equations describing the motion of the rotor and aircraft; the eigenvalues of these equations define the system stability.

In this discussion, dimensionless quantities are generally used, based on the air density ρ , the rotor radius R and the rotor rotational speed Ω .

2. ROTOR MODEL

2.1. Structural analysis

The structural model of the rotor is based on engineering beam theory (i.e. the Bernoulli-Euler theory of bending) for the coupled flap-lag bending and torsion of a blade with large pitch and twist. The basic assumption is that the structural elements of the blade have a high aspect ratio. This assumption is normally well satisfied for rotor blades, although engineering beam theory may be suspect at the root for hingeless rotors. The use of engineering beam theory is almost universal in helicopter analyses, but there are some variations. Often the blade pitch and twist are assumed to be small; and nonlinear terms may be introduced in the structural model (here all the nonlinearity considered is accounted for in the inertial and aerodynamic forces).

Figure 1 shows the geometry of the undeformed blade. It is assumed that the undeformed elastic axis is a straight line. The span variable r is measured from the center of rotation; the coordinates x and z are the structural principal axes of the section, with origin at the elastic axis. The tension center (modulus weighted centroid) is on the x axis, at a distance x_c aft of the elastic axis. The angle of the major principal axis (the x axis) with respect to the hub plane is θ . The blade pitch is described by root pitch $\theta^\circ(\psi)$ (rigid

pitch about system), but $\theta = \theta^\circ + \theta$ is small, but axis system (i, j and k)

Figure 2 described by section due ϕ_z and θ_c a

lements the
r dynamics
itation in a
ed in such
terized by
a model is

athematical
r describes
behind the
and limita-
-exposition
prehensive
ormulation
to be de-
ode calcul-
el; and the
otion and
on; and for

he descrip-
l positions
The per-
ise can be
onuniform
metry. The
n solution.
atives, and
the poles,
The tran-
prescribed
r differen-
s of these

air density

y (i.e. the
sion of a
ements of
for rotor
ess rotors.
but there
mall; and
nlinearity

the unde-
-center of
tion, with
he x axis,
he x axis)
 ψ (rigid

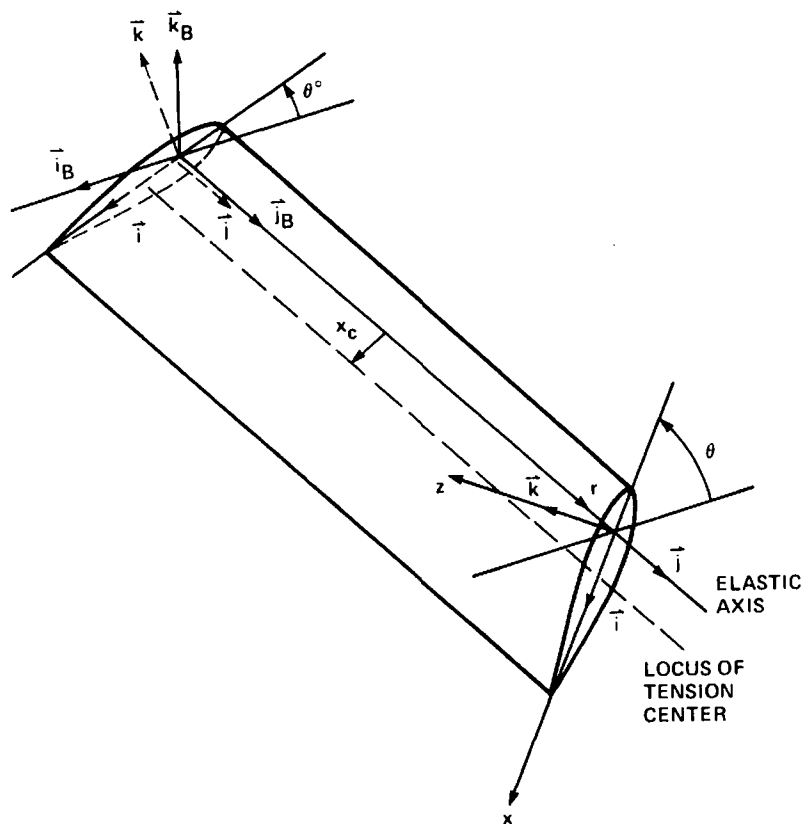


Fig. 1. Geometry of the undeformed blade.

pitch about the feathering axis, including that due to the elastic distortion of the control system), built-in twist $\theta_{iw}(r)$, and torsion deflection about the elastic axis $\theta_e(r, \psi)$; so $\theta = \theta^\circ + \theta_{iw} + \theta_e$. There is shear stress in the blade due to θ_e only. It is assumed that θ_e is small, but θ° and θ_{iw} can be large angles. The unit vectors in the rotating hub plane axis system are i_B, j_B and k_B (Fig. 1). The unit vectors for the principal axes of the section (i, j and k) are rotated by the angle θ from the hub plane axis.

Figure 2 shows the geometry of the deformed section. The deformation of the blade is described by (a) deflections x_o, r_o and z_o of the elastic axis; (b) rotations ϕ_x and ϕ_z of the section due to bending; and (c) twist θ_e about the elastic axis. The quantities $x_o, r_o, z_o, \phi_x, \phi_z$, and θ_e are assumed to be small. (Since the present structural model includes only the

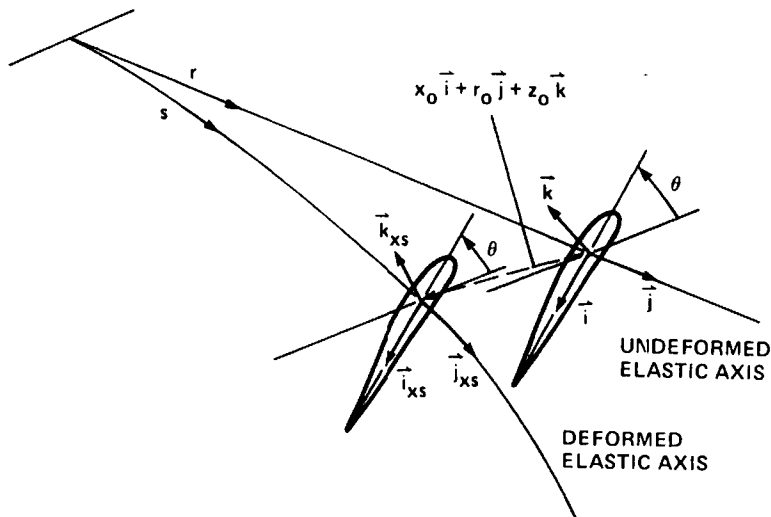


Fig. 2. Geometry of the deformed blade.

lowest order terms, a more precise definition of the order of these quantities is not necessary). The unit vectors of the bent cross section are i_{xs} , j_{xs} , and k_{xs} , which are obtained from i , j , and k by rotating about the x and z axes by the angles ϕ_x and ϕ_z respectively. By definition, j_{xs} is tangent to the deformed elastic axis, so $j_{xs} = dr/ds$ where $r = x_0i + (r + r_0)j + x_0k$ and s is the arc length (Fig. 2). It follows that $\phi_z = -x'_0 - z_0\theta'$ and $\phi_x = z'_0 - x_0\theta'$; or $\phi_x i + \phi_z k = (z_0 i - x_0 k)'$. The position of a blade element is $r = xi + rj + zk$ in the undeformed blade, and $r = (x_0 + x)i + (r + r_0 + x\phi_z - z\phi_x)j + (z_0 + z)k$ is the deflected position.

The basic assumptions of engineering beam theory are that plane sections perpendicular to the elastic axis remain so after bending of the blade; and that all stresses except the axial component are negligible. The structural analysis follows the work of Houbolt and Brooks [3]. The strain tensor is defined by $2\gamma_{mn}dx_m dx_n = (dS)^2 - (ds)^2$, or $\gamma_{mn} = \frac{1}{2}(G_{mn} - g_{mn})$. Here G_{mn} and g_{mn} are the metric tensors of the deformed and undeformed blade [4]; dS and ds are the corresponding differential lengths in the material; and x_m are general curvilinear coordinates. The axial component of the metric tensor is obtained from $|\partial r/\partial r|^2$, using the position vector r of the deformed or undeformed blade. The strain analysis is simplified by neglecting the elastic extension r_0 , since then to first order the arc length along the deformed elastic axis is $s = r$. The linear strain ϵ_{rr} is obtained from the axial component of γ_{rr} ; it takes the form

$$\epsilon_{rr} = \epsilon_T + (x - x_C)\epsilon_x + z\epsilon_z + \theta'_{tw}\theta'_c(x^2 + z^2 - k_p^2)$$

where the terms ϵ_T , ϵ_x , and ϵ_z are linear functions of x_0 , z_0 , r_0 , θ_c , ϕ_x , and ϕ_z (the strain due to the blade extension r_0 is included in ϵ_T at this point). Here k_p is the modulus weighted radius of gyration about the elastic axis; and the strain ϵ_T is related to the blade tension by $T = \int E\epsilon_{rr} dA = \epsilon_T \int E dA$.

The axial stress is given by $\sigma_{rr} = E\epsilon_{rr}$, where E is the modulus of elasticity. The direction of σ_{rr} is assumed to be given by the vector $\partial r/\partial r$ (which does not give the torsion moment due to tension quite correctly, but the error is not usually important for rotor blades). The moment on the deformed cross section, $M = M_x i_{xs} + M_r j_{xs} + M_z k_{xs}$, is obtained by integrating the cross product of the elemental force $\sigma_{rr} dA$ and its moment arm about the elastic axis. The torsion moment due to the shear stresses produced by elastic torsion, $GJ\theta'_c$, is introduced at this point; and for the bending it is convenient to deal with moments about the tension center at $x = x_C$.

The section bending moment vector and flap-lag deflection vector are defined as follows: $M_{2E} = M_x i + M_z k$ and $w = z_0 i - x_0 k$. Then the result of the blade structural analysis is

$$M_{2E} = (EI_{zz}ii + EI_{xx}kk) \cdot w'' + \theta'_{tw}\theta'_c(EI_{xp}k - EI_{zp}i)$$

$$M_{rE} = (GJ + k_p^2 T + \theta'^2_{tw} EI_{pp})\theta'_c + \theta'_{tw} k_p^2 T + \theta'_{tw}(EI_{xp}k - EI_{zp}i) \cdot w''$$

where EI_{zz} and EI_{xx} are the flapwise and chordwise bending stiffness; and EI_{xp} , EI_{zp} and EI_{pp} are higher order integrals [2]. (Dyadic notation is used in the expression for M_{2E} . A dyadic D is a sum of terms of the form (cab) , where a and b are vectors and c is a scalar; then the operation of a dyadic on a vector x is defined by $D \cdot x = (ca b) \cdot x = ca (b \cdot x)$, using the vector dot product). The vector form allows a simultaneous treatment of the coupled inplane and out-of-plane bending of the blade, even for large pitch angles, with considerable simplification of the equations as a consequence.

2.2. Inertia analysis

An integrated Newtonian approach is used to derive the partial differential equations describing the motion of the rotor blade. The same or equivalent equations could be obtained by Lagrangian or differential Newtonian techniques. A modal representation is used to transform the partial differential equations to ordinary differential equations (in time) for the degrees of freedom. The approach used is equivalent to a Galerkin analysis, based on the orthogonal modes of free vibration for the rotating blade. A formal modal

derivation true orthogary conditi the pitch c

The sele representat the rotor n half of the to accurate many force modal corr of motion, possible. In motion of different or marily due modes are coupling o forces is si body mod two-bladed by a rigid equivalent condition, or teeterin calculate n mode is us some ineffi blade. How conditions obtained d mode is us

There ha of the work oped in th shaft moti preclude tl rived for t mathemati to be requi forces and here inclu shaft moti derive the required). lished kno ency in the this sectio deflection good agre isolated bl

Conside is at the az sionless ti reference f

derivation is most convenient, and gives the same results as the Galerkin approach. A true orthogonal mode analysis is not possible however, since it cannot handle the boundary conditions correctly (particularly those associated with the lag damper moment and the pitch control moment at the blade root).

The selection of modes affects the efficiency of the solution procedure. The modal representation separates the solution for the spacial variation and the time variation of the rotor motion. Certain forces that couple aspects of the motion can be put in either half of the solution. The modes should be chosen such that as few as possible are needed to accurately represent the forced response of the structure, which suggests including as many forces as possible in the modal solution. However, the increase in complexity of the modal computation is not compensated by any significant simplification of the equations of motion, so it is desirable to limit what is included in the modal solution as far as possible. In the present analysis, separate modes are used for the bending and torsion motion of the blade. The differential equations for the bending and torsion modes are of different order. Also, for most blades the coupling between bending and torsion is primarily due to aerodynamic and nonlinear dynamic forces. Coupled flap-lag bending modes are used (including the rigid flap and lag modes for an articulated blade). The coupling of the inplane and out-of-plane blade motion by the structural and inertial forces is significant, especially at large pitch angles or with large twist. Separate rigid body modes are used for the gimbal pitch and roll motion, or the teeter motion of a two-bladed rotor. Representing the motion of the blade on a gimballed or teetering rotor by a rigid flap mode plus K elastic modes with a cantilever root boundary condition is equivalent to modelling the blade by K elastic modes with a pinned root boundary condition, although $K + 1$ degrees of freedom are used. Hence the model for a gimballed or teetering rotor will be somewhat inefficient. The alternative however would be to calculate modes for the entire rotor, not just for a single blade. A separate rigid body mode is used for the blade pitch motion due to control system flexibility. Again there is some inefficiency involved in combining this mode with the elastic torsion modes of the blade. However it is simpler to handle the pitch control input and the root boundary conditions by working directly with the rigid pitch mode (since the equation of motion is obtained directly from equilibrium of moments about the pitch axis). Also, the rigid pitch mode is usually more important than the elastic torsion motion.

There have been numerous investigations of rotor and helicopter dynamics, with much of the work in recent years focused on hingeless rotor characteristics. The models developed in these investigations generally are restricted to uniform blade properties or no shaft motion, or involve other limitations on the geometry or degrees of freedom that preclude their use here. Consequently the equations of motion were independently derived for the present analysis. While recent investigations have tended to deal with the mathematics of the problem rather than the physics, certain nonlinear effects are known to be required for an adequate representation of rotor dynamics, particularly the Coriolis forces and the equivalent pitch-flap and pitch-lag coupling. The inertial analysis used here includes nonlinear accelerations and forces to some extent. The rotor blade and shaft motion are assumed to be small, but no formal ordering scheme is introduced to derive the equations of motion (hence no precise definition of what small means is required). The retention of nonlinear terms in the equations is based generally on established knowledge of certain important nonlinear effects, and the requirement of consistency in the derivation. The structure of the resulting equations is described at the end of this section. Basically the equations are linearized about the time-averaged bending deflection of the blade. It has been found [5] that this model gives results that are in good agreement with calculations based on independently developed models for an isolated blade in hover.

Consider an N -bladed rotor, rotating at speed Ω (Fig. 3). The m -th blade ($m = 1$ to N) is at the azimuth location $\psi_m = \psi + m\Delta\psi$, where $\Delta\psi = 2\pi/N$ and $\psi = \Omega t$ is the dimensionless time variable. The S coordinate system (i_s, j_s, k_s) is a nonrotating, inertial reference frame. The B system (i_B, j_B, k_B) is a coordinate frame rotating with the m -th

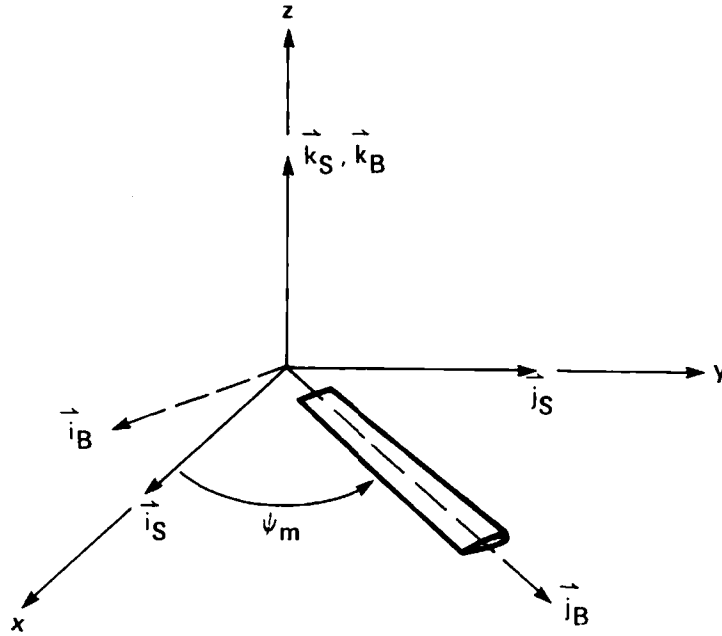


Fig. 3. Nonrotating and rotating hub coordinate systems.

blade. The acceleration, angular velocity and angular acceleration of the hub, and the forces and moments exerted by the rotor on the hub are defined in the nonrotating frame (the *S* system). The rotor blade equations of motion will be derived in the rotating frame. The origin of the *B* and *S* systems is the location of the optional gimbal or teeter hinge. The hub of the rotor is a distance z_{FA} below the origin (gimbal undersling). The blade has a torque offset x_{FA} . The precone angle δ_{FA1} gives the orientation of the blade elastic axis inboard of the pitch bearing with respect to the hub plane: δ_{FA1} is positive upward and is assumed to be a small angle. The pitch bearing is offset radially from the center of rotation by r_{FA} . The droop angle δ_{FA2} and sweep angle δ_{FA3} give the orientation of the elastic axis of the blade outboard of the pitch bearing, with respect to the precone. Both δ_{FA2} and δ_{FA3} are assumed to be small angles, positive downward and positive aft respectively. Feathering axis droop δ_{FA4} and sweep δ_{FA5} define the orientation of the feathering axis with respect to the precone: these angles are positive downward and aft respectively and both are small.

The geometry of the blade was shown in Fig. 1. The undeformed elastic axis is a straight line (except for the droop and sweep angles at the pitch bearing). The unit vector \hat{j} is in the direction of the elastic axis; \hat{i} and \hat{k} are the section mass principal axes, with origin at the elastic axis. The corresponding coordinates are r (measured from the center of rotation), x , and z . It is assumed that the direction of the mass principal axes is the same as the direction of the modulus principal axes. The inertial characteristics of the blade are described by the section mass m , the chordwise center of gravity offset x_l , and the section polar moment of inertia about the elastic axis I_θ . The distance x_l is positive aft, measured from the elastic axis. The corresponding z displacement is neglected. The rotor blade motion is described by the following degrees of freedom: (a) gimbal pitch and roll motion of the rotor disk (omitted for articulated and hingeless rotors), or teeter motion of the blade (for two-bladed rotors only); (b) rotor rotational speed perturbation; (c) rigid pitch motion about the feathering axis and torsion about the elastic axis; and (d) coupled flap-lag bending deflection of the elastic axis, including rigid flap and lag motion if the blade is articulated. The gimbal degrees of freedom are β_{GC} and β_{GS} , respectively pitch and roll of the rotor disk. The rotor rotational speed perturbation is ψ_s . The degrees of freedom of the gimbal motion in the rotating frame are $\beta_G = \beta_{GC} \cos \psi_m + \beta_{GS} \sin \psi_m$ and $\theta_G = -\beta_{GC} \sin \psi_m + \beta_{GS} \cos \psi_m$. For two-bladed rotors, the teetering degree of freedom β_T may be included. The teetering motion is defined in

the rotating geometry of the elastic axis of the section. The blade axis (the x axis) angle at the kinematic definition of the blade. The trim value of the perturbation is time dependent root pitch motion due to Hence, the

The pitch The trim $\tilde{\theta} = (\theta^0 -$ at the blade

For the rigid The velocity $v_r = dr/dt$ gravity of system. Balance expressed as blade torsion bent blade Coriolis acceleration the change blade is re coordinate frame. The the *S* frame shaft have

It is assumed The acceleration of the shaft, then for the acceleration follows:

where $a_{r,s}$ rotates at and no an

the rotating frame, hence $\beta_G = \beta_T(-1)^m$ and $\theta_G = 0$ for this case. Figure 2 showed the geometry of the deformed blade. The deformation is described by twist θ_e about the elastic axis; bending deflections x_0 and z_0 of the elastic axis; and rotations ϕ_x and ϕ_z of the section due to the bending.

The blade pitch angle θ is measured from the hub plane to the section major principal axis (the x axis). The pitch of the deformed blade is composed of the root pitch $\theta^0(\psi)$ (the angle at the pitch bearing, due to control commands, control system flexibility and kinematic coupling); the built-in twist $\theta_{tw}(r)$; and torsion about the elastic axis $\theta_e(r, \psi)$. By definition, both θ_{tw} and θ_e are zero at $r = r_{FA}$, and only θ_e produces shear stress in the blade. The commanded root pitch angle is defined as $\theta^c = \theta_{coll} + \theta_{con}$. Here θ_{coll} is the trim value of the collective pitch, which may be large but is steady in time; and θ_{con} is the perturbation control input (including the cyclic control required to trim the rotor), which is time dependent but is assumed to be a small angle. The difference between the actual root pitch and the pitch commanded by the control system, $(\theta^0 - \theta^c)$, is the rigid pitch motion due to control system flexibility or kinematic coupling in the control system. Hence, the blade pitch may be written as

$$\theta = \theta^0 + \theta_{tw} + \theta_e = (\theta_{coll} + \theta_{tw}) + (\theta^0 - \theta^c) + \theta_{con} + \theta_e$$

The pitch angle may now be separated into trim and perturbation terms, $\theta = \theta_m + \tilde{\theta}$. The trim term $\theta_m = \theta_{coll} + \theta_{tw}$ is a large steady angle; and the perturbation term $\tilde{\theta} = (\theta^0 - \theta^c) + \theta_{con} + \theta_e$ is a small angle since all the components are small. The pitch at the blade root ($r = r_{FA}$) is then

$$\theta^0 = \theta_{coll} + (\theta^0 - \theta^c) + \theta_{con} = \theta_m^0 + \tilde{\theta}^0$$

For the rigid pitch motion the following notation is used: $p_0 = \tilde{\theta}^0 = (\theta^0 - \theta^c) + \theta_{con}$.

The velocity and acceleration of the blade section relative to the rotating frame are $\mathbf{v}_r = d\mathbf{r}/dt$ and $\mathbf{a}_r = d\mathbf{v}_r/dt$, where r is the distance from the rotor hub to the center of gravity of the section, and the time derivative is taken relative to the B coordinate system. Based on the model described above, the distance, velocity and acceleration are expressed as linear functions of the degrees of freedom, except that the coefficients of the blade torsion degrees of freedom depend on the bending deflection (since torsion of a bent blade produces inplane and out-of-plane motion of the elastic axis). For the blade Coriolis acceleration the radial velocity component $\mathbf{j} \cdot \mathbf{v}_r$ is required, including the effect of the change in the radial position of the section due to bending. The acceleration of the blade is required with respect to an inertial frame, specifically the S system. The B coordinate frame rotates at a constant angular velocity $\boldsymbol{\Omega} = \Omega \mathbf{k}_B$ with respect to the S frame. The shaft motion is composed of linear and angular displacement of the origin of the S frame. The acceleration, angular velocity, and angular acceleration of the rotor shaft have the following components in the nonrotating, inertial frame:

$$\mathbf{a}_0 = x_h \mathbf{i}_S + y_h \mathbf{j}_S + z_h \mathbf{k}_S$$

$$\boldsymbol{\omega}_0 = \dot{\alpha}_x \mathbf{i}_S + \dot{\alpha}_y \mathbf{j}_S + \dot{\alpha}_z \mathbf{k}_S$$

$$\dot{\boldsymbol{\omega}}_0 = \ddot{\alpha}_x \mathbf{i}_S + \ddot{\alpha}_y \mathbf{j}_S + \ddot{\alpha}_z \mathbf{k}_S$$

It is assumed that \mathbf{a}_0 , $\boldsymbol{\omega}_0$ and $\dot{\boldsymbol{\omega}}_0$ are small quantities.

The acceleration of a blade point in inertial space is required, in terms of the motion of the shaft, the rotation of the rotor and the blade motion in the B frame. From the result for the acceleration in a rotating coordinate frame (S frame, rotating a rate $\boldsymbol{\omega}_0$), there follows:

$$\mathbf{a} = \mathbf{a}_0 + \mathbf{a}_{r,s} + 2\boldsymbol{\omega}_0 \times \mathbf{v}_{r,s} + \boldsymbol{\omega}_0 \times (\boldsymbol{\omega}_0 \times \mathbf{r}) + \dot{\boldsymbol{\omega}}_0 \times \mathbf{r}$$

where $\mathbf{a}_{r,s}$ and $\mathbf{v}_{r,s}$ are the acceleration and velocity relative to the S frame. The B system rotates at angular velocity $\boldsymbol{\Omega} = \Omega \mathbf{k}_B$ with respect to the S frame. Hence with Ω constant and no angular or linear acceleration of the B frame with respect to the S frame, there

follows:

$$\mathbf{a}_{r,s} = \mathbf{a}_r + 2\boldsymbol{\Omega} \times \mathbf{r} + \boldsymbol{\Omega} \times (\boldsymbol{\Omega} \times \mathbf{r})$$

$$\mathbf{v}_{r,s} = \mathbf{v}_r + \boldsymbol{\Omega} \times \mathbf{r}$$

where \mathbf{a}_r and \mathbf{v}_r are the acceleration and velocity relative to the B frame.

Thus:

$$\mathbf{a} = \mathbf{a}_0 + \mathbf{a}_r + 2\boldsymbol{\Omega} \times \mathbf{v}_r + \boldsymbol{\Omega} \times (\boldsymbol{\Omega} \times \mathbf{r}) + 2\boldsymbol{\omega}_0 \times \mathbf{r} + 2\boldsymbol{\omega}_0 \times (\boldsymbol{\Omega} \times \mathbf{r}) + \boldsymbol{\omega}_0 \times (\boldsymbol{\omega}_0 \times \mathbf{r}) + \dot{\boldsymbol{\omega}}_0 \times \mathbf{r}$$

To first order in the velocity and angular velocity, this becomes finally:

$$\begin{aligned} \mathbf{a} &\cong \mathbf{a}_0 + 2\boldsymbol{\omega}_0 \times (\boldsymbol{\Omega} \times \mathbf{r}) + \dot{\boldsymbol{\omega}}_0 \times \mathbf{r} + \mathbf{a}_r + 2\boldsymbol{\Omega} \times \mathbf{v}_r + \boldsymbol{\Omega} \times (\boldsymbol{\Omega} \times \mathbf{r}) \\ &= \mathbf{a}_0 + 2\boldsymbol{\Omega}(\mathbf{k}_B \mathbf{r} - r \mathbf{k}_B)\boldsymbol{\omega}_0 - (r \times)\dot{\boldsymbol{\omega}}_0 + \mathbf{a}_r + 2\boldsymbol{\Omega}(\mathbf{j}_B \mathbf{i}_B - \mathbf{i}_B \mathbf{j}_B)\mathbf{v}_r - \boldsymbol{\Omega}^2(\mathbf{i}_B \mathbf{i}_B + \mathbf{j}_B \mathbf{j}_B)\mathbf{r} \end{aligned}$$

(using dyadic notation for the final form). The approximation $\mathbf{r} = r\mathbf{j}_B$ is used to evaluate the hub motion terms.

The aerodynamic forces acting on the blade section are F_x , F_r and F_z . These are the components of the aerodynamic lift and drag forces in the hub plane axis system (the B frame). The directions of F_x , F_r , and F_z are respectively in the hub plane, radial, and normal to the hub plane. (The aerodynamic forces are defined in more detail in section 2.4). There are also radial components of F_x and F_z due to the tilt of the section by blade bending; here F_r is just the radial drag force. Thus the aerodynamic force acting on the section at the deformed elastic axis is

$$\mathbf{F}_{\text{aero}} = F_x \mathbf{i}_B + \tilde{F}_r \mathbf{j}_B + F_z \mathbf{k}_B,$$

where

$$\begin{aligned} \tilde{F}_r &= F_r - F_z[\beta_G + \delta_{FA1} - \delta_{FA2} + \mathbf{k}_B \cdot (x_0 \mathbf{i} + z_0 \mathbf{k})] \\ &\quad - F_x[-\psi_s + \delta_{FA3} + \mathbf{i}_B \cdot (x_0 \mathbf{i} + z_0 \mathbf{k})]. \end{aligned}$$

The section aerodynamic moment about the elastic axis is M_a . These section aerodynamic loads are integrated over the blade span to obtain the total forces and moments.

The equations of motion for elastic bending, torsion and rigid pitch of the blade are obtained from equilibrium of inertial, aerodynamic and elastic moments on the portion of the blade outboard of r : $\mathbf{M}_I = \mathbf{M}_A - \mathbf{M}_E$, where \mathbf{M}_E is the structural moment on the inboard face of the deformed cross section; \mathbf{M}_A is the total aerodynamic moment on the blade surface outboard of r ; and \mathbf{M}_I is the total inertial moment of the blade outboard of r . The structural moment \mathbf{M}_E is obtained from the engineering beam theory for bending and torsion, from the control system flexibility for rigid pitch, or from the hub spring for gimbal or teeter motion. \mathbf{M}_I is the inertial moment of the blade outboard of r , about the point $\mathbf{r}_0(r)$, obtained by integrating the acceleration times the blade density over the volume of the blade:

$$\mathbf{M}_I = \int_r^1 \int_{\text{section}} [\mathbf{r}(\rho) - \mathbf{r}_0(r)] \times \mathbf{a} \, dm \, d\rho$$

The aerodynamic moment \mathbf{M}_A is obtained by integrating the section aerodynamic forces over the length of the blade:

$$\mathbf{M}_A = \int_r^1 [\mathbf{r}(\rho) - \mathbf{r}_0(r)] \times \mathbf{F}_{\text{aero}} \, d\rho + \int_r^1 M_a \mathbf{j}_{xs} \, d\rho$$

For bending of the blade, engineering beam theory gives

$$\mathbf{M}_{2E} = M_x \mathbf{i} + M_z \mathbf{k} = (\mathbf{ii}_{xs} + \mathbf{kk}_{xs})\mathbf{M}_E = [\mathbf{ii} + \mathbf{kk} - (x_0 \mathbf{i} + z_0 \mathbf{k})\mathbf{j}]\mathbf{M}_E.$$

Therefore the operator $(\mathbf{ii}_{xs} + \mathbf{kk}_{xs})$ is applied to \mathbf{M}_I and \mathbf{M}_A also. For bending, moments about the tension center ($x = x_C$) are required. Then the desired partial differential equation for bending is obtained from $\partial^2 \mathbf{M}_2 / \partial^2 r$. Finally the ordinary differential equation

for the k -th

where η_k is
theory give

So this op
elastic axis
 r_{FA} . The d
The ordin
with

where ζ_k is
The equ
equilibrium
moment a
feathering

The aerody
due to the
is given by
system stiff
coupling a

The first tv
terms are
bending. T
system and
is the pitch
blade, this
 $K_p = \tan \epsilon$
ameters, or
system. Th
a fixed sw
reduces to
well. Also,
frequency

The tota
force of the

The compo

for the k -th bending mode of the blade is obtained by operating with

$$\int_0^1 \eta_k \cdot (\dots) dr$$

where η_k is the flap-lag bending mode shape. For elastic torsion, engineering beam theory gives

$$M_{rE} = \mathbf{j}_{xs} \cdot \mathbf{M}_E = [\mathbf{j} + (x_0 \mathbf{i} + z_0 \mathbf{k})'] \cdot \mathbf{M}_E$$

So this operator is applied to \mathbf{M}_I and \mathbf{M}_A . For torsion, moments about the section elastic axis ($x = 0$) at r are required; and torsion involves only the blade outboard of r_{FA} . The desired partial differential equation for torsion is then obtained from $\partial M_r / \partial r$.

The ordinary differential equation for the k -th torsion mode is obtained by operating with

$$\int_0^1 \xi_k (\dots) dr$$

where ξ_k is the elastic torsion mode shape.

The equation of motion for the rigid pitch degree of freedom p_0 is obtained from equilibrium of moments about the feathering axis, $M_{FA} = \mathbf{e}_{FA} \cdot \mathbf{M}(r_{FA})$. Here \mathbf{M} is the moment about the feathering axis ($x = 0$) at $r = r_{FA}$ and \mathbf{e}_{FA} is the direction of the feathering axis, including perturbations due to blade bending:

$$\mathbf{e}_{FA} = \mathbf{j}_{FA} + (x_0 \mathbf{i} + z_0 \mathbf{k})'|_{r_{FA}} - \delta_{FA4} \mathbf{k}_B + \delta_{FA5} \mathbf{i}_B$$

The aerodynamic and inertial moments about the feathering axis are reacted by moments due to the deformation of the control system. The restoring moment acting on the blade is given by the product of the elastic deformation in the control system, and the control system stiffness K_θ : $M_{con} = K_\theta(p_0 - p_r)$, where the rigid pitch consists of the kinematic coupling and the blade commanded pitch angle:

$$p_r = \theta_{1c} \cos \psi_m + \theta_{1s} \sin \psi_m + \Delta \theta_{govr} + \Delta \theta_{mast} \\ - \sum_i K_{Pi} q_i - K_{PG} \beta_G + (\theta_{1s} \cos \psi_m - \theta_{1c} \sin \psi_m) \psi_s$$

The first two terms are the lateral and longitudinal cyclic pitch control inputs; the next terms are feedback from the governor, and kinematic coupling due to the rotor mast bending. The constant K_{Pi} is the kinematic pitch-bending coupling due to the control system and blade root geometry (q_i is the i -th bending degree of freedom). Similarly, K_{PG} is the pitch-flap coupling for the gimbal or teeter motion. For the rigid flap motion of the blade, this coupling is usually expressed in terms of a delta-three angle, such that $K_P = \tan \delta_3$. The values of the kinematic pitch-bending coupling may be input parameters, or K_{Pi} may be calculated from the geometry of the blade root and control system. The last term in p_r is the pitch change due to the rotor azimuth perturbation with a fixed swashplate. For a rigid control system (K_θ very large) the rigid pitch equation reduces to $p_0 = p_r$. Control system damping can be included in the restoring moment as well. Also, the control system stiffness can be written in terms of the nonrotating natural frequency of the blade rigid pitch motion, ω_0 .

The total force exerted by the rotor on the hub is the sum over N blades of the net force of the m -th blade, $\mathbf{F}^{(m)} = \mathbf{F}_A - \mathbf{F}_I$. The inertial and aerodynamic forces are

$$\mathbf{F}_I = \int_0^1 \mathbf{a} m dr$$

$$\mathbf{F}_A = \int_0^1 (F_x \mathbf{i}_B + F_z \mathbf{i}_B + \tilde{F}_r \mathbf{j}_B) dr$$

The components of the total hub force in the nonrotating frame are

$$\mathbf{F} = \sum_{m=1}^N \mathbf{F}^{(m)} = H \mathbf{i}_S + Y \mathbf{j}_S + T \mathbf{k}_S$$

The total moment acting on the hub is the sum over N blades of the net moment $\mathbf{M}^{(m)} = \mathbf{M}_A - \mathbf{M}_I$. The inertial and aerodynamic moments are

$$\mathbf{M}_I = \int_0^1 \mathbf{r} \times \mathbf{a} m \, dr$$

$$\mathbf{M}_A = \int_0^1 (F_z \mathbf{i}_B - F_x \mathbf{k}_B) r \, dr.$$

The components of the total hub moment in the nonrotating frame are

$$\mathbf{M} = \sum_{m=1}^N \mathbf{M}^{(m)} = M_x \mathbf{i}_S + M_y \mathbf{j}_S - Q \mathbf{k}_S.$$

The torsion component of the root moment in the rotating frame is neglected compared to the flap and lag components.

The equations of motion for the gimbal degrees of freedom are obtained from the pitch and roll components of the total rotor hub moment. Allowing for a gimbal spring and damper in the nonrotating frame reacting the rotor moments, the equations of motion are

$$\begin{aligned} M_y + C_{GC} \dot{\beta}_{GC} + K_{GC} \beta_{GC} &= 0 \\ -M_x + C_{GS} \dot{\beta}_{GS} + K_{GS} \beta_{GS} &= 0 \end{aligned}$$

The gimbal hub spring can be written as $K_G = \frac{1}{2} N I_0 \Omega^2 (v_G^2 - 1)$, where I_0 is the flapwise moment of inertia of one blade about the hub center of rotation, and v_G is the rotating natural frequency of the gimbal flap motion. The equation of motion for the teeter degree of freedom of a two-bladed rotor is obtained from equilibrium of flap moments about the teeter hinge. Allowing for a teeter spring and damper in the rotating frame, the equation of motion is

$$-2M_T + C_T \dot{\beta}_T + K_T \beta_T = 0$$

where M_T is the total root flapwise moment:

$$2M_T = \sum_{m=1}^2 (-1)^m \mathbf{i}_B \cdot \mathbf{M}^{(m)}.$$

Again the spring constant can be written in terms of the flap natural frequency: $K_T = 2I_0 \Omega^2 (v_T^2 - 1)$. The equation of motion for the rotor speed perturbation is obtained from equilibrium of the shaft torque moments. The helicopter transmission couples the torque perturbations of the two rotors, hence this equation is best considered with the helicopter body equations of motion.

To derive the modal equation, consider the equilibrium of the elastic, inertial, and centrifugal bending moments, which gives the following homogeneous equation for bending of the blade:

$$\begin{aligned} [(EI_{zz} \mathbf{i}\mathbf{i} + EI_{xx} \mathbf{k}\mathbf{k})(z_0 \mathbf{i} - x_0 \mathbf{k})'''] - \Omega^2 \left[\int_r^1 \rho m \, d\rho (z_0 \mathbf{i} - x_0 \mathbf{k})' \right]' \\ - \Omega m \Omega \cdot (z_0 \mathbf{i} - x_0 \mathbf{k}) + m(z_0 \mathbf{i} - x_0 \mathbf{k})'' = 0 \end{aligned}$$

This equation may be solved by the method of separation of variables. Writing $(z_0 \mathbf{i} - x_0 \mathbf{k}) = \boldsymbol{\eta}(r) e^{i\nu t}$, it becomes

$$(EI\boldsymbol{\eta}''') - \Omega^2 \left(\int_r^1 \rho m \, d\rho \boldsymbol{\eta}' \right)' - \Omega m \Omega \cdot \boldsymbol{\eta} - m\nu^2 \boldsymbol{\eta} = 0.$$

This is the modal equation for coupled flap-lag bending of the rotating blade. It is an ordinary differential equation for the mode shape $\boldsymbol{\eta}(r)$; this mode may be interpreted as the free vibration of the rotating beam at natural frequency ν . This equation, with the

appropriate
Liouville ei
and corres
function m :

The bendin
The hom
given by the

The equati
and some a
torsional st
representat
write $\theta_e =$

There are a
 ω_k^2 ($k \geq 1$).
quency ω_k .
unity at the
The bend
modes. By
converted to
the bending

where η_i ar
 q_i are the d
torsion we v

where ξ_i ar
degrees of f
for rigid pit
is simply ξ_0

The ordinar
the partial c
span. The m
the equation
onality of th
ordinary dif
replace the
orthogonalit

net moment

Appropriate boundary conditions for a cantilevered or hinged blade. is a proper Sturm-Liouville eigenvalue problem. It follows that there exists a series of eigensolutions $\eta_k(r)$ and corresponding eigenvalues v_k^2 . The eigensolutions are orthogonal with weighting function m ; so if $i \neq k$,

$$\int_0^1 \eta_i \cdot \eta_k m \, dr = 0.$$

The bending modes are normalized to unit amplitude (dimensionless) at the tip.

The homogeneous equation for the elastic torsion motion of the nonrotating blade is given by the balance of structural and inertial torsion moments:

$$-(GJ\theta_e') + I_\theta \ddot{\theta}_e = 0.$$

ed compared

The equation for the torsion motion of a rotating blade, including centrifugal forces and some additional structural torsion moments could be used instead. However, for the torsional stiffness typical of rotor blades, the nonrotating torsion modes are an accurate representation of the blade motion. Solving this equation by separation of variables, write $\theta_e = \zeta(r)e^{i\omega t}$, so

$$(GJ\zeta') + I_\theta \omega^2 \zeta = 0.$$

om the pitch
il spring and
is of motion

There are a series of eigensolutions $\zeta_k(r)$ of this equation, and corresponding eigenvalues ω_k^2 ($k \geq 1$). These modes are the free vibration shape of the nonrotating blade. at frequency ω_k . The modes are orthogonal with weighting function I_θ , and are normalized to unity at the tip.

the flapwise
the rotating
teeter degree
its about the
the equation

The bending and torsion motion of the blade are expanded as series in the normal modes. By this means the partial differential equations for the motion (in r and t) are converted to ordinary differential equations (in time only) for the degrees of freedom. For the bending we write:

$$(z_0 \dot{\mathbf{i}} - x_0 \mathbf{k}) = \sum_{i=1}^{\infty} q_i(t) \eta_i(r)$$

where η_i are the rotating coupled flap-lag bending modes defined above. The variables q_i are the degrees of freedom for the bending motion of the blade. For the blade elastic torsion we write

l frequency:
turbation is
transmission
t considered

$$\theta_e = \sum_{i=1}^{\infty} p_i(t) \zeta_i(r)$$

inertial, and
on for bend-

where ζ_i are the nonrotating elastic torsion modes. The variables p_i ($i \geq 1$) are the degrees of freedom for the elastic torsion motion of the blade. The degree of freedom for rigid pitch motion is p_0 . For rigid rotation about the feathering axis, the mode shape is simply $\zeta_0 = 1$. Thus the total blade pitch perturbation is expanded as the series

:o k)'' = 0

$$\tilde{\theta} = \sum_{i=0}^{\infty} p_i(t) \zeta_i(r).$$

es. Writing

The ordinary differential equation for the k -th bending mode is obtained by multiplying the partial differential equation by the mode shape η_k and integrating over the blade span. The modal equation is used to introduce the bending mode natural frequency into the equation, replacing the structural and centrifugal stiffness terms, and the orthogonality of the bending modes decouples the inertia and spring terms. Similarly, in the ordinary differential equation for the k -th torsion mode, the modal equation is used to replace the structural stiffness term with the torsion mode natural frequency and the orthogonality of the modes decouples the inertia and spring terms.

de. It is an
terpreted as
n, with the

Articulated rotors usually have a lag damper, which has an important influence on the blade loads and stability. For a linear lag damper, the moment on the blade is $g_{lag} \zeta$, where

$$\zeta = \sum_{i=1}^{\infty} \mathbf{k}_B \cdot \boldsymbol{\eta}'_i(e) \dot{q}_i$$

and g_{lag} is the viscous lag damping coefficient. The quantity $\mathbf{k}_B \cdot \boldsymbol{\eta}'_i(e)$ is the slope of the i -th bending mode in the lagwise direction, just outboard of the lag hinge. The manner in which the lag damping enters the equation of motion is obtained by a Galerkin or Rayleigh-Ritz analysis, so the term $\mathbf{k}_B \cdot \boldsymbol{\eta}'_k(e) g_{lag} \zeta$ is added to the equation of motion for the k -th bending mode. A nonlinear lag damper moment $M_{lag}(\zeta, \dot{\zeta})$ can also be included, by adding the term

$$\mathbf{k}_B \cdot \boldsymbol{\eta}'_k(e) (g_{lag} \dot{\zeta} - M_{lag})$$

to the right-hand side of the bending equation. Here linear damping is included on the left-hand side still, but only to improve the convergence of the solution; so the g_{lag} term must be subtracted from M_{lag} . Structural damping is also included in the bending and torsion equations, modelled as equivalent viscous damping.

The acceleration due to gravity is $\mathbf{g} = g \mathbf{k}_E$, where g is the gravitational constant and \mathbf{k}_E is the vertical vector. The gravitational forces acting on the rotor blades may be accounted for by substituting $\mathbf{a}_0 - \mathbf{g}$ for \mathbf{a}_0 . Thus the components of \mathbf{g} in the S frame are subtracted from the components of the hub acceleration in the nonrotating shaft axes.

The rotor blade equations of motion are finally obtained by substituting the expansion of the bending and torsion motion as series in the modes of free vibration. Also, the equations of motion, hub reactions and inertial constants are normalized at this point in the analysis, using the characteristic blade inertia I_b (usually the flap inertia); and the blade Lock number $\gamma = \rho a c R^4 / I_b$ is introduced (where a is the two-dimensional lift curve slope, and c is here the blade mean chord). The inertia constants and the blade equations of motion are divided by I_b . The hub forces and moments are divided by NI_b , so they appear in rotor coefficient form. The equations of motion for blade coupled flap-lag bending and for blade rigid pitch and elastic torsion take the form

$$M \begin{pmatrix} \ddot{q}_k \\ \ddot{p}_k \end{pmatrix} + C \begin{pmatrix} \dot{q}_k \\ \dot{p}_k \end{pmatrix} + K \begin{pmatrix} q_k \\ p_k \end{pmatrix} = F + \frac{\gamma}{ac} \begin{pmatrix} M_{qk} \\ M_{pk} \end{pmatrix}_{aero}$$

The coefficient matrices M , C and K contain terms that are functions of the blade bending deflection q_j . The generalized force F is a linear function of the gimbal and rotational speed degrees of freedom (displacement, velocity, and acceleration), and of the shaft motion components (angular velocity, angular acceleration, and linear acceleration). Some coefficients of the terms in F are functions of the blade bending deflection. In addition, F contains the nonlinear lag damper moment in the bending equation, and the control moment (due to p_r) in the pitch equation. The time-average of the bending deflection is used in the coefficient matrices, so the inertia terms in these equations are nonlinear but time-invariant (except for the shaft motion terms, where the transformation from the nonrotating to the rotating frame introduces $\sin \psi_m$ and $\cos \psi_m$ factors). The aerodynamic forces produce periodic coefficients in forward flight.

In rotor coefficient form, the rotor hub force and moment are

$$\frac{\mathbf{F}}{NI_b} = \frac{\gamma}{\sigma a} (C_H \mathbf{i}_S + C_Y \mathbf{j}_S + C_T \mathbf{k}_S) = \frac{1}{N} \sum_{m=1}^N \frac{\gamma}{\sigma a} (C_{f_x} \mathbf{i}_B + C_{f_y} \mathbf{j}_B + C_{f_z} \mathbf{k}_B)$$

$$\frac{\mathbf{M}}{NI_b} = \frac{\gamma}{\sigma a} (C_{M_x} \mathbf{i}_S + C_{M_y} \mathbf{j}_S - C_Q \mathbf{k}_S) = \frac{1}{N} \sum_{m=1}^N \frac{\gamma}{\sigma a} (C_{m_x} \mathbf{i}_B - C_{m_z} \mathbf{k}_B)$$

or

Hence the then filtered

The inertial speed of motion components. Some of the terms). From gimbal or t

To improve for the aerodynamic equations of aerodynamic and β_G is motion, as

2.3. Blade b

The required efficient, an distribution able. In the method [6] does the Ra

The mod.

where $\boldsymbol{\eta}(r) = \boldsymbol{\Omega} = \boldsymbol{\Omega}_B$ is bending stiff frequently the ary condition at the root blade. K_s is offset $r = e$ hingeless rot the modified

uence on the
blade is g_{lag} ,

slope of the
in manner in
Galerkin or
of motion for
be included,

uded on the
the g_{lag} term
bending and

stant and k_E
des may be
S frame are
shaft axes.

ie expansion
n. Also, the
this point in
ia); and the
al lift curve
le equations
 VI_b , so they
led flap-lag

f the blade
gimbal and
, and of the
acceleration).
eflection. In
on, and the
he bending
uations are
nsformation
ctors). The

k_B)

$$\begin{pmatrix} C_H \\ C_Y \\ C_T \\ C_{M_x} \\ C_{M_y} \\ C_Q \end{pmatrix} = \frac{1}{N} \sum_{m=1}^N \begin{pmatrix} \sin \psi_m C_{f_x} + \cos \psi_m C_{f_r} \\ -\cos \psi_m C_{f_x} + \sin \psi_m C_{f_r} \\ C_{f_z} \\ \sin \psi_m C_{m_x} \\ -\cos \psi_m C_{m_x} \\ C_{m_z} \end{pmatrix}$$

Hence the blade root force and moment are resolved in the nonrotating frame, and then filtered by the summation operator. The blade root forces take the form

$$\frac{\gamma}{\sigma a} \begin{pmatrix} C_f \\ C_m \end{pmatrix} = G + \frac{\gamma}{\sigma a} \begin{pmatrix} C_f \\ C_m \end{pmatrix}_{aero}$$

The inertia term G is a linear function of the blade bending, torsion, gimbal, and rotational speed degrees of freedom (displacement, velocity, and acceleration) and of the shaft motion components (angular velocity, angular acceleration, and linear acceleration). Some of the coefficients in G are functions of the blade bending deflections (nonlinear terms). From the expressions for the hub reactions, the equations of motion for the gimbal or teeter degrees of freedom can be constructed.

To improve the convergence of the solution for the blade motion, an approximation for the aerodynamic spring and damping forces is included on the left-hand-side of the equations of motion (see section 5.1). Hence a linear, constant coefficient expansion of the aerodynamic forces M_{qk} , M_{pk} , and C_{m_x} in terms of the rotor degrees of freedom (\dot{q}_i , p_i , \dot{p}_i , and β_G) is derived [2]. These terms will be added to both sides of the equations of motion, as described in section 5.1.

2.3. Blade bending and torsion modes

The requirements for the blade mode calculation procedure are that it be numerically efficient, and that it work well for blades with rapid radial variations in mass and stiffness distributions. There are numerous satisfactory mode shape calculation methods available. In the present analysis the modal equations will be solved by a modified Galerkin method [6], which works better for large radial variations of the blade properties than does the Rayleigh-Ritz method in standard form.

The modal equation for coupled flap-lag bending of the rotating blade is

$$(EI\eta'')'' - \Omega^2 \left(\int_r^R \rho m d\rho \eta' \right)' - m\Omega\Omega \cdot \eta - mv^2\eta = 0$$

where $\eta(r) = z_0\mathbf{i} - x_0\mathbf{k}$ is the bending deflection, EI is the bending stiffness dyadic, $\Omega = \Omega\mathbf{k}_B$ is the rotor rotational speed, and v is the natural frequency of the mode. The bending stiffness dyadic depends on the blade collective pitch and twist angles, consequently the frequencies and mode shapes depend on these parameters also. The boundary conditions are as follows: (a) $EI\eta'' = (EI\eta'')' = 0$ at the tip ($r = R$); and (b) $\eta = \eta' = 0$ at the root ($r = e$) for a cantilever blade, or $\eta = 0$ and $EI\eta'' = K_s\eta'$ for an articulated blade. K_s is the hinge spring dyadic [2]. The root boundary condition is applied at the offset $r = e$ to allow for hinge offset of an articulated rotor, or a very stiff hub of a hingeless rotor. Different offsets can be used for the out of plane and inplane motion. For the modified Galerkin solution, the differential equation is written as

$$\begin{aligned} \mathbf{M}'' - \left(\int_r^1 \rho m d\rho \eta' \right)' - m\mathbf{k}_B\mathbf{k}_B \cdot \eta - mv^2\eta &= 0 \\ \eta'' - (EI/\Omega^2 R^4)^{-1} \mathbf{M} &= 0 \end{aligned}$$

The deflection and moment are expanded as finite series in the functions f_i and g_i :

$$\eta = \sum c_i f_i(r)$$

$$M = \sum d_i g_i(r)$$

For simplicity the functions used for the moment expansion are $g_i = f_i'$ (using $g_i = EI f_i'$ would reduce the solution to the standard Galerkin form). A convenient set of functions for f_i are the bending mode shapes of a nonrotating, uniform beam. Such functions satisfy the required boundary conditions, and furthermore are orthogonal (necessary for good numerical conditioning of the matrices). The series for η and M are substituted into the differential equations, and the following operators are applied to the equations:

$$\int_e^1 f_k \cdot (\dots) dr \quad \text{and} \quad \int_e^1 g_k \cdot (\dots) dr$$

The equations are integrated by parts and the boundary conditions are introduced. The result is a set of algebraic equations for c and d :

$$Cd + Dc - v^2 Bc = 0$$

$$C^T c - Ad = 0$$

So the eigenvalues of the matrix $B^{-1}(CA^{-1}C^T + D)$ are the natural frequencies v^2 of the coupled bending vibration of the blade; and the corresponding eigenvectors c give the mode shape η . A similar procedure is used to solve the equation for the elastic torsion natural frequencies and modes.

2.4. Aerodynamic analysis

The rotor blade aerodynamic loading is calculated using lifting line theory and steady, two-dimensional airfoil characteristics, with corrections for unsteady and three-dimensional flow effects. The model is applicable to rotors operating in low or high inflow, and in axial or nonaxial flight. The assumptions of lifting line theory are generally well satisfied for helicopter rotor blades: that the wing has a high aspect ratio, or more correctly that spanwise variations of the aerodynamic environment are small. In addition, for the rotary wing it is essential to have the capability to treat compressible and viscous flow effects, which are present to some degree in almost all helicopter operating conditions. These effects are included in lifting line theory by using experimental data for the two-dimensional airfoil characteristics. Lifting surface theory models offer more accuracy in the treatment of three-dimensional and perhaps compressible flow effects at low angles of attack, but are no more accurate and cause more difficulties than lifting line theory when calculating the loading at high angles of attack. Computational fluid dynamics (CFD) methods are just beginning to be applied to the type of flows encountered on helicopter rotors. Finally, lifting line theory is far more efficient than lifting surface theory or CFD methods, to the extent that with current computers lifting line theory is probably the only practical approach for a comprehensive analysis of the rotary wing in forward flight.

Lifting line theory is not accurate at the tip of a wing or for a close vortex-blade interaction. The calculation of the loading at the blade tip is corrected for three-dimensional effects by using a tip loss factor in the conventional manner of rotor analyses. The calculation of the loading induced by a vortex passing close to the blade is corrected by using the solution for a model problem, obtained from linear lifting surface theory (described further below). The steady section aerodynamic characteristics must be corrected to account for unsteady flow effects. For low angles of attack, thin airfoil theory results are used to calculate the unsteady aerodynamic loading. For high angles of attack an empirical dynamic stall model is used. The dynamic stall model must be based on the steady, two-dimensional airfoil characteristics in order to be widely applicable. Two such models are implemented in the present analysis. The section aerodynamic characteristics are also corrected for the effects of yawed flow.

The aero
the lowest
here. To in
the aerodyn
and thin ai
first order i
velocity me
empirical c
ground effe
forward flig
as an empir
nonuniform
scribed and

A hub pl
ties are resc
of the blade
ence plane.
and u_R ; U
 $\phi = \tan^{-1} u$
 $\alpha = \theta + \theta_z$,
relative to t
span, and s
coefficients
the blade d
namic load:
drag forces:
resolved wi
blade; and
forces due t
radial drag

where ρ is th
since all qu.

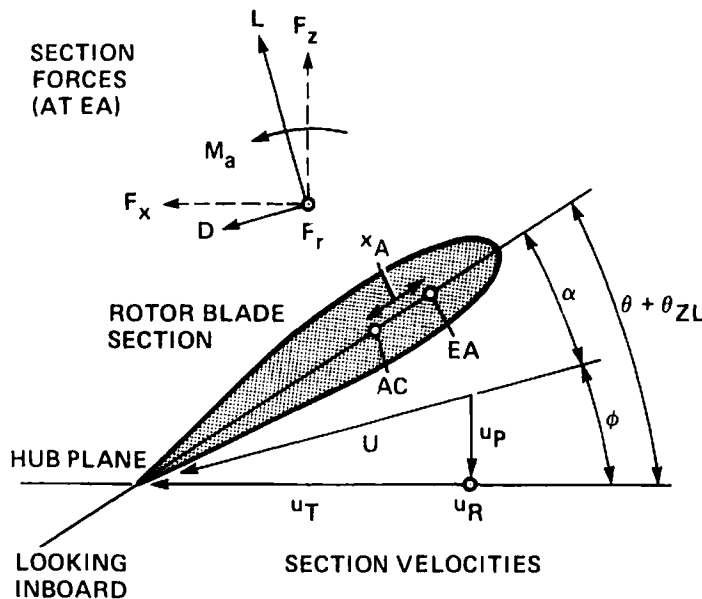


Fig. 4. Rotor blade section aerodynamics.

and g_i :
 sing $g_i = EI f_i$
 et of functions
 nctions satisfy
 ssary for good
 ituted into the
 tions:

roduced. The

ncies v^2 of the
 ors c give the
 elastic torsion

y and steady,
 ree-dimensio-
 inflow, and in
 well satisfied
 correctly that
 ition, for the
 viscous flow
 g conditions.

for the two-
 accuracy in
 low angles of
 theory when
 amics (CFD)
 on helicopter
 eory or CFD
 probably the
 orward flight.
 vortex-blade
 three-dimen-
 analyses. The
 corrected by
 rface theory
 must be cor-
 airfoil theory
 gles of attack
 based on the
 le. Two such
 characteristics

The aerodynamic loading is determined by the air velocity at the blade section. Only the lowest order contribution of each degree of freedom to the velocity is considered here. To include higher order terms would not be consistent since the basic elements of the aerodynamic model are obtained from first order theories (such as lifting line theory and thin airfoil theory). Nonlinear effects, such as stall, are included when they have a first order influence on the loading. Both momentum theory and vortex theory induced velocity models are included in the present analysis. The momentum theory model has empirical corrections for nonideal induced power losses, rotor-rotor interference, and ground effect; and a linear variation of the induced velocity over the rotor disk due to forward flight or aerodynamic moments on the rotor. Such a model is very efficient, and as an empirical model is reliable when used within its limits. A detailed wake model for a nonuniform inflow calculation is also developed for the analysis, using available prescribed and free wake geometry models.

A hub plane reference frame is used for the aerodynamic forces. All forces and velocities are resolved in the B coordinate system. Figure 4 illustrates the forces and velocities of the blade section aerodynamics. The blade pitch angle is θ , measured from the reference plane. The velocity of the air as seen by the moving blade has components u_T , u_P , and u_R ; $U = (u_T^2 + u_P^2)^{1/2}$ is the resultant air velocity in the plane of the section; and $\phi = \tan^{-1} u_P / u_T$ is the induced angle. The section angle of attack is then $\alpha = \theta + \theta_{ZL} - \phi$, where θ_{ZL} is the pitch of the aerodynamic zero-lift axis of the section relative to the structural-inertial principal axis at pitch angle θ (θ_{ZL} may vary along the span, and should not therefore be included in the definition of the section aerodynamic coefficients as a function of α). The velocity components u_T , u_R , and u_P are respectively in the blade drag direction, radially outward and normal to the hub plane. The aerodynamic loads on the section are defined as follows: L and D are the aerodynamic lift and drag forces; F_z and F_x are the components of the total aerodynamic force on the section resolved with respect to the hub plane coordinates; F_r is the radial drag force on the blade; and M_a is the section aerodynamic moment about the elastic axis. The radial forces due to the tilt of F_z and F_x are considered separately, hence F_r consists only of the radial drag forces. The section lift and drag are

$$L = \frac{1}{2} \rho U^2 c c_l + L_{us}$$

$$D = \frac{1}{2} \rho U^2 c c_d$$

where ρ is the air density, and c is the chord of the blade. (The air density can be dropped since all quantities are actually dimensionless.) The section lift and drag coefficients, c_l

and c_d are functions of the angle of attack and Mach number. The section Mach number is $M = M_{tip} U$ (where M_{tip} is the rotor tip speed ΩR divided by the speed of sound). L_{us} is the unsteady aerodynamic lift force. The radial drag force is $F_r = (u_R/U)D = \frac{1}{2}\rho U u_R c c_d$. This radial drag force is based on the assumption that the viscous drag force on the section has the same sweep angle as the local section velocity. The moment about the elastic axis is

$$M_a = -x_A L + M_{ac} + M_{us} = -x_A \frac{1}{2}\rho U^2 c c_l + \frac{1}{2}\rho U^2 c^2 c_m + M_{us}$$

where x_A is the distance the aerodynamic center is behind the elastic axis, c_m is the section moment about the aerodynamic center, and M_{us} is the unsteady aerodynamic moment. The components of the section aerodynamic forces relative to the hub plane axes are then

$$\begin{aligned} F_z &= L \cos \phi - D \sin \phi = (L u_T - D u_P)/U \\ F_x &= L \sin \phi + D \cos \phi = (L u_P + D u_T)/U \end{aligned}$$

The net rotor forces required are obtained by integration of these section forces over the span of the blade

$$\begin{aligned} \frac{M_{qk}}{ac} &= \int_0^1 \eta_k \cdot \left(\frac{F_z}{ac} i_B - \frac{F_x}{ac} k_B \right) dr \\ \frac{M_{pk}}{ac} &= \int_0^1 \xi_k \frac{M_a}{ac} dr - \int_0^1 X_{Ak} \cdot \left(\frac{F_x}{ac} i_B + \frac{F_z}{ac} k_B \right) dr \\ \frac{C_{m_x}}{\sigma a} &= \int_0^1 \frac{F_z}{ac} r dr \\ \frac{C_{m_z}}{\sigma a} &= \int_0^1 \frac{F_x}{ac} r dr \\ \frac{C_{f_x}}{\sigma a} &= \int_0^1 \frac{F_x}{ac} dr \\ \frac{C_{f_z}}{\sigma a} &= \int_0^1 \frac{F_z}{ac} dr \\ \frac{C_{f_r}}{\sigma a} &= \int_0^1 \frac{\tilde{F}_r}{ac} dr \end{aligned}$$

where X_{Ak} is essentially the moment arm about the elastic axis at r , due to the blade bending deflection. The section forces are divided by the two-dimensional lift-curve slope a , and by the mean chord c_{mean} (which enter the definition of the Lock number also).

The air velocity seen by the blade section is due to the rotor rotation, the helicopter forward speed and aerodynamic gusts, the rotor and shaft motion, and the wake induced velocity. The rotor is rotating at speed Ω . The velocity of the air as seen by the rotor disk has the dimensionless components μ_x , μ_y , and μ_z in the shaft axis system: $\mu = \mu_x i_s - \mu_y j_s - \mu_z k_s$. The rotor wake-induced velocity is $\lambda_i = v_i/\Omega R$, normal to the rotor disk and positive downward. A simple model may be used, such as a uniform or linear variation over the disk, or calculated nonuniform induced velocities can be used. For the latter case, all three components of the wake induced velocity (in shaft axes) are considered. The aerodynamic gust velocity has components u_G , v_G , and w_G in the shaft axis system, normalized by dividing by the tip speed ΩR : $V_{gust} = u_G i_s - v_G j_s + w_G k_s$ relative to the rotor. This gust velocity is evaluated at azimuth angle ψ and radial station r on the rotor disk. The quasisteady shaft motion and the gust velocity at the rotor hub will be included in the advance ratio components. The velocity components u_T , u_P , and u_R are thus expressed as linear functions of the rotor degrees of freedom (displacement and velocity of q_k , β_G , and ψ_s), the shaft angular motion (displacement and velocity), the

shaft line; these expressions; the induced velocity; the trim velocity. With inner change in terms in the to the trim axis motion of α . The rotor

where $\lambda =$ for the effective flight. An expression in theory results in the present using the

where z is radius; an approach expression radius. As linear variation mean value κ_y is small following

with typical net aerodynamic theory give aircraft in wake-induced combination velocity of the two rotor

where κ_{12} The section coefficients aerodynamic to $\alpha =$

shaft linear velocity components, and the gust velocity components. The coefficients in these expressions are functions of the radial station r ; the velocity components μ_x , μ_y , and μ_z ; the induced velocity; and are periodic functions of the azimuth angle ψ . In body axes, the trim velocity vector is fixed with the reference frame, and would therefore tilt with it. With inertial axes however, a tilt of the rotor by the shaft motion results in a small change in the directions of the components of μ as seen in the reference frame. Several $\mu\alpha$ terms in the expressions for u_T , u_P , and u_R result from such tilt of the inertial axes relative to the trim velocity vector. The aircraft body yaw, pitch, and roll will be defined as body axis motion however. Hence the body Euler angles are not to be included in the evaluation of α_x , α_y and α_z for the blade velocities.

The rotor wake-induced velocity can be obtained from the momentum theory result

$$\lambda_i = \frac{C_T}{2\sqrt{\lambda^2/\kappa_h^4 + \mu^2/\kappa_f^2}}$$

where $\lambda = \mu_z + \lambda_i$ and $\mu^2 = \mu_x^2 + \mu_y^2$. Empirical correction factors κ_h and κ_f are included for the effects of nonuniform inflow, tip losses, swirl, blockage, etc., in hover and forward flight. An iterative solution of this equation for λ_i is necessary; and an empirical expression is used in the vortex ring and turbulent wake states where the momentum theory result is not applicable. The wake-induced velocity is reduced when the rotor disk is in the proximity of the ground plane. The effect of the ground will be accounted for using the following approximate expression [7] for the induced velocity in ground effect:

$$(\lambda_i)_{IGE} = (1 - \cos^2\epsilon/16z^2) (\lambda_i)_{OGE}$$

where z is the height of the rotor hub above ground level, normalized by the rotor radius; and ϵ is the angle between the ground and rotor wake ($\epsilon = 0$ for hover and ϵ approaches 90° in forward flight), which accounts for the effect of forward speed. This expression compares well with test results, down to an altitude of about one-half rotor radius. As a first approximation to the rotor nonuniform induced velocity distribution, a linear variation over the disk is considered: $\Delta\lambda = \lambda_i(\kappa_x r \cos\psi + \kappa_y r \sin\psi)$, where λ_i is the mean value of the induced velocity. Typically κ_x is positive, roughly 1 at high speed; and κ_y is smaller in magnitude and negative. Both κ_x and κ_y must be zero in hover. Here the following expressions are used:

$$\kappa_x = f_x \mu_x / (\sqrt{\mu^2 + \lambda^2} + |\lambda|) - f_y 2\mu_y - 4f_m C_{M_y} / C_T$$

$$\kappa_y = -f_x \mu_y / (\sqrt{\mu^2 + \lambda^2} + |\lambda|) - f_y 2\mu_x + 4f_m C_{M_x} / C_T$$

with typically $f_x = 1.5$ and $f_y = 1.0$ [8]. There will also be an inflow variation due to any net aerodynamic moment on the rotor disk. Hence the differential form of momentum theory gives the last terms in κ_x and κ_y , including an empirical factor f_m . With twin-rotor aircraft it is also necessary to account for the rotor-rotor aerodynamic interference in the wake-induced inflow velocities. The induced velocity at each rotor is expressed as a linear combination of the isolated rotor induced velocity. Let λ_{i1} and λ_{i2} be the trim induced velocity of the two isolated rotors, calculated as above. Then the trim inflow ratios for the two rotors are

$$\lambda_1 = \mu_{z1} + \lambda_{i1}(1 + \kappa_x r \cos\psi + \kappa_y r \sin\psi) + \kappa_{12} \lambda_{i2} (\Omega R)_2 / (\Omega R)_1$$

$$\lambda_2 = \mu_{z2} + \lambda_{i2}(1 + \kappa_x r \cos\psi + \kappa_y r \sin\psi) + \kappa_{21} \lambda_{i1} (\Omega R)_1 / (\Omega R)_2$$

where κ_{12} and κ_{21} are the rotor-rotor aerodynamic interference factors.

The section aerodynamic characteristics required are the static lift, drag and moment coefficients as a function of angle of attack, Mach number, and blade radial station. The aerodynamic description of the blade also requires θ_{zL} , the pitch of the axis corresponding to $\alpha = 0$ in the airfoil data, relative to the principal axis at pitch angle θ ; and x_A , the

distance aft of the elastic axis to the axis about which the moment coefficient data are given. (It is convenient, but not necessary, for θ_{ZL} to give the pitch of the zero lift axis, and x_A the location of the aerodynamic center.) The two-dimensional airfoil data is used in tabular form. The use of airfoil tables is a nearly universal practice in helicopter analyses. The data are linearly interpolated between the table entries, to obtain the coefficient values at the specified angle of attack and Mach number.

Three-dimensional flow effects at the blade tips significantly alter the loading. Lifting line theory can be formulated as a singular perturbation problem [9], in which the small parameter is the inverse of the aspect ratio, or c/R here. The classical result, which is the basis for the present analysis, is the first order solution, which is not valid within distances the order of the chord from the blade tip (unless the tip platform has a cusp). The rigorous approach is to obtain an inner solution for the tip region, that can be matched to the loading distribution away from the tip to produce a uniformly valid solution. A simpler approach is to make use of the fact that the bound circulation must be zero at the tip and to introduce an empirical function or factor to account for the fall-off of the loading at the tip. Applications of lifting line theory for fixed wings often represent the loading by a series of continuous functions, thereby constraining the loading to fall off proportional to the square root of the distance from the tip. The corresponding approach for rotary wings is provided by the solution of Goldstein or Prandtl [8], which cannot however account for the rolled up tip vortex, and is applicable only to rotors in axial flow. In a discretized application of lifting line theory, the continuous wake is represented by a series of finite strength vortices, trailed from various points along the span. Such a model cannot account for the details of the loading at the tip (using many closely-spaced trailers is not really consistent with the first-order nature of lifting line theory). The net effect of the reduced loading at the tip can be accounted for however by setting the loading to zero over a small distance at the tip. Setting the loading to zero gives zero trailed wake strength, so an alternative approach is to directly move the last trailer inboard by that distance. This can be viewed as modelling the position of the rolled up tip vortex, which usually is slightly inboard of the geometric tip even with a rectangular platform. With the rotary wing it is also necessary to account for the corresponding inboard movement of the tip vortices when they pass under the following blades; but that effect is usually implicit in a separate definition of the wake geometry. The interpretation of the tip loss for a rotary wing is complicated by the fact that the actuator disk model (infinite number of blades, hence infinite aspect ratio) can be related to finite span wing theory; in fact in forward flight the actuator disk is just a circular wing, and uniform disk loading gives the ideal of elliptical loading. The tip loss effect is a correction of the blade loading however, not the disk loading. It accounts for the effects introduced by having a finite number of blades, with finite (but large) aspect ratio. The interpretation is further complicated by the fact that the outer problem, the calculation of the induced velocity at the bound vortex, can be solved in various ways. Momentum theory can be used, if an empirical multiplicative factor is introduced (that includes the effects of the tip loss on the induced velocity); or the nonuniform inflow distribution can be calculated from a detailed wake model. While the latter method produces a more accurate solution for the loading, the limit to the validity of lifting line theory near the blade tip remains. As a consequence of this complexity, the tip loss on a rotary wing has been viewed in several ways [8]: as the reduced effective area of the actuator disk; as the reduced effective wake cross sectional area due to discrete vorticity in the wake; as the reduced section loading on the blade tip; and as the inboard shift of the rolled up tip vortex.

In the present analysis the correction of the lifting line loading calculation at the tip is accomplished using the standard tip loss correction of rotor analyses. It is assumed that the blade has drag but no lift outboard of radial station $r = BR$. The parameter B is called the tip loss factor. The three-dimensional flow at the blade tip increases the critical Mach number of the tip sections, compared to the two-dimensional flow characteristics. This compressible tip relief may be accounted for by reducing the effective section Mach number by the factor $f_M = M_{eff}/M$, which must be specified at each blade station. The tip

platform
relief factor
Yawed
assumption
dimension
by yawed
velocity V
unyawed
layer, then
Accounting
relative to
 $\cos A$, c_m
dimension
data for y

Dynamics
the blade
edge when
It has been
normalized
of $\tau_L = 4.8$
angle of at
value of th
values of τ
model, rat
attack. He

Including

Here Δc_l is
is discussed
moment fi
aerodynam

including
($|\alpha| > 90^\circ$)
leading ed;
induces lar
the pitch r
expressions
 $\Delta c_l = 2.0$ a
loads it is a
the peak v

planform should also be considered in choosing the tip loss factor and compressible tip relief factors for the rotor blade.

Yawed flow over the blade section may be accounted for using the equivalence assumption for swept wings: that the yawed section drag coefficient is given by two-dimensional airfoil characteristics, and the normal section lift coefficient is not influenced by yawed flow below stall. Since the wing viewed in a frame moving spanwise at a velocity $V \sin \Lambda$ (where V is the wing velocity, yawed at angle Λ) is equivalent to an unyawed wing with free stream velocity $V \cos \Lambda$, except for changes in the boundary layer, there should then be no effect of spanwise flow on the loading below stall. Accounting for the effective dynamic pressure and angle of attack of the yawed section relative to the normal section leads to $c_l(\alpha) = c_{l_{2D}}(\alpha \cos^2 \Lambda) / \cos^2 \Lambda$, $c_d(\alpha) = c_{d_{2D}}(\alpha \cos \Lambda) / \cos \Lambda$, $c_m(\alpha) = c_{m_{2D}}(\alpha \cos^2 \Lambda)$ for the section aerodynamic coefficients in terms of two-dimensional airfoil characteristics. These results are largely verified by the experimental data for yawed wings. The section yaw angle is given by

$$\cos \Lambda = \sqrt{\frac{u_T^2 + u_P^2}{u_T^2 + u_P^2 + u_R^2}}$$

Dynamic stall is characterized by a delay in the occurrence of separated flow due to the blade motion, and high transient loads induced by a vortex shed from the leading edge when stall does occur. These features are modelled by the following procedure [10]. It has been found that the dynamic stall delay correlates fairly well in terms of the normalized time constant $\tau = \Delta t V / c$, with approximate values for lift and moment stall of $\tau_L = 4.8$ and $\tau_M = 2.7$ [11, 12]. Hence the section lift will be evaluated at the delayed angle of attack $\alpha_d = \alpha(\psi - \Delta\psi_L) \cong \alpha - \Delta\psi_L \dot{\alpha}$, where $\Delta\psi_L = \Omega \Delta t_L = \tau_L c / u_T$. A maximum value of the angle increment should be specified in order to avoid difficulties at small values of u_T . The lift coefficient below stall should not be affected by the dynamic stall model, rather the stall delay should extend the linear range above the static stall angle of attack. Hence the correction lift coefficient takes the form

$$c_l = \frac{\alpha}{\alpha_d} [c_{l_{2D}}(\alpha_d) - c_{l_{2D}}(0)] + c_{l_{2D}}(0) + \Delta c_l$$

Including the yawed flow correction this becomes

$$c_l = \frac{1}{\cos^2 \Lambda} \left\{ \frac{\alpha}{\alpha_d} [c_{l_{2D}}(\alpha_d \cos^2 \Lambda) - c_{l_{2D}}(0)] + c_{l_{2D}}(0) \right\} + \Delta c_l$$

Here Δc_l is the lift increment due to the leading edge vortex shed at dynamic stall, which is discussed below. Similarly a delayed angle of attack is calculated for the drag and moment from appropriate time constants τ_D and τ_M , and the corrected section aerodynamic coefficients are

$$c_d = \frac{1}{\cos \Lambda} c_{d_{2D}}(\alpha_d \cos \Lambda) + \Delta c_d$$

$$c_m = c_{m_{2D}}(\alpha_d \cos^2 \Lambda) + \Delta c_m$$

Including the yawed flow correction. Similar expressions are used for reverse flow ($|\alpha| > 90^\circ$). When the blade section angle of attack reaches the dynamic stall angle α_{ds} , a leading edge vortex is shed. As this vortex passes aft over the airfoil upper surface it induces large transient loads. The peak incremental aerodynamic coefficients depend on the pitch rate at the instant of stall, $\dot{\alpha}c/V$. This dependence is approximated by analytical expressions based on experimental data [13], with maximum values of approximately $\Delta c_l = 2.0$ and $\Delta c_m = -0.65$ at high pitch rate. In the present model of the dynamic stall loads it is assumed that the incremental coefficients due to the shed vortex rise linearly to the peak values in the small azimuth increment $\Delta\psi_{ds}$ (typically 10° to 15°), and then fall

linearly to zero in the time $\Delta\psi_{ds}$ again. Hence the model involves impulsive lift and nose down moment increases when dynamic stall occurs, which produce the blade motion and loads characteristic of rotor stall. After these transient loads decay the blade section is assumed to be in deep stall, and dynamic stall is not allowed to occur again until the flow has reattached. Flow reattachment takes place when the angle of attack drops below the angle α_{re} . Generally a dynamic stall angle about three degrees above the static stall angle gives good results. Different values of α_{ds} , $\Delta\psi_{ds}$, and α_{re} can be used for the lift, drag, and moment characteristic if necessary to adequately model the dynamic stall of an airfoil.

An alternative dynamic stall model [14] is also implemented in the present analysis. An effective angle of attack of the form

$$\alpha_{dyn} = \alpha - \tau_L \sqrt{|\dot{\alpha}c/2u_T|} \text{ sign } \dot{\alpha}$$

is introduced, where τ_L is a function of Mach number and the airfoil section that is obtained from oscillating airfoil tests. This angle α_{dyn} can be used in place of α_d in the expression for c_l given above, with $\Delta c_l = 0$. Similar corrected angles of attack are calculated for the moment and drag coefficients, using appropriate factors τ_M and τ_D . One or two other dynamic stall models have been developed and described in the literature well enough that they could also be used. The two models implemented in the present analysis are the ones that are most fully documented.

The thin airfoil theory result for the unsteady aerodynamic lift and moment about the pitch axis for the rotary wing is [8]

$$\frac{L_{us}}{ac} = \frac{c}{4} VB(1 + 2x_{AC}/c) + \frac{c}{8} (\dot{w} + u_R w')$$

$$\frac{M_{us}}{ac} = -\frac{c^2}{32} VB(1 + 4x_{AC}/c)^2 - \frac{c^2}{32} (\dot{w} + u_R w')(1 + 4x_{AC}/c)$$

where x_{AC} is the distance between the aerodynamic center and the elastic axis. Here $w = u_T \sin\theta - u_P \cos\theta$ is the upwash velocity normal to the blade surface (with no order c terms); $B = dw/dx$ is the gradient of the upwash along the chord, as due to a pitch rate and $V = u_T \cos\theta + u_P \sin\theta$. In this result the order c^2 lift and order c^3 moment terms have been neglected. Radial flow effects are included in the slender body pressure terms (from the radial derivative w') and in the contributions to the upwash w . The time derivative \dot{w} includes terms due to the time varying free stream. Corrections for real flow effects on the lift-curve slope and aerodynamic center have been included. The sign changes in reverse flow are also accounted for [2].

The blade bound circulation is required for the wake induced velocity calculation $\Gamma = \frac{1}{2} U c c_l + \Gamma_{us}$. Thin airfoil theory gives for the unsteady circulation (below stall) $\Gamma_{us}/ac = \frac{1}{4} c B(1 + 2x_{AC}/c)$.

3. ROTOR WAKE ANALYSIS

The rotor nonuniform inflow is calculated using a vortex wake model developed for the analysis. The wake analysis involves two tasks: calculation of the wake-induced velocities and calculation of the resulting aerodynamic loading on the rotor blade. The blade loading is calculated using lifting line theory, as described above. It is necessary to include corrections for the case of a close blade-vortex interaction: three-dimensional flow effects are accounted for using a linear lifting surface theory solution; and viscous flow effects are accounted for using an empirical model based on the vortex core radius. The induced velocity calculation depends on the strength and geometry of the vorticity in the rotor wake. The tip vortex rollup process is not calculated in the present analysis. Several details of the rollup have a major influence on the solution: the effect of the vortex rollup on the tip loading of the generating blade; the strength of the tip vortex when it encounters the following blade; and the core radius when the vortex is fully

rolled up. Empirical geometry relation [15] geometry

3.1. Nonuniform

Conservation is circulation at the tip produce sl vorticity is at the time the tip of trailed vor quickly re influenced by the time strength n a small co tip vortex viscosity velocity. T limits the the vortex vortex she gradient c vortex is g

The tra blades rot consists o transporte induced ve disk by th the wake vected wit locking he

The stro ant featur from the p highly no encounter does not required t economic vortex-bla nonrotati present a velocity a of measur when the

rolled up. These key features are modelled, not calculated, primarily because the techniques are not well developed to calculate them accurately and efficiently. As a result the model for the rolled up wake is quite simple, hence efficient, emphasizing the properties of the tip vortex—which is in fact the most important component in the rotor wake. Empirical models are available for the wake geometry in hover. These prescribed wake geometry models are incorporated in the analysis. An existing free wake geometry calculation [15] has also been incorporated. This analysis efficiently calculates the distorted geometry of the tip vortices of the rotor in forward flight.

3.1. Nonuniform wake-induced velocity

Conservation of vorticity on a three-dimensional wing requires that the bound circulation is trailed into the wake from the blade tip and root. Radial variation of the bound circulation produces trailed vorticity in the wake, parallel to the local free stream direction at the instant it leaves the blade. Azimuthal variation of the bound circulation will produce shed vorticity, oriented radially in the wake. The strength of the trailed and shed vorticity is determined by the radial and azimuthal derivatives of the bound circulation at the time the wake element left the blade. The lift and circulation are concentrated at the tip of the rotating wing, due to the larger dynamic pressure there. Consequently the trailed vorticity strength is high at the outer edge of the rotor wake, and the vortex sheet quickly rolls up into a concentrated tip vortex. The formation of this tip vortex is influenced by the blade tip geometry. With square tips, much of the roll up has occurred by the time the vortex leaves the trailing edge. The rolled up tip vortex quickly attains a strength nearly equal to the maximum bound circulation of the blade. The tip vortex has a small core radius, depending on the blade geometry and loading. The vorticity in the tip vortex is distributed over a small but finite region, called the vortex core, due to the viscosity of the fluid. The vortex core radius is defined at the maximum tangential velocity. The vortex core is an important factor in the wake induced velocity, since it limits the maximum velocity induced near a tip vortex. Only a limited amount of data on the vortex core radius is available, particularly for rotary wings. There is an inboard vortex sheet of trailed vorticity in the wake, with opposite sign as the tip vortex. Since the gradient of the bound circulation is low on the inboard portion of the blade, the root vortex is generally much weaker and more diffuse than the tip vortex.

The trailed and shed vorticity of the rotor wake is created in the flow field as the blades rotate, and then convected with the local velocity of the fluid. This local velocity consists of the free stream velocity and the wake self-induced velocity. The wake is transported downward, normal to the disk plane, by a combination of the mean wake induced velocity and the free stream velocity. The wake is transported aft of the rotor disk by the inplane component of the free stream velocity. The self-induced velocity of the wake also produces substantial distortion of the vortex filaments as they are convected with the local flow. Thus the wake geometry basically consists of distorted interlocking helices, one behind each blade, skewed aft in forward flight.

The strong concentrated tip vortices trailed in helices from each blade are the dominant feature of the rotor wake. Due to its rotation, a rotor blade encounters the tip vortex from the preceding blade in both hover and forward flight. These tip vortices produce a highly nonuniform flow field in which the blades must operate. For close vortex-blade encounters, the induced loading varies rapidly along the blade span. Lifting line theory does not give an accurate prediction of such loading. Thus lifting surface theory is required to accurately estimate the vortex-induced loads on a rotary wing. The most economical approach is to use lifting line theory with a correction factor for close vortex-blade encounters, based on a lifting surface solution for an infinite aspect-ratio, nonrotating wing encountering a straight, infinite, constant-strength free vortex. In the present analysis this correction will be incorporated as a factor reducing the induced velocity as required to obtain the correct loading by lifting line theory. An examination of measured rotor airloads indicates that the vortex induced loading is generally high when the blade first encounters a vortex, but decreases as the blade sweeps over the

vortex. There is evidently some phenomenon limiting the loads [16,17]. Local flow separation due to the high vortex-induced radial pressure gradients on the blade appears at present to be the most likely explanation for the reduction in loading after the initial encounter. Bursting of the vortex core induced by the blade is also a possibility. Another possibility is that the vortex interacts with the trailed wake it induces behind the blade, with the effect of diffusing the circulation in the vortex. The phenomenon limiting vortex induced loads after the initial encounter will be modelled by increasing the core radius of a segment after it encounters the blade, with upstream propagation along the vortex to produce the loads reduction [15]. An increase in core size is a convenient means to reduce the influence of the vortex; the exact physical explanation for this phenomenon is at present speculative.

The rotor wake induced velocity is calculated by integrating the Biot-Savart law over the vortex elements in the rotor wake. The wake strength is determined by the radial and azimuthal variation of the bound circulation. For the wake geometry a simple assumed model, experimental measurements, or a calculated geometry can be used. With the helical geometry of the rotary wing wake, it is not possible to analytically evaluate the induced velocity, even if the self-induced distortion of the wake is neglected. A direct numerical integration of the Biot-Savart law is not satisfactory either, because the large variations in the induced velocity at close vortex-blade encounters requires a small integration step size for accurate results. It is most accurate and most efficient to calculate the rotor nonuniform inflow with the wake modelled using a set of discrete vortex elements. For each vortex element in the wake the induced velocity at a point in the flow field is evaluated by an analytical expression, and the total induced velocity is obtained by summing contributions from all elements. The tip vortex is well represented by a connected series of straight-line vortex segments, with a small viscous core radius. The inboard trailed and shed vorticity can be modelled by planar, rectangular vortex sheets, or a lattice of discrete straight-line vortex segments (with a large effective core to limit the induced velocity close to individual line segments). A large-core vortex-line element is more economical than a vortex sheet panel, and might in some cases even be a better model than a sheet, if the inboard wake has partially rolled up to form a root vortex. The inboard wake is less important to the nonuniform inflow calculation than the tip vortices, so a more approximate model may be used. The approximations involved in modelling the rotor wake using a set of discrete vortex elements include replacing the curvilinear geometry by a series of straight-line or planar segments; a simplified distribution of vorticity over the individual wake elements (linear variation, or even constant strength); and perhaps physical approximations such as the use of line elements to represent the inboard vortex sheet. The development of a practical model involves a balance between the accuracy and efficiency resulting from such approximations.

The blade bound circulation will be calculated at discrete points on the rotor disk radially and azimuthally. Assuming a linear variation of the bound circulation between these known points results in a wake model consisting of vortex sheet panels (Fig. 5). Assume that the blade bound circulation $\Gamma(r, \psi)$ is given at the radial stations r_i ($i = 1$ to M) and at the azimuthal stations $\psi_j = j\Delta\psi$ ($j = 1$ to J , $\Delta\psi = 2\pi/J$). Let ϕ be the age of vortex elements in the wake ($\phi_k = k\Delta\psi$, $k = 0$ to ∞). The strength of the trailed and shed vorticity of a wake element is determined by the bound circulation of the blade at the time the vorticity was created. Consider a wake panel of age $\phi = \phi_k$ to ϕ_{k+1} , arising from the blade between radial stations r_i and r_{i+1} . The strength of the vorticity in this panel is determined by the bound circulation at the time it was created, which is known at the four corners of the panel. The bound circulation corresponding to the panel leading edge is that at time $\psi - \phi_k$, where ψ is the current blade position (dimensionless time) and ϕ_k is the age of the panel at the leading edge. The bound circulation corresponding to the panel trailing edge is that at $\psi - \phi_{k+1}$, $\Delta\psi$ earlier than the leading edge. The difference between the bound circulation at r_i and r_{i+1} defines the trailed vorticity strength δ , which is constant radially along the panel assuming a linear variation of the bound circulation from r_i to r_{i+1} . When the bound circulation varies azimuthally, how-

ever, the t
linear var
difference
vorticity s
variation
edges.

A vorte
trailed line
induced v
produced
the line se
and bound
radially a
panels to
approxim
of the line
where it c
strength l
lation, az
where the

The rot
vortex. Be
model the
the inboa
 $\Gamma_{\max}(\psi)$ b
far wake,
concentra
small but
along its
single she
model ma

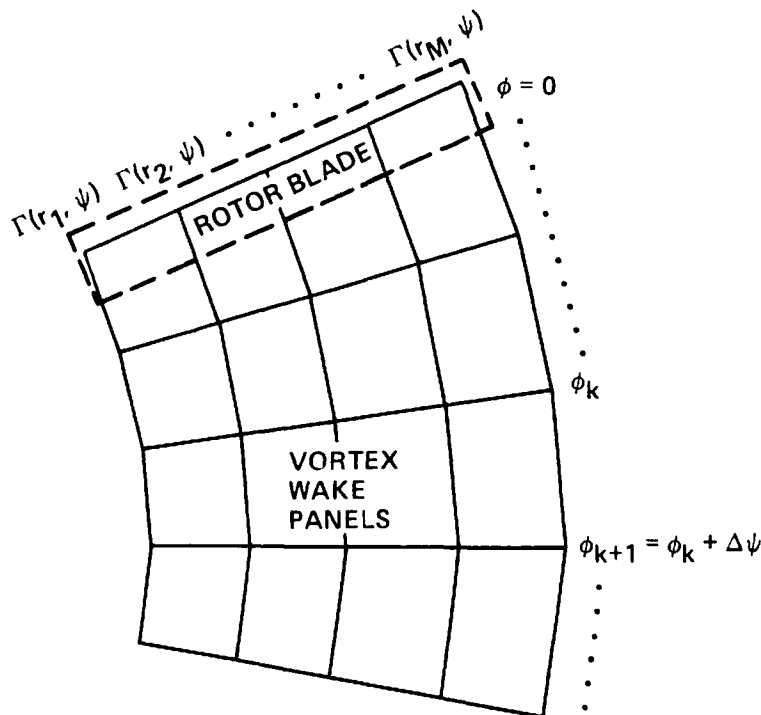


Fig. 5. Wake model with bound circulation calculated at discrete points on rotor disk.

ever, the trailed vorticity strength δ is different at the panel leading and trailing edges; a linear variation of δ in the direction of the trailed vorticity will be used. Similarly, the difference between the bound circulation at $\psi - \phi_k$ and $\psi - \phi_{k+1}$ defines the shed vorticity strength γ , which is constant azimuthally along the panel (for a linear azimuthal variation of the bound circulation) but varies linearly from the left to the right panel edges.

A vortex sheet panel in the wake may be economically approximated by shed and trailed line vortices located in the middle of the panel, with a large core to avoid the induced velocity singularity near a vortex line. A vortex lattice model of the rotor wake is produced by collapsing all the wake panels to such finite strength line segments. Since the line segments are in the center of the sheets, the points at which the induced velocity and bound circulation are evaluated lie at the midpoints of the vortex lattice grid, both radially and azimuthally. Simply collapsing the shed and trailed vorticity in the wake panels to lines, the strength of the line segments will vary along their length. As a further approximation, a stepped (piecewise constant) variation of strength can be used instead of the linear variation, with the jump in strength occurring at the center of the segment where it crosses the other vortex line. Such a vortex lattice wake model with constant strength line segments corresponds to a stepped distribution of the blade bound circulation, azimuthally and radially (with the jumps occurring midway between the points where the circulation is evaluated).

The rotor vortex wake quickly rolls up at the outer edge to form a concentrated tip vortex. Because of the dominant role of the tip vortex in the flow field, it is important to model these rolled up tip vortices in the induced velocity calculation. The lesser role of the inboard wake vorticity allows a more approximate model to be used for it. Let $\Gamma_{\max}(\psi)$ be the radial maximum of the blade bound circulation. It is assumed that in the far wake, where the rollup process is complete, that all of the bound circulation Γ_{\max} is concentrated in the tip vortex. The tip vortex will be modelled by a line segment with a small but finite core radius. When Γ_{\max} varies azimuthally, the tip vortex strength varies along its length. Furthermore, the inboard portion of the wake will be modelled by a single sheet panel, with trailed and shed vorticity as described above. This far wake model may be viewed as corresponding to the circulation distribution sketched in Fig. 6.

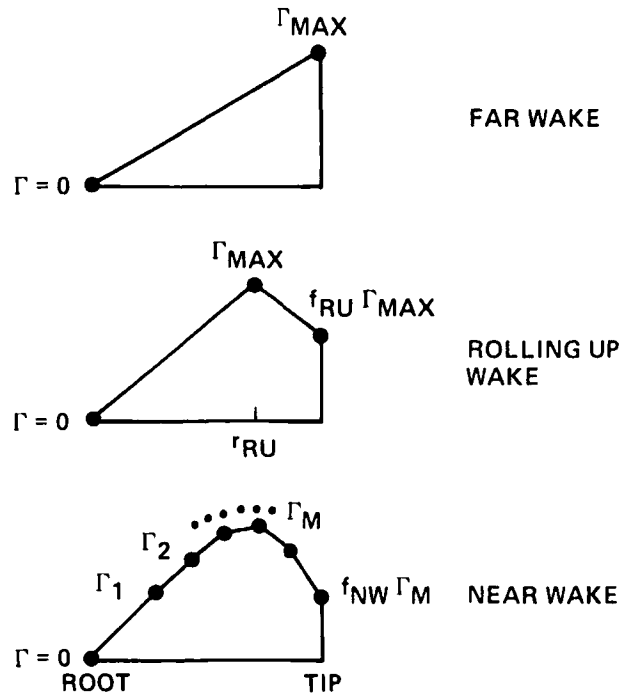


Fig. 6. Equivalent circulation distribution for models of far wake, rolling up wake, and near wake.

The linear variation for $\Gamma = 0$ at the root to $\Gamma = \Gamma_{\max}$ at the tip defines the single inboard sheet, and the sharp drop from Γ_{\max} to zero at the tip defines the tip vortex line. (This circulation distribution should not be associated with the actual bound circulation at the rotor blade. Rather it is an approximation for the vorticity distribution in the far wake, which is determined by the rollup process. Since an analysis of the rollup is not attempted here, the actual vorticity distribution over the inboard sheet is not known. An approximation involving constant strength determined by the known maximum bound circulation is therefore appropriate. This far wake model is computationally efficient, since it depends only on the maximum bound circulation.)

The rollup process may not be complete by the time the tip vortex encounters the following blade. The induced loads will be significantly lower if the tip vortex has strength less than the maximum bound circulation. Therefore the tip vortex rollup must be included in the wake model. Figure 6 sketches the radial circulation distribution assumed, which produces the model for the rolling up wake. The circulation goes from zero at the root to Γ_{\max} at radial station r_{ru} ; to $f_{ru}\Gamma_{\max}$ at the tip. Thus there is a line tip vortex of strength $f_{ru}\Gamma_{\max}$, and two inboard wake panels. The rollup process will take place over the wake from $\phi = 0$ to $\phi = \phi_{ru}$. The position of the maximum circulation and the rollup fraction will vary linearly from r_{ru} and f_{ru} at $\phi = 0$, to $r = 1$ and $f = 1$ at $\phi = \phi_{ru}$. An analysis of the rollup process is not part of the present work, so the parameters ϕ_{ru} , r_{ru} , and f_{ru} must be prescribed inputs to the calculation procedure. Note that the velocity induced by the rolling up wake also depends only on the maximum bound circulation Γ_{\max} .

Just behind the reference blade, where the induced velocity is being evaluated, it is the detailed radial and azimuthal variation of the wake vorticity which is important, not the rollup process (except for the influence of the rollup on the tip loads). Hence for the near wake of the reference blade the full vortex panel representation is retained. The corresponding radial distribution of the circulation is also sketched in Fig. 6 for the near wake; in this case it is the actual blade bound circulation distribution. The tip vortex rollup is often partially complete at the blade trailing edge, so a line vortex at the tip is included, with strength equal to a fraction f_{nw} of the calculated bound circulation at the most outboard radial station. The complete model of the rotor wake is shown in Fig. 7.

The ver
correctly c
chord beh
vortex she
immediate
junction b
point well
using line
panel side
panels sho
A nonro
the induce
velocity ca
hub plane
contrast. t
is less sens
metry is s
evaluated
blade is r_b
rotor disk

The very first panels of the near wake require special consideration. In order to correctly calculate the unsteady aerodynamic effects, the shed wake is stopped a quarter chord behind the bound vortex [18]. The singularity near the side edges of the trailed vortex sheets presents a difficulty in calculating the induced velocity at a point due to the immediately adjacent panels. Thus if the induced velocity is to be calculated near a junction between two panels, they should be replaced by one panel with the collocation point well away from the edges of the single panel. This difficulty can be also avoided by using line vortex elements for the trailed vorticity in the near wake, or by moving the panel side edge away from the collocation point. Finally, the front edges of the individual panels should all be aligned with the bound vortex.

A nonrotating tip path plane coordinate frame with origin at the rotor hub is used for the induced velocity calculation. The solution process will iterate between the induced velocity calculation, and the solution for the blade motion and helicopter trim. Thus the hub plane orientation will be updated based on a new induced velocity estimate. In contrast, the tip path plane orientation is well defined by the operating condition, hence is less sensitive to changes in the induced velocity estimate. Also, the rotor wake geometry is simplest when defined relative to the tip-path plane. The induced velocity is evaluated at the radial stations r_n along the rotor blade. The position vector of the rotor blade is $r_b(r_n)$. The wake-induced velocity is also required at points in the flow field off the rotor disk: (a) at the wing-body, horizontal tail, and vertical tail for the rotor-airframe

near

the single
vortex line.
circulation
in the far
wake is not
known. An
approximate
bound
efficiency,

enters the
vortex has
the wake must
distribution
goes from
a line tip
will take
circulation
and $f = 1$ at
tip, so the
wake. Note
maximum

1. it is the
tip, not the
near the near
the corre-
the near
tip vortex
the tip is
on at the
in Fig. 7.

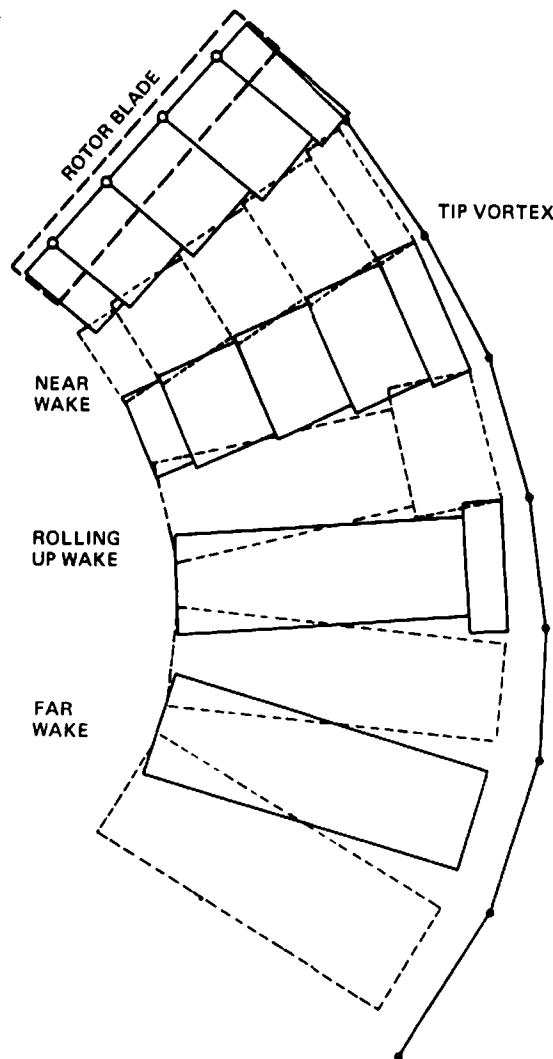


Fig. 7. Sketch of wake model for nonuniform induced velocity calculation.

aerodynamic interference: (b) at the other rotor hub for rotor-rotor aerodynamic interference; (c) at an arbitrary point in the flow field; and (d) at the reference blade of the other rotor, for detailed rotor-rotor interference. For the first two, only the mean value of the induced velocity will be used in the present analysis. The induced velocity distribution over the disk of the other rotor can be used in the present analysis only if the two rotors have the same rotational speed; so for the single main rotor and tail rotor configuration the rotor-rotor interference can be accounted for only in terms of the induced velocity at the rotor hub. The position vectors of these points off the rotor disk are required relative to the hub-centered, tip-path plane coordinate system of the rotor.

The geometry of the tip vortex behind the blade will be defined by the vector $\mathbf{r}_w(\psi, \phi)$, where ψ is the present azimuth angle of the blade and ϕ is the age of the vortex element. The wake geometry is required at the discrete azimuth positions $\psi_l = l\Delta\psi$ and wake ages $\phi_k = k\Delta\psi$, where l ranges from 1 to J (one revolution of the blade, with $\Delta\psi = 2\pi/J$) and k ranges from zero to the specified number of wake spirals for the induced velocity calculation. The tip vortex geometry behind the other blades of the rotor can be obtained from \mathbf{r}_w at the appropriate azimuth angle. The tip vortex elements are created at the blade tip (\mathbf{r}_b at radial station $r = 1$), convected with the free stream velocity μ and distorted by the self-induced velocity in the wake. The rotation of the wing together with convection by the free stream velocity produces the basic helical geometry of the rotor wake. The resulting geometry is

$$\mathbf{r}_w(\psi, \phi) = \mathbf{r}_b(\psi - \phi) + \mu\phi + \mathbf{D}(\psi, \phi)$$

where $\mathbf{D}(\psi, \phi)$ is the distortion due to the wake self-induced velocity, and μ is the free stream convection velocity in the tip-path plane coordinate frame. Similarly the geometry of the inboard wake sheet will be defined at the root and tip edges, trailing from the blade position \mathbf{r}_b at radial stations $r = r_{\text{root}}$ and $r = 1$ respectively. The distortion \mathbf{D} will be different for the tip vortex and the inboard sheet. The induced velocity calculation may require the wake geometry beyond the point where the stored distortion ends. For this portion of the wake, rigid geometry will be used. Consider the distortion when the age ϕ is greater than the age of the last element in the known distortion, ϕ_{last} . The wake geometry will be extrapolated from ϕ_{last} to ϕ , using only vertical convection due to the mean induced velocity:

$$\mathbf{D}(\psi, \phi) = \mathbf{D}(\psi - \phi + \phi_{\text{last}}, \phi_{\text{last}}) - (\phi - \phi_{\text{last}})K_2\mathbf{k}$$

where K_2 is defined below. Note that the azimuth angle of the blade at the time the wake element was created, $\psi - \phi$, has been held constant.

For the self-induced distortion of the rotor wake geometry, the following models are considered: (a) rigid or prescribed wake, with contraction and two-stage convection; and (b) a calculated free wake geometry. The prescribed wake geometry is defined by the radial and axial coordinates D_r and D_z , such that

$$\mathbf{D} = D_r \cos(\psi - \phi) \mathbf{i} + D_r \sin(\psi - \phi) \mathbf{j} + D_z \mathbf{k}$$

where D_r and D_z depend only on the wake age ϕ . For a rigid wake model it is assumed that all elements are convected downward by the mean induced velocity at the rotor disk, with no contraction: $D_z = -\phi\lambda_i$, $D_r = 0$. A more general model consists of two-stage convection:

$$D_z = \begin{cases} -K_1\phi, & \phi < 2\pi/N \\ -K_1 2\pi/N - K_2(\phi - 2\pi/N), & \phi > 2\pi/N \end{cases}$$

with $K_1 = f_1\lambda_i$ and $K_2 = f_2\lambda_i$ determined by the constants f_1 and f_2 . To improve convergence, $\bar{\lambda} = \frac{1}{2}(\lambda_i + \bar{\lambda}_{\text{old}})$ should be used in place of λ_i . Including the contraction of the wake, the radial displacement is modelled as

$$D_r = -(1 - e^{-K_3\phi})(1 - K_4)r_i$$

($r_i = 1$ for inside edge and K_4 , w constants, wake geom experiment K_1, K_2, K_3 defined for developed from low a
The bla $\Gamma_{ij} = \Gamma(r_i$, the blade: subset of tl strength in defined as azimuth ψ induced ve

The second reference b each point azimuth ar blade span the hub of vertical tail

The calc involves th. The solutio discrete po induced vel the rotor (ψ_m blade is ψ_m , $\phi = k\Delta\psi$ (k wake age c behind the evaluated: inboard sh circulation at $\psi_m - \phi$ velocity of is part of th The near w calculating vortex line: inboard wa separate inl velocity exp The contrit By this p Then the ir during the

($r_i = 1$ for the tip vortex and the outside edge of the inboard sheet and $r_i = r_{\text{root}}$ for the inside edge). Hence the rigid wake geometry is determined by the parameters $f_1, f_2, K_3,$ and K_4 , which may be different for the tip vortex and inboard sheet. Alternatively, the constants K_1 and K_2 can be specified, instead of f_1 and f_2 . This form for the prescribed wake geometry of a hovering rotor was introduced by Gray [19]. Landgrebe [20] used experimental model rotor flow visualization data to develop equations for the constants $K_1, K_2, K_3,$ and K_4 as a function of $C_T, C_T/\sigma$ and the rotor twist. Separate equations are defined for the tip vortex and for the sheet tip and root edges. Kocurek and Tangler [21] developed revised expressions for the tip vortex constants based on experimental data from low aspect-ratio two-bladed rotors.

The blade bound circulation is calculated at discrete points on the rotor disk: $\Gamma_{ij} = \Gamma(r_i, \psi_j)$. The solution is periodic, so the azimuthal points cover one revolution of the blade: $\psi_j = j\Delta\psi$ for $j = 1$ to J ($\Delta\psi = 2\pi/J$). The radial stations r_i ($i = 1$ to M) are a subset of the aerodynamic loading radial stations. Except for the near wake, the vorticity strength in the present model actually depends only on the maximum circulation Γ_j , defined as the value of Γ_{ij} with maximum magnitude over all radial stations r_i at a given azimuth ψ_j . Summing the contributions from all vortex elements in the wake gives the induced velocity as the product of the blade bound circulation and influence coefficients:

$$\mathbf{v} = \sum_{j=1}^J \Gamma_j \mathbf{C}_j + \sum_{j=l-K}^l \sum_{i=1}^M \Gamma_{ij} \mathbf{C}_{ij}.$$

The second term is due to the near wake (extending from $\phi = 0$ to $\phi = K\Delta\psi$ behind the reference blade at azimuth angle $\psi = l\Delta\psi$). A set of influence coefficients is obtained for each point in the flow field at which the induced velocity is calculated. At a given azimuth angle ψ_l the field points consist of the induced velocity points along the rotor blade span; perhaps the induced velocity points along the blade of the other rotor, or at the hub of the other rotor; and perhaps the points at the wing-body, horizontal tail, vertical tail, or an arbitrary field point.

The calculation of the influence coefficients proceeds as follows. The outermost loop involves the dimensionless time ψ , which is also the azimuth angle of the reference blade. The solution is periodic so the induced velocity is evaluated for $\psi = 0$ to 2π (at the discrete points $\psi_l = l\Delta\psi$, $l = 1$ to J). For a given ψ , the position vectors at which the induced velocity is required can be evaluated. Next there is a loop over all the blades of the rotor ($m = 0$ to $N - 1$; $m = 0$ is the reference blade). The azimuth angle of the m -th blade is $\psi_m = \psi + m2\pi/N = (l + mJ/N)\Delta\psi$. Finally there is a loop over the wake age $\phi = k\Delta\psi$ ($k = 0$ to the maximum extent of the far wake). The blade specification plus the wake age determines the vortex panel being considered, extending from ϕ to $\phi + \Delta\psi$ behind the m -th blade. Given ψ_m and ϕ , the position vectors of this wake panel can be evaluated: the end points of the tip vortex line segment, and the four corners of the inboard sheet. The wake strength at the panel leading edge is determined by the bound circulation at $\psi_m - \phi$, and the strength at the trailing edge by the bound circulation at $\psi_m - \phi - \Delta\psi$. These azimuth angles define to which influence coefficients the induced velocity of this panel contributes. The wake age determines whether the panel considered is part of the near wake, the rolling up wake, or the far wake models (as described above). The near wake model is only used behind the reference blade ($m = 0$), and is not used in calculating the velocity at points off the rotor disk. The far wake model consists of a tip vortex line segment and a single inboard wake panel. The rolling up wake model has two inboard wake panels. The near wake model consists of a tip vortex line segment and separate inboard wake panels between the bound circulation radial stations. The induced velocity expressions for these elements give the contributions to the influence coefficients. The contribution of the bound vortices of the other blades is also included.

By this procedure the influence coefficients are calculated for a given wake geometry. Then the induced velocity \mathbf{v} can be evaluated from the circulation estimate as required during the solution for the blade motion and helicopter trim. The velocity \mathbf{v} is obtained

in the tip path plane coordinate system. Hence it must be transformed to the hub plane coordinate system for use in the aerodynamic analysis of the rotor. The induced velocity for the rotor-airframe interference must be transformed to the body coordinate system. Also to be accounted for are differences in normalization factors for the velocity induced by the two rotors; sign changes for a clockwise rotating rotor; and a possible azimuthal phase difference between the two rotors [2].

The nonuniform inflow calculation can be simplified in hover or vertical flight due to the axial symmetry of the wake geometry. For the hover case the influence coefficients will be the same for the induced velocity at all azimuth angles, except for an azimuth shift and axis rotation:

$$C_j(\psi = l\Delta\psi) = \begin{bmatrix} \cos(\psi - \Delta\psi) & -\sin(\psi - \Delta\psi) & 0 \\ \sin(\psi - \Delta\psi) & \cos(\psi - \Delta\psi) & 0 \\ 0 & 0 & 1 \end{bmatrix} C_{j-l+1}(\psi = \Delta\psi).$$

Even in hover the rotor may have a net pitch or roll moment (with offset hinges or a hingeless rotor) if the center of gravity is offset from the shaft. Hence in general the hover case will not involve induced velocity and bound circulation independent of azimuth angle. An accurate calculation of the induced velocity of a rotor in axial flight requires consideration of the wake very far from the rotor disk. The detailed wake model described above is required only close to the disk however. Very far from the disk a more approximate and more efficient model is used, obtained by spreading the vorticity vertically over the distance h between successive sheets, as sketched in Fig. 8. The axial convection velocity in the far wake is taken from the prescribed wake model: $v = -k \cdot \mu_{i,pp} + K_2$, giving for the spiral axial spacing $h = 2\pi v$. The tip vortex elements are spread vertically to form a vortex sheet with axial and circumferential components. There is a corresponding axial root vortex from the inboard trailing vorticity. The shed vorticity is spread vertically to form a vortex sheet. This wake model extends L turns (an axial distance Lh) beyond the last spiral of the detailed wake model from each blade.

The induced velocity of a finite length line vortex element must be evaluated. Consider an element of length s , with circulation varying linearly between Γ_1 and Γ_2 at the end points. The induced velocity is required at the point P , defined by the position vectors r_1 and r_2 from the ends of the segment to P . The Biot-Savart law gives the induced velocity

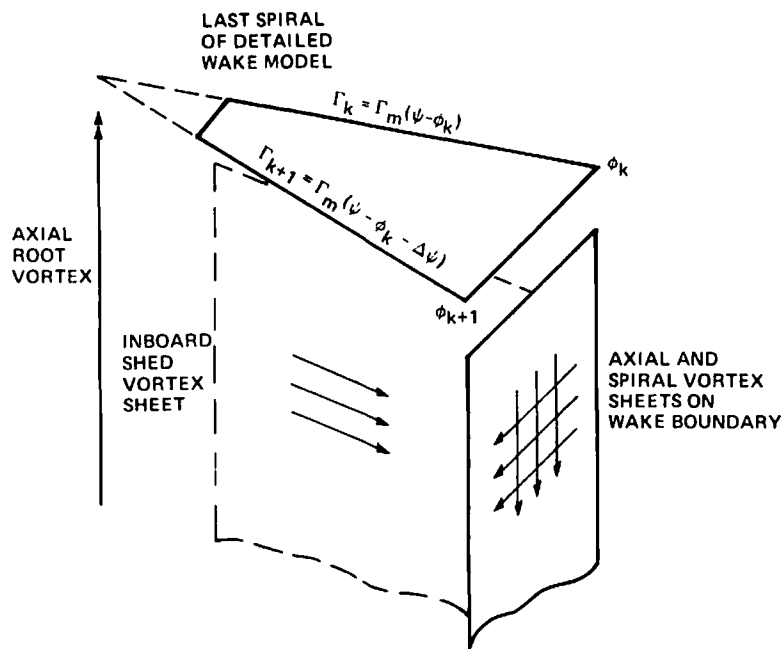


Fig. 8. Far wake model for hover or vertical flight.

due to thi

where r is:
Evaluatin

A similar possible n all the voi mum tang plying Δv line (inclu Measured outside th which is o that one-l circulator obtained v

A lifting infinite asj Λ with the and is cor interaction and wake solved for to the vort to the nun can be ob and the sa solution. T range of v the velocit

(where r at solution fo

The corres obtained in

For each l surface effi ment is mu theory will

The use to model s loads. Let blade, with if the line increment rate $V_b = \dot{c}$

due to this line segment:

$$\Delta \mathbf{v} = -\frac{1}{4\pi} \int \frac{\Gamma \mathbf{r} \times d\boldsymbol{\sigma}}{r^3}$$

where \mathbf{r} is the vector from the element $d\boldsymbol{\sigma}$ on the segment to the point P , and $r = |\mathbf{r}|$. Evaluating the integral gives an expression of the form

$$\Delta \mathbf{v} = \Gamma_1 \mathbf{f}_1(\mathbf{r}_1, \mathbf{r}_2) + \Gamma_2 \mathbf{f}_2(\mathbf{r}_1, \mathbf{r}_2).$$

A similar result is obtained for a line segment with a stepped circulation distribution. A possible model for the tip vortex viscous core is solid body rotation, which implies that all the vorticity is concentrated within the core radius r_c (defined at the point of maximum tangential velocity). The influence of such a vortex core is accounted for by multiplying $\Delta \mathbf{v}$ by the factor $\min(r_m^2/r_c^2, 1)$, where r_m is the minimum distance from the vortex line (including its extension beyond the end points of the segment) to the point P . Measured vortex velocity distributions show that a significant fraction of the vorticity is outside the core radius however. Hence a distributed vorticity core model is preferred, which is obtained by multiplying $\Delta \mathbf{v}$ by the factor [15] $r_m^2/(r_m^2 + r_c^2)$. This factor implies that one-half of the vorticity is outside the core radius, and hence for a given total circulation the maximum tangential velocity (at r_c) with this core model is one-half that obtained with solid body rotation.

A lifting surface theory solution has been developed for the vortex induced loads on an infinite aspect-ratio, nonrotating wing encountering a straight, infinite vortex at an angle A with the wing [22]. The vortex lies in a plane parallel to the wing, a distance h below it and is convected past the wing by the free stream. The distortion of the vortex line by interaction with the wing was not considered. In linear lifting surface theory, the blade and wake are represented by a planar distribution of vorticity. This model problem was solved for the case of a sinusoidal induced velocity distribution, with wave fronts parallel to the vortex line. An approximate solution was obtained by fitting analytical expressions to the numerical solution for sinusoidal loading. The vortex induced velocity distribution can be obtained by a suitable combination of sinusoidal waves of various wavelengths, and the same superposition gives the vortex induced loading from the sinusoidal loading solution. The approximate solution is not valid for extremely small wavelengths, but the range of validity is sufficient to handle the cases arising in rotary wing applications. For the velocity induced along the wing span by a vortex of strength Γ :

$$w = \frac{\Gamma}{2\pi(c/2)} \frac{(-r \sin A)}{(r \sin A)^2 + h^2}$$

(where r and h are here divided by the wing semichord) the approximate lifting surface solution for the section lift takes the form

$$L_{ls} = \rho V \Gamma F(r \sin A, h, A).$$

The corresponding lifting line theory solution for the vortex induced loading can be obtained in the form

$$L_{ll} = \rho V \Gamma G(r \sin A, h).$$

For each line segment it is determined whether it is close enough to the blade for lifting surface effects to be important. If so, the induced velocity contribution of the line segment is multiplied by the ratio L_{ls}/L_{ll} . Then the blade loading calculation from lifting line theory will give the correct vortex induced loads.

The use of a large viscous core radius after a blade-vortex interaction will be allowed, to model such effects as vortex induced stall or core bursting, which limit the induced loads. Let $\phi_{inter}(\psi)$ be the age of the tip vortex segment which first intersects the following blade, with the generating blade at azimuth angle ψ . Then a larger core radius r_b is used if the line segment age is greater than $\phi_b(\psi)$. The transition at ϕ_b occurs initially a fixed increment $\Delta\phi_b$ after the intersection at ϕ_{inter} and then propagates up the tip vortex at a rate $V_b = \partial\phi/\partial\psi$. The wake age ϕ_{inter} at the first blade-vortex intersection can be deter-

mined by examining the projection of the tip vortex wake geometry $r_w(\psi, \phi)$ on the disk plane.

The induced velocity of a planar rectangular vortex sheet element is also required. The velocity is to be evaluated at a point P in the flow field. The vortex panel location is defined by the vectors $r_1, r_2, r_3,$ and r_4 from the four corners to the point P . The strength of the sheet is defined by the circulation value at the four corners. This panel is approximated by a planar, rectangular sheet with sides s and t . The trailed vorticity δ and shed vorticity γ vary linearly along the length of the vortex filaments. The Biot-Savart law gives the induced velocity of this vortex sheet:

$$\Delta v = -\frac{1}{4\pi} \int \frac{r \times \omega}{r^3} dA.$$

Evaluating the integral gives an expression of the form

$$\Delta v = (\Gamma_1 - \Gamma_3)v_{t1} + (\Gamma_2 - \Gamma_4)v_{t2} + (\Gamma_1 - \Gamma_2)v_{s1} + (\Gamma_3 - \Gamma_4)v_{s3}$$

where the subscripts t and s refer to the trailed and shed vorticity respectively and the v vectors are all functions of $r_1, r_2, r_3,$ and r_4 .

There is a logarithmic singularity in the velocity induced at the vortex sheet side edges, which is avoided by replacing the trailed or shed vorticity by a line segment with a large core radius if the point P is too near an edge or corner. An economical approximation is to replace the vortex sheet by a line segment with a large core size to eliminate the singularity of the induced velocity near a line (in this case the core does not have physical significance, rather it is just a convenient means for limiting the velocity magnitude).

3.2. Free-wake geometry

The present analysis incorporates an existing method [15] for calculating the free wake geometry of a single rotor in steady state flight, out of ground effect. This model is not applicable in hover, and only calculates the distorted geometry of the tip vortices. Several other free wake geometry analyses are also available. The method incorporated here appears to be the most sophisticated, and is also quite economical.

The wake model for the free wake geometry calculation consists of line segments for the tip vortices; and rectangular sheets or line segments for the inboard shed and trailed wake. The distortion of the tip vortex geometry from the basic helix is defined as a vector $D_s(\psi, \delta)$, giving the displacement of the wake element with current age δ which was created when the blade was at azimuth angle ψ . A tip path plane coordinate frame is used. The procedure for calculating the wake geometry consists basically of integrating the induced velocity at each wake element. The outer loop in the calculation is an iteration on the wake age δ . The induced velocity $q(\psi)$ is calculated at all wake elements for a given age δ and all azimuth angles ψ . Then the increment in the distortion as the wake age increases by $\Delta\psi$ is

$$D_s(\psi, \delta) = D_s(\psi, \delta - \Delta\psi) + \Delta\psi q(\psi)$$

An efficient calculation of the wake geometry requires many variations in this basic procedure. The near-wake and far-wake scheme for reducing the computation is used. The first time the induced velocity is evaluated at a point in the wake, the contributions from all wake elements must be found. For subsequent evaluations of the induced velocity at that point, only the induced velocity due to the nearby wake elements are recalculated. The other major consideration for minimizing the computation is the matter of updating the induced velocity calculation. At a given point in the wake geometry calculation, there is a boundary in the wake between the distorted geometry and the initial, rigid geometry. The distortion has been calculated between the rotor disk and the boundary; downstream of the boundary the wake is undistorted. As time increases by $\Delta\psi$, the entire wake is convected downstream, and the rotor blades move forward by $\Delta\psi$, adding new trailed and shed vorticity at the beginning of the wake. If there were no distortion of the wake during the time $\Delta\psi$, then the induced velocity at a given wake

element w
vorticity j
induced ve
new wake
and as the
tion of the
recalculate
wake. In g
upstream
and rear p
greater. G
often if the
and conver
accuracy v
where m c
consists of
iterations :

1. W. Johns
2. W. Johns
81182 (19
3. J. C. Ho
Chordwi
4. R. L. Bis
Massach
5. W. John
73248 (19
6. K.-W. La
Rotor Bl.
7. I. C. Che
ARC R d
8. W. Johns
9. M. Van I
10. W. Johns
setts Inst
11. W. J. Mc
Arizona,
12. T. S. Bed
(1976).
13. N. D. Ha
13, No 2.
14. R. E. Go
Helicopte
15. M. P. Sc
Airloads.
16. W. Johns
Lifting-St
17. N. D. Ha
20, No. 4
18. R. H. Mi
19. R. B. Gre
Rotor an
20. A. J. Lan
ance. J. /
21. J. D. Koc
Helicopte
22. W. Johns

element would not change except for the contributions from the newly created wake vorticity just behind the blade. Thus the normal procedure consists of calculating the induced velocity at the boundary, by adding at each step just the contribution from the new wake directly behind the blade. Of course, the wake does distort as it is convected and as the estimate of the distortion improves, thus it is necessary to update the calculation of the induced velocity in the wake. In boundary updating, the induced velocity is recalculated at the boundary only, by summing the contributions from all elements in the wake. In general updating, the induced velocity is recalculated at all points in the wake upstream of the boundary. Boundary updating is typically done every 90° on the front and rear portions of the helices, and every 45° along the sides where the distortion is greater. General updating is typically done every 180° . General updating cannot be done often if the amount of computation is to be kept low, but it does improve the accuracy and convergence. Numerous techniques for secondary improvements in the efficiency and accuracy were also included. The distorted wake geometry is required for m revolutions, where m decreases with forward speed. A single iteration of the free wake analysis consists of calculating the distortion for $\psi = 0$ to 2π and $\delta = 0$ to $2\pi m$. Usually two iterations are sufficient to obtain the converged solution for the wake geometry.

(To be concluded)

REFERENCES

1. W. Johnson. Comprehensive Helicopter Analyses—A State of the Art Review. *NASA TM 78539* (1979).
2. W. Johnson. A Comprehensive Analytical Model of Rotorcraft Aerodynamics and Dynamics. *NASA TM 81182* (1980).
3. J. C. Houbolt, and G. W. Brooks. Differential Equations of Motion for Combined Flapwise Bending, Chordwise Bending and Torsion of Twisted Nonuniform Rotor Blades. *NACA Report 1346* (1958).
4. R. L. Bisplinghoff, J. W. Mar, and T. H. H. Pian, *Statics of Deformable Solids*. Addison-Wesley, Reading, Massachusetts (1965).
5. W. Johnson, Flap/Lag/Torsion Dynamics of a Uniform, Cantilever Rotor Blade in Hover. *NASA TM 73248* (1977).
6. K.-W. Lang, and S. Nemat Nasser. An Approach for Estimating Vibration Characteristics of Nonuniform Rotor Blades. *AIAA Journal*, 17, No. 9 (1979).
7. I. C. Cheeseman, and W. E. Bennett. The Effect of the Ground on a Helicopter Rotor in Forward Flight. *ARC R & M 3021* (1955).
8. W. Johnson. *Helicopter Theory*. Princeton University Press, Princeton, New Jersey (1980).
9. M. Van Dyke. *Perturbation Methods in Fluid Mechanics*. Academic Press, New York (1964).
10. W. Johnson. The Response and Airloading of Helicopter Rotor Blades Due to Dynamic Stall. Massachusetts Institute of Technology. *ASRLTR 130-1* (1970).
11. W. J. McCroskey. *Recent Developments in Dynamic Stall. Symposium on Unsteady Aerodynamics*, Tucson, Arizona, March 1975.
12. T. S. Beddoes. A Synthesis of Unsteady Aerodynamic Effects Including Stall Hysteresis. *Vertica*, 1, 113–123 (1976).
13. N. D. Ham, and M. S. Garelick. Dynamic Stall Considerations in Helicopter Rotors. *J. Am. Helicopter. Soc.* 13, No. 2. (April 1968).
14. R. E. Gormont. A Mathematical Model of Unsteady Aerodynamics and Radial Flow for Application to Helicopter Rotors. *USAAVLABS TR 72-67* (1973).
15. M. P. Scully. Computation of Helicopter Rotor Wake Geometry and its Influence on Rotor Harmonic Airloads. Massachusetts Institute of Technology. *ASRLTR 178-1*, (1975).
16. W. Johnson, A Comparison Between Experimental Data and Helicopter Airloads Calculated Using a Lifting-Surface Theory. Massachusetts Institute of Technology. *ASRLTR 157-1* (1970).
17. N. D. Ham. Some Conclusions from an Investigation of Blade-Vortex Interaction. *J. Am. Helicopter. Soc.* 20, No. 4 (1975).
18. R. H. Miller. Rotor Blade Harmonic Air Loading. *AIAA Journal*, 2, No. 7 (1964).
19. R. B. Gray. On the Motion of the Helical Vortex Shed from a Single-Bladed Hovering Model Helicopter Rotor and Its Application to the Calculation of the Spanwise Aerodynamic Loading. Princeton University, Aeronautical Engineering Department, Report No. 313, September (1955).
20. A. J. Landgrebe, The Wake Geometry of a Hovering Helicopter Rotor and its Influence on Rotor Performance. *J. Am. Helicopter. Soc.* 17, No. 4 (1972).
21. J. D. Kocurek, and J. L. Tangler. A Prescribed Wake Lifting Surface Hover Performance Analysis. *J. Am. Helicopter. Soc.* 22, No. 1 (1977).
22. W. Johnson. A Lifting-Surface Solution for Vortex-Induced Airloads. *AIAA Journal*, 9, 4 (1971).

DEVELOPMENT OF A COMPREHENSIVE ANALYSIS FOR ROTORCRAFT—II. AIRCRAFT MODEL, SOLUTION PROCEDURE AND APPLICATIONS

WAYNE JOHNSON

NASA Ames Research Center and Aeromechanics Laboratory, AVRADCOM Research and
Technology Laboratories, Moffett Field, CA, U.S.A.

(Received 26 May 1981)

Abstract—The development of a comprehensive analytical model of rotorcraft aerodynamics and dynamics is described. Particular emphasis is given to describing the reasons behind the choices and decisions involved in constructing the model. The analysis is designed to calculate rotor performance, loads and noise; helicopter vibration and gust response; flight dynamics and handling qualities; and system aeroelastic stability. It is intended for use in the design, testing and evaluation of a wide class of rotors and rotorcraft and to be the basis for further development of rotary wing theories. The general characteristics of the geometric, structural, inertial and aerodynamic models used for the rotorcraft components are described, including the assumptions introduced by the chosen models and the resulting capabilities and limitations. Finally, some examples from recent applications of the analysis are given.

1. AIRCRAFT MODEL

A general two-rotor aircraft is considered, with rigid body and elastic motion of the airframe. The model is applicable to the case of a rotor or helicopter on a flexible support in a wind tunnel as well. An arbitrary, nonlinear representation of the aircraft geometry and trim orientation is included, since all that requires is properly defined rotation matrices. An orthogonal mode representation of the body elastic motion is used. The modal approach is efficient, yet allows a completely general representation of the airframe. The airframe structural vibration modes must be obtained from a separate analysis. The linearized equations of motion for the rigid body degrees of freedom are used in the calculation of the aircraft vibration and transient motion. Linearized equations are consistent with the assumption in the rotor analysis that the perturbation shaft motion is small. The trim orientation angles of the helicopter can be large however.

Aerodynamic forces on the wing-body, horizontal tail and vertical tail are modelled, including control surfaces. Static aircraft aerodynamic characteristics are used, which must be defined based on experimental results. Current theories are not able to accurately and reliably calculate the aerodynamic loads for the geometries and operating conditions of the typical helicopter fuselage. The aerodynamic characteristics are specified separately for the tail surfaces since the angle of attack and dynamic pressure may be different at the tail due to interference effects. An empirical model for the interference between the rotors and the airframe is included in the present analysis. It is also possible to calculate the mean rotor-induced velocity at the airframe components as part of the nonuniform inflow analysis. The generalized aerodynamic damping and control forces on the airframe elastic modes are included; these terms should be estimated for the frequency of the principal excitation of the mode. The airframe aerodynamic representation is basically a quasistatic model however. High frequency aerodynamic forces on the fuselage and tail can be important for some problems, but the theories to calculate these forces are even less well developed than the theories for the static forces, particularly on a helicopter, for which the rotor-induced flow field and separated flow effects are major factors. The technology is well enough developed to calculate the body-induced interference flow at the rotor disk, at least with sufficient accuracy to model the general features of the interaction. Such a calculation can be readily coupled with the rotor aerodynamic solution, but is not included in the present analysis.

The rotational speed degrees of freedom of the two rotors, coupled through the drive system, can be important factors in the helicopter dynamics. To complete the equations

raft

issues
nes are
ilm and
ble on
on and
at the

Barton,
; Telex

ineously
nsferred
authors
uce and
ure, and
by any
writing

U.S.A.,
7 or 108
e of the
s of the
oes not
in must

of motion for these degrees of freedom, a model for the drive train is required, including the engine dynamics and a rotor speed governor. An elementary model of the transmission and engine dynamics is used in the present analysis, so that at least the principal features may be included in the calculations.

1.1 Aircraft configuration definition

The aircraft flight path is specified by the velocity magnitude V , and the orientation of the velocity vector with respect to earth axes. The velocity vector has a yaw angle ψ_{FP} and a pitch angle θ_{FP} . The aircraft attitude with respect to earth axes is specified by the trim Euler angles, first pitch θ_{FT} and then roll ϕ_{FT} . The rotation matrix R_{FV} between the velocity axes (V system) and the body axes (F system) is defined by these four angles. Airplane convention is followed for the coordinate systems— x is positive forward, y positive to the right and z positive downward [1]. The velocity of the aircraft is $\mathbf{V} = V R_{FV} \mathbf{i}_V$, with components in the body axes. The acceleration due to gravity is $\mathbf{g} = g \mathbf{k}_E$, where in body axes

$$\mathbf{k}_E = -\sin\theta_{FT} \mathbf{i}_F + \cos\theta_{FT} \sin\phi_{FT} \mathbf{j}_F + \cos\theta_{FT} \cos\phi_{FT} \mathbf{k}_F$$

The rotor hub position is specified by the x , y and z coordinates in the body axes relative to the aircraft center of gravity position. The rotor orientation is defined by the rotation matrix R_{SF} between the shaft axes (S system) and the aircraft body axes (F system). For example, the orientation of a main rotor relative to the body axes is specified by a shaft angle of attack and a roll angle. The orientation of a tail rotor is specified by a cant angle and a shaft angle of attack. The position and orientation of the rotors relative to the body axes are fixed geometric parameters. So the components in shaft axes of the velocity seen by the rotor are

$$-\mu_x \mathbf{i}_S + \mu_y \mathbf{j}_S + \mu_z \mathbf{k}_S = V R_{SF} R_{FV} \mathbf{i}_V$$

The sign of the lateral velocity μ_y must be changed for a clockwise rotating rotor; and for the second rotor the velocity components must be multiplied by $(\Omega R)_1/(\Omega R)_2$. The quasistatic hub motion and the gust velocity at the rotor hub will be included in the advance ratio components:

$$-\mu_x \mathbf{i}_S + \mu_y \mathbf{j}_S + \mu_z \mathbf{k}_S = R_{SF} R_{FV} ((V + u_G) \mathbf{i}_V + v_G \mathbf{j}_V + w_G \mathbf{k}_V) + (\dot{x}_h \mathbf{i}_S + \dot{y}_h \mathbf{j}_S + \dot{z}_h \mathbf{k}_S)_{\text{static}}$$

The aerodynamic gust velocity is defined relative to the velocity axes, with longitudinal component u_G positive rearward, lateral component v_G positive from the right and vertical component w_G positive upward. The components in the body axes are then

$$(u_G \mathbf{i} + v_G \mathbf{j} + w_G \mathbf{k})_F = R_{FV} (u_G \mathbf{i} + v_G \mathbf{j} + w_G \mathbf{k})_V$$

The components in the rotor shaft axes are

$$(u_G \mathbf{i} - v_G \mathbf{j} + w_G \mathbf{k})_S = R_{SF} R_{FV} (-u_G \mathbf{i} - v_G \mathbf{j} - w_G \mathbf{k})_V$$

Hence the matrix $R_G = (-\mathbf{ii} + \mathbf{jj} - \mathbf{kk}) R_{SF} R_{FV}$ defines the transformation of the gust components to shaft axes. (Also, for a clockwise rotating rotor the sign of v_G is changed; and for the second rotor the gust velocities must be multiplied by $(\Omega R)_1/(\Omega R)_2$.)

The control variables included in the rotorcraft model are collective and cyclic pitch of the two rotors and the aircraft controls, which consist of engine throttle θ_t , wing flaperon angle δ_f , wing aileron angle δ_a , elevator angle δ_e , and rudder angle δ_r . The control vector is thus

$$\mathbf{v} = [(\theta_0 \theta_{1c} \theta_{1s})_1 (\theta_0 \theta_{1c} \theta_{1s})_2 \delta_f \delta_e \delta_a \delta_r \theta_t]^T$$

The pilot's controls consist of collective stick δ_0 , lateral cyclic stick δ_c , longitudinal cyclic stick δ_s , pedal δ_p , and throttle δ_t :

$$\mathbf{v}_p = [\delta_0 \delta_c \delta_s \delta_p \delta_t]^T$$

For the pur
inputs and
is the contro
the control
coupling be
copters that
and gain scl
that the ma
aircraft con
ual controls
control syst

1.2. Aircraft

The aircr
free vibratic
gravity (the
followed for
frame used i
 x -axis with
consider the
ties dimensi
forces in rot
the characte
The linear d
The linear d
on the rotor
speed ΩR ra
freedom are
angular velo

where

For the el
arbitrary poi

The first six
 ϕ_F, θ_F, ψ_F
of the aircra

For the purpose of trimming the helicopter, a linear relation between the pilot's control inputs and the rotor and aircraft control variables is assumed: $\mathbf{v} = T_C \mathbf{v}_p + \mathbf{v}_0$, where \mathbf{v}_0 is the control input with all sticks centered, and T_C is a transformation matrix defined by the control system geometry. It is not intended that the matrix T_C account for the true coupling between the pilot's control and the rotor-aircraft controls. For modern helicopters that coupling is often quite complex, and may involve some nonlinear functions and gain scheduling with flight condition. All that is necessary for the present purposes is that the matrix T_C correctly account for the coupling between the redundant rotor and aircraft controls. Then the trim solution will produce the correct positions of the individual controls, and the true position of the pilot's sticks can be determined from the actual control system geometry if necessary.

2. Aircraft analysis

The aircraft motion consists of the six rigid body degrees of freedom and the elastic free vibration modes. A body axis coordinate frame with origin at the aircraft center of gravity (the F system) is used for the description of the motion. Airplane practice is followed for these axes— x is forward, y is to the right and z is downward. The coordinate frame used is not a principal axis system; moreover, the airplane practice of aligning the x axis with the trim velocity is not followed, since for rotorcraft it is necessary to consider the hovering case. The parameters of the first rotor are used in making quantities dimensionless and in normalizing the aircraft equations of motion. With the hub forces in rotor coefficient form it is convenient to normalize the equations by dividing by the characteristic inertia ($\frac{1}{2} N I_b$).

The linear and angular rigid body motion of the aircraft is defined in the body axes. The linear degrees of freedom are x_F , y_F and z_F . These variables are dimensionless based on the rotor radius R ; thus the velocity perturbations are normalized using the rotor tip speed ΩR rather than the forward speed V as is airplane practice. The angular degrees of freedom are the Euler angles ψ_F , θ_F and ϕ_F (yaw, pitch and roll). Then the linear and angular velocity perturbations are

$$\begin{aligned} \mathbf{u}_F &= \dot{x}_F \mathbf{i}_F + \dot{y}_F \mathbf{j}_F + \dot{z}_F \mathbf{k}_F \\ \boldsymbol{\omega}_F &= R_c (\dot{\phi}_F \mathbf{i}_F + \dot{\theta}_F \mathbf{j}_F + \dot{\psi}_F \mathbf{k}_F) \end{aligned}$$

where

$$R_c = \begin{bmatrix} 1 & 0 & -\sin \theta_{FT} \\ 0 & \cos \phi_{FT} & \sin \phi_{FT} \cos \theta_{FT} \\ 0 & -\sin \phi_{FT} & \cos \phi_{FT} \cos \theta_{FT} \end{bmatrix}.$$

For the elastic motion of the aircraft in flight, the displacement \mathbf{u} and rotation $\boldsymbol{\theta}$ at an arbitrary point \mathbf{r} are expanded in a series of the orthogonal free vibration modes:

$$\mathbf{u}(\mathbf{r}, t) = \sum_{k=1}^{\infty} q_{s_k}(t) \boldsymbol{\xi}_k(\mathbf{r})$$

$$\boldsymbol{\theta}(\mathbf{r}, t) = \sum_{k=1}^{\infty} q_{s_k}(t) \boldsymbol{\gamma}_k(\mathbf{r}).$$

The first six degrees of freedom are the rigid body motions: $q_{s_1} \dots q_{s_6}$ are respectively ϕ_F , θ_F , ψ_F , x_F , y_F , and z_F . The generalized coordinates for $k \geq 7$ are the elastic modes of the aircraft. For the rigid body motions the mode shapes are simply

$$[\boldsymbol{\xi}_1 \quad \dots \quad \boldsymbol{\xi}_6] = [(-\mathbf{r} \times) R_c \quad I]$$

$$[\boldsymbol{\gamma}_1 \quad \dots \quad \boldsymbol{\gamma}_6] = [R_c \quad 0]$$

The rotor equations of motion require the six components of the hub linear and angular motion in the shaft axis system:

$$\begin{pmatrix} x_h \\ y_h \\ z_h \\ \alpha_x \\ \alpha_y \\ \alpha_z \end{pmatrix} = \begin{bmatrix} R_{SF} \xi_k(\mathbf{r}_{hub}) \\ \dots \\ R_{SF} \gamma_k(\mathbf{r}_{hub}) \dots \end{bmatrix} (q_{sk})$$

or $\alpha = c \mathbf{x}_s$. The total velocity of a point is the sum of the trim and perturbation velocities, $\dot{\mathbf{u}} = \mathbf{V} + \sum \dot{q}_{sk} \xi_k$ (in body axes). The rotor equations require the velocity components at the hub in an inertial frame (the S system), and the Euler angle rotations between the body and inertial axes introduce perturbations of the trim velocity \mathbf{V} . So the perturbation velocity becomes $\alpha_F \times \mathbf{V} + \sum \dot{q}_{sk} \xi_k$, where $\dot{\alpha}_F = \omega_F$. The contributions of $\alpha_F \times \mathbf{V}$ to the hub velocities ($\dot{x}_h, \dot{y}_h, \dot{z}_h$) cancel the terms in the blade velocity due to the Euler angle rotation of the inertial axes relative to the trim velocity. Thus the evaluation of the hub rotation ($\alpha_x, \alpha_y, \alpha_z$) for the aerodynamic analysis should not include the body Euler angle contributions. Finally, the rotor hub acceleration is $\ddot{\mathbf{u}} = \omega_F \times \mathbf{V} + \sum \ddot{q}_{sk} \xi_k$, where the first term is the inertial acceleration due to the rotation of the trim velocity vector by the body axes angular velocity. This additional contribution of the Euler angle velocity to the hub linear acceleration, in the shaft axes system, is

$$\Delta(\ddot{x}_h \mathbf{i}_S + \ddot{y}_h \mathbf{j}_S + \ddot{z}_h \mathbf{k}_S) = \omega_F \times \mathbf{V} = R_{SF}(-\mathbf{V} \times) R_c(\dot{\phi}_F \mathbf{i}_F + \dot{\theta}_F \mathbf{j}_F + \dot{\psi}_F \mathbf{k}_F)$$

which can be written $\Delta \ddot{\alpha} = \bar{c} \ddot{\mathbf{x}}_s$. For the second rotor the linear hub displacement must be multiplied by R_1/R_2 to account for the differences in normalization, c being based on the parameters of the first rotor, while α is based on the parameters of the second rotor in this case. For a clockwise rotating rotor it is necessary to change the signs of y_h, α_x and α_z . In addition, the derivatives of the hub motion of the second rotor must be corrected for the different time base, by multiplying the velocities by Ω_1/Ω_2 and the acceleration by Ω_1^2/Ω_2^2 .

Flexibility between the rotor swashplate and hub will produce a blade pitch change due to elastic motion of the airframe. This coupling between the rotor pitch and mast bending is accounted for by introducing kinematic feedback of the following form:

$$\Delta \theta_{mast} = - \sum_{i=7}^{\infty} q_{s_i} (K_{MC_i} \cos \psi_m + K_{MS_i} \sin \psi_m)$$

which is used in the expression for p_r (see Ref. [2] section 2.2).

Following the usual steps of airplane flight dynamics analysis [1], the linearized rigid body equations of motion are obtained by equating the angular and linear acceleration to the net moments and forces on the aircraft: $I \dot{\omega}_F = \Sigma \mathbf{M}$ and $M(\dot{\mathbf{u}}_F + \omega_F \times \mathbf{V}) = \Sigma \mathbf{F}$. In terms of the body axis degrees of freedom, including the gravitational forces, the equations are

$$\begin{aligned} R_c^T I^* R_c (\dot{\phi}_F \mathbf{i}_F + \dot{\theta}_F \mathbf{j}_F + \dot{\psi}_F \mathbf{k}_F) &= (Q_1^* \mathbf{i}_F + Q_2^* \mathbf{j}_F + Q_3^* \mathbf{k}_F) \\ M^* (\ddot{x}_F \mathbf{i}_F + \ddot{y}_F \mathbf{j}_F + \ddot{z}_F \mathbf{k}_F) - M^* (\mathbf{V} \times) R_c (\dot{\phi}_F \mathbf{i}_F + \dot{\theta}_F \mathbf{j}_F + \dot{\psi}_F \mathbf{k}_F) \\ &= (Q_4^* \mathbf{i}_F + Q_5^* \mathbf{j}_F + Q_6^* \mathbf{k}_F) + M^* g \mathbf{k}_E - G(\phi_F \mathbf{i}_F + \theta_F \mathbf{j}_F + \psi_F \mathbf{k}_F) \end{aligned}$$

where

$$G = -M^* g [\partial \mathbf{k}_E / \partial \phi_F \quad \partial \mathbf{k}_E / \partial \theta_F \quad \partial \mathbf{k}_E / \partial \psi_F]$$

Here M is the aircraft mass, including the rotors, and I is the moment of inertia matrix. These equations are dimensionless, and have been normalized by dividing by the characteristic inertia $(\frac{1}{2} N I_b)_1$. Thus $M^* = M / (\frac{1}{2} N I_b R^2)$ and $I^* = I / (\frac{1}{2} N I_b)$. Note that the gravi-

tational co
 $M^* g = \gamma 2C$
since ortho;

for $k \geq 7$,
frequency o
ing is here r
the hub rea
rotor mass
be included
the rotor g
weight is in
The gene

Normalizin

or $Q = c^T F$
to account
parameters
is necessary

The aircr
zonal tail
body lift, c
deflection;
angle and a
attack and
attack and
divided by
the approp
form from
necessary;
aircraft rigi
experiment;
including th

The aircr
and on the
ocity, the pe
the rotor-in
thus

(u_i)_F

which must
The rate o
interference
calculation,
aerodynami

linear and rotational constant g is also dimensionless, based on the acceleration $\Omega^2 R$; and $g = \gamma^2 C_W / \sigma a$, where $W = Mg$ is the gross weight. For the elastic degrees of freedom, since orthogonal free vibration modes are used the equations of motion are simply

$$M_k^* (\ddot{q}_{s_k} + g_s \omega_k \dot{q}_{s_k} + \omega_k^2 q_{s_k}) = Q_k^*$$

for $k \geq 7$, where M_k is the generalized mass including the rotors, ω_k is the natural frequency of the mode and g_s is the structural damping coefficient. (The structural damping is here represented by a viscous damping term.) The generalized forces Q_k^* are due to the hub reactions of the two rotors, and the aerodynamic forces on the aircraft. Since the rotor mass is included in the aircraft inertia, the hub linear acceleration terms should not be included in the evaluation of the hub forces for these equations of motion. Similarly, the rotor gravitational forces are not included in the rotor hub forces, since the rotor weight is included in the aircraft gross weight.

The generalized force on the aircraft due to the rotor hub reactions is

$$Q_k = \xi_k(\mathbf{r}_{\text{hub}}) \cdot \mathbf{F}_{\text{hub}} + \gamma_k(\mathbf{r}_{\text{hub}}) \cdot \mathbf{M}_{\text{hub}}$$

Normalizing Q_k by dividing by $(\frac{1}{2} N I_b)$ gives then

$$(Q_k^*) = \begin{bmatrix} \vdots \\ (R_{SF} \xi_k)^T (R_{SF} \gamma_k)^T \\ \vdots \end{bmatrix} \frac{\gamma^2}{\sigma a} (C_H C_Y C_T C_{M_x} C_{M_y} - C_Q)^T$$

or $\mathbf{Q} = \mathbf{c}^T \mathbf{F}$, with \mathbf{c} defined above for the hub motion. For rotor No. 2 it is also necessary to account for the differences in normalization, \mathbf{Q} and \mathbf{c} being based on rotor No. 1 parameters while \mathbf{F} is based on rotor No. 2 parameters. For a clockwise rotating rotor it is necessary to change the signs of C_Y , C_{M_x} and C_Q .

The aircraft aerodynamic forces considered are those acting on the wing-body, horizontal tail and vertical tail. Specifically, the aerodynamic forces needed are the wing-body lift, drag and pitch moment as a function of angle of attack and the flaperon deflection; wing-body side force, roll moment and yaw moment as a function of sideslip angle and aileron deflection; the horizontal tail lift and drag as a function of angle of attack and elevator deflection; and the vertical tail lift and drag as a function of angle of attack and rudder deflection. These loads are defined in terms of the force or moment divided by dynamic pressure. The forces are multiplied by the dynamic pressure, and by the appropriate arm for the moments; they are rotated by the angle of attack to transform from wind axes to the body axes; they are rotated by the tail cant angles if necessary; and they are divided by $(\frac{1}{2} N I_b)$. The result is the generalized forces for the aircraft rigid body degrees of freedom, due to the aerodynamic loads. For best results, experimental data should be used to define the aircraft aerodynamic characteristics, including the airframe interference effects.

The aircraft aerodynamic forces depend on the air velocity seen by the components and on the aircraft control positions. The air velocity consists of the trim aircraft velocity, the perturbation linear and angular rigid body contributions, the gust velocity and the rotor-induced aerodynamic interference velocity. In body axes, the total velocity is thus

$$(v_i \mathbf{i}_F + v_j \mathbf{j}_F + w_k \mathbf{k}_F) = R_{FV} ((V + u_G) \mathbf{i}_V + v_G \mathbf{j}_V + w_G \mathbf{k}_V) + \mathbf{u}_F + \omega_F \times \mathbf{r} - \lambda$$

which must be evaluated at the wing-body, at the horizontal tail, and at the vertical tail. The rate of change of angle of attack is also required ($\dot{\alpha} = \dot{z}_F / V$). The aerodynamic interference velocity due to each rotor is required. With a nonuniform induced velocity calculation, λ is the mean value of the velocity calculated at the position of the fixed aerodynamic surface. As a simple model for the aerodynamic interference, the rotor-

induced velocities at the wing-body, horizontal tail, and vertical tail can be obtained as a linear combination of the mean induced velocity at the two rotors:

$$\lambda = K_1 C_1 \lambda_{i1} R_{SF}^T(-k_S) + K_2 C_2 \lambda_{i2} R_{SF}^T(-k_S)$$

assuming that the induced velocity is normal to the disk plane. The K factors account for the maximum fraction of the aerodynamic surface which is affected by the wake, and the fraction of the fully developed wake velocity that is achieved. The C multiplicative factors account for the decrease in the wake induced velocity away from the wake surface, using the expression $C = 1/\max(1, 1 + l)$, where l is the perpendicular distance from the aerodynamic surface to the nearest wake boundary ($l < 0$ if the surface is inside the rotor wake cylinder). C is calculated from the position of the aerodynamic component relative to the rotor, and the velocity of the rotor relative to the air.

From the velocity components at the wing-body, the angle of attack, sideslip angle and dynamic pressure are $\alpha_{WB} = \tan^{-1} w/u$, $\beta_{WB} = \tan^{-1} v/u$, and $q_{WB} = \frac{1}{2}(u^2 + v^2 + w^2)$. The angles of attack of the tail surfaces are calculated in a similar manner. The aircraft aerodynamic interference at the tail is accounted for by an angle of attack change ϵ and a sideslip angle σ , which are evaluated using procedures developed for fixed wing aircraft [3]. The time-varying nonuniform inflow will increase the mean dynamic pressure in the wake:

$$q = \frac{1}{2}(u^2 + v^2 + w^2) + \frac{1}{2}\sigma^2$$

where σ^2 is the mean-square wake velocity perturbation, at the wing-body or tail as appropriate.

The only generalized aerodynamic forces considered for the airframe elastic modes are the direct damping and control forces. In dimensional form, these forces are

$$(Q_k)_{aero} = \frac{1}{2}\rho V^2 [-F_{q_k \dot{q}_k} \dot{q}_{sk}/V + F_{q_k \delta} (\delta_f \delta_e \delta_a \delta_r)^T].$$

1.3 Transmission and Engine Analysis

An elementary model is used that accounts for the coupling of the two rotors through the flexible drive-train, and for the engine damping and inertia. The drive train dynamics are described by the rotor speed, the interconnect shaft torsion, and the engine shaft torsion degrees of freedom. The equations of motion are derived from the balance of rotor and engine torques. A model for a governor with throttle or collective feedback of the rotor speed error is also considered. The engine model includes the inertia, damping and control torques:

$$I_E \dot{\Omega}_E = Q_E - Q_{\Omega} \Omega_E + Q_t \theta_t$$

The engine speed is Ω_E and Q_E is the torque on the engine. The engine rotary inertia is I_E . The engine speed damping coefficient Q_{Ω} is the torque per unit speed change at constant throttle setting. The variable θ_t is the engine throttle control position. Q_t is the torque applied due to a throttle change at constant speed.

In the model considered for asymmetric drive train configurations, such as for a single main and tail rotor helicopter, the two rotors are connected by a shaft and the engine is geared to one rotor. The torsional flexibility of the drive train is represented by shaft springs for each rotor, an interconnect shaft spring and an engine shaft spring. The transmission gear ratios are r_E (the ratio of the engine speed to the speed of the first rotor), and r_{I1} and r_{I2} (the ratio of the interconnect shaft speed to the rotor speeds). Thus $r_{I1}/r_{I2} = \Omega_2/\Omega_1$ is the ratio of the trim rotational speeds of the two rotors. The degrees of freedom are rotational speed perturbations of the two rotors (ψ_{s1} and ψ_{s2}) and the engine speed perturbation ψ_e . The engine shaft azimuth perturbation is defined relative to the rotation of the first rotor, so the total engine speed perturbation with respect to space is $r_E(\psi_{s1} + \psi_e)$. With the rotation of the two rotors coupled by the drive system, it is more appropriate to use the following degrees of freedom: $\psi_s = \psi_{s1}$ and $\psi_l = \psi_{s2} - (r_{I1}/r_{I2})\psi_{s1}$. Here ψ_l is the differential azimuth perturbation between the two rotors. The

degrees of freedom are ψ_s , ψ_l and ψ_e . The differential azimuth perturbation ψ_l is a control, and the engine speed perturbation ψ_e is a forcing function of the linearized equations of the rotor. The governor is modeled with a second-order transfer function

where $\Delta\theta$ is the differential azimuth perturbation between the two rotors.

It is now necessary to determine the steady state performance and transient response of the trim without blade unacceleration. Usually it is necessary to determine the steady state solution for the trim state variables of the rotor and engine forces and state. Unfortunately, the velocity perturbation angles, zero (and the y) and aircraft remaining solution. The procedure of the periodic motion in the presence of a steady motion is a solution for the steady state with simultaneous match the

The trim without blade unacceleration. Usually it is necessary to determine the steady state solution for the trim state variables of the rotor and engine forces and state. Unfortunately, the velocity perturbation angles, zero (and the y) and aircraft remaining solution. The procedure of the periodic motion in the presence of a steady motion is a solution for the steady state with simultaneous match the

The trim without blade unacceleration. Usually it is necessary to determine the steady state solution for the trim state variables of the rotor and engine forces and state. Unfortunately, the velocity perturbation angles, zero (and the y) and aircraft remaining solution. The procedure of the periodic motion in the presence of a steady motion is a solution for the steady state with simultaneous match the

The trim without blade unacceleration. Usually it is necessary to determine the steady state solution for the trim state variables of the rotor and engine forces and state. Unfortunately, the velocity perturbation angles, zero (and the y) and aircraft remaining solution. The procedure of the periodic motion in the presence of a steady motion is a solution for the steady state with simultaneous match the

The trim without blade unacceleration. Usually it is necessary to determine the steady state solution for the trim state variables of the rotor and engine forces and state. Unfortunately, the velocity perturbation angles, zero (and the y) and aircraft remaining solution. The procedure of the periodic motion in the presence of a steady motion is a solution for the steady state with simultaneous match the

The trim without blade unacceleration. Usually it is necessary to determine the steady state solution for the trim state variables of the rotor and engine forces and state. Unfortunately, the velocity perturbation angles, zero (and the y) and aircraft remaining solution. The procedure of the periodic motion in the presence of a steady motion is a solution for the steady state with simultaneous match the

The trim without blade unacceleration. Usually it is necessary to determine the steady state solution for the trim state variables of the rotor and engine forces and state. Unfortunately, the velocity perturbation angles, zero (and the y) and aircraft remaining solution. The procedure of the periodic motion in the presence of a steady motion is a solution for the steady state with simultaneous match the

degrees of freedom ψ_1 and ψ_e therefore involve elastic torsion in the drive train. The degree of freedom ψ_s is the rotational speed perturbation of the drive system as a whole. The differential equations of motion for the rotor speed dynamics are obtained from equilibrium of the torques on the two rotors and the engine. The resulting equations for ψ_s , ψ_1 and ψ_e have linear terms due to the engine inertia and damping, the throttle control, and various shaft springs; and the shaft torques of the two rotors appear as forcing functions. These equations are applicable (with different values for the coefficients of the linear terms) to an asymmetric drive train configuration with the engine by either rotor, to a symmetric configuration with two engines, and to the case of a single rotor. The governor model considered is integral and proportional feedback of the rotor speed, with a second order lag to represent the governor dynamics:

$$\tau_2 \Delta \ddot{\theta} + \tau_1 \Delta \dot{\theta} + \Delta \theta = K_p \dot{\psi}_s + K_I \psi_s$$

where $\Delta \theta$ is the throttle perturbation, or the collective pitch perturbation of either or both rotors. The collective pitch perturbation is used in p_r (see Ref. [2] section 2.2).

2. SOLUTION FOR THE ROTORCRAFT MOTION

It is now necessary to develop the solution procedures for the problem defined above. The first task is the trim analysis, in which the equations are solved for the case of a steady state flight condition. After the blade motion solution has been obtained, the rotor performance, loads and noise can be evaluated. The aeroelastic stability, flight dynamics and transient analyses begin from the trim solution.

The trim solution is the steady state condition achieved by the system as time increases without bound with the controls fixed and no external input. Steady state means either unaccelerated flight, including climbs and descents as well as level flight, or a steady turn. Usually it is the inverse problem that is to be solved: determining the control settings necessary to achieve a specified flight condition. The system considered here has nonrotating and rotating components, the latter consisting of N identical, equally spaced blades attached to a central hub. The equations of motion for such a system are not in general time invariant, but rather have periodic coefficients. It follows that the steady state solution will also be periodic. The trim problem is concerned with the average values of the periodic state variables. Unaccelerated motion implies that the net force and moment on the entire aircraft are zero. Setting to zero the six components of the forces and moments provides algebraic equations that must be satisfied in the trimmed state. Unaccelerated flight also implies that the aircraft linear velocity is constant and that the angular velocity is zero (except for the Euler yaw rate in a steady turn). The velocity vector can be specified by its magnitude, and the pitch and yaw flight path angles. Zero angular velocity implies that the pitch and roll Euler angles are constant (and the yaw angle also, except in a turn). Some of the flight path angles, Euler angles, and aircraft controls may be specified by the definition of the trim flight state. The remaining angles and controls constitute the set of trim variables to be determined in the solution. These variables are adjusted so that the relevant trim criteria are satisfied. The procedure is readily generalized to other cases, such as trim in a wind tunnel or specification of the power. The trim problem therefore naturally separates into two parts: the periodic rotor motion and airframe vibration, described by differential equations; and the steady state flight criteria, described by algebraic equations. The trim procedure used in the present analysis consists of an inner loop in which the solution for the periodic motion is obtained with fixed values of the trim variables; and an outer loop in which the solution for the trim variables is obtained. The two parts of the problem could be dealt with simultaneously, but by treating them separately it is possible to use procedures that match the individual characteristics of the two parts.

The rotor and airframe equations are solved for the periodic motion by a harmonic analysis method, which directly calculates the harmonics of a Fourier series representation of the motion. Basically the procedure advances the rotor around the azimuth, calculating the forcing functions in the time domain and then updating the harmonics of

quasistatic airframe motion is not applicable. The solution for general transient motions would require a direct time integration solution procedure for the rotor motion, in place of the harmonic analysis method used in the present analysis.

While the details of the solution procedure remain to be defined, an overview can be given at this point. The job begins with data input and initial calculations. Next the trim solution is obtained. Then the aeroelastic stability analysis, flight dynamics analysis, or transient analysis is performed as required. In the trim analysis the aircraft controls and orientation are incremented until the equilibrium of forces and moments required for the specified operating state is achieved. Since the nonuniform inflow influence coefficients depend on the rotor thrust (through the wake geometry) it is necessary to iterate between the influence coefficient calculation and the trimmed motion and forces calculation (unless the rotor thrust is specified as part of the definition of the trim operating state). The trim analysis is performed first for uniform inflow, then the nonuniform inflow with a prescribed wake, and finally for nonuniform inflow with a free wake geometry (the analysis can stop at any of these three stages). After obtaining the trim solution, the aircraft performance and loads can be calculated. In the transient analysis, the rigid body equations of motion are numerically integrated for a prescribed gust or control input. In the flight dynamics analysis, the stability derivatives are calculated and the matrices are constructed that describe the linear differential equations of motion. For each motion or control increment in the stability derivative calculation there is an iteration between the influence coefficient calculation and the calculation of the rotor motion and forces. Finally the system of linear differential equations is analyzed (optionally including a numerical integration as for the transient analysis). In the flutter analysis the matrices are constructed that describe the linear differential equations of motion, and the constant coefficient or periodic coefficient equations are analyzed. Optionally the equations are reduced to just the aircraft rigid body degrees of freedom by assuming quasistatic response of the other degrees of freedom, and the equations are analyzed as for the flight dynamics task.

The periodic rotor motion and airframe vibration are calculated for an operating state defined by the control positions; the aircraft velocity, orientation and flight path; the linear and angular hub motion due to quasistatic aircraft rigid body motions; and any gust velocity components. The solution procedure begins with the calculation of the blade bending and torsion modes. If nonuniform inflow is to be used, the rotor wake influence coefficients are calculated, which also requires a calculation of the prescribed or free wake geometry. The outermost loop in the solution procedure is an iteration on the rotor induced velocity and bound circulation. An iteration begins with an evaluation of the uniform or nonuniform induced velocity from the rotor thrust or bound circulation. The next loop is an iteration on the motion calculation, for a fixed induced velocity distribution. The motion calculation procedure consists of a number of cycles of successive evaluation of the rotor and airframe motion. First the hub motion harmonics are evaluated. Next there is an azimuth loop for the rotor. At each azimuth step the rotor blade motion harmonics and the aerodynamic hub reactions are updated. After the rotor motion has been updated over a number of steps (typically one rotor revolution), the total hub reactions are evaluated, and the aircraft equations are solved to update the harmonics of the body motion. Within the azimuth loop of the motion calculation there are the following steps. At a given azimuth the hub motion and blade motion are evaluated from the current estimate of the harmonics. At each radial station the blade section pitch, velocity, angle of attack and Mach number are evaluated; the lift, drag and moment coefficients are evaluated; and the section aerodynamic forces are evaluated. The generalized aerodynamic forces of the blade modes are calculated by integrating the section forces over the blade span, and then the rotor equations are solved to update the blade motion harmonics. After each iteration of the motion calculation, the convergence is tested by comparing the blade and airframe motion harmonics with the values at the beginning of the iteration. After the converged motion is obtained, the circulation convergence is determined by comparing the rotor thrust or bound circulation used to

calculate the induced velocity with the values resulting at the end of the iteration. When the solution has converged, it is possible to evaluate the generalized forces due to the mean hub reactions of the rotors; the body aerodynamic generalized forces; as well as various performance parameters of the rotor and aircraft.

2.1. Rotor motion and airframe vibration

The equations of motion are solved by a harmonic analysis method. For the case of steady state flight, all the rotor blades execute the same periodic motion. It follows that the blade motion in the rotating frame can be written as a Fourier series:

$$q_k = \sum_{n=-\infty}^{\infty} \beta_n^{(k)} e^{in\psi_m}$$

$$p_k = \sum_{n=-\infty}^{\infty} \theta_n^{(k)} e^{in\psi_m}$$

where $\psi_m = \psi + m\Delta\psi$ is the azimuth angle of the m -th blade ($\Delta\psi = 2\pi/N$, $m = 1$ to N) and $\psi = \Omega t$ is the dimensionless time variable. The complex representation is most convenient for solving the equations of motion. The corresponding cosine and sine harmonics are obtained from $\beta_n = (\beta_{nc} - i\beta_{ns})/2$ for $n \geq 1$. The degrees of freedom in the nonrotating frame are the aircraft rigid body and elastic motion, and the rotor speed perturbations. These degrees of freedom are excited by the net rotor hub reactions, obtained by summing the root forces and moments from all N blades. Ideally, the rotor hub acts as a filter, transmitting to the nonrotating frame only those harmonics at multiples of N/rev . The vibratory motion in the nonrotating frame is then also periodic, with fundamental frequency $N\Omega$, and can be written as a Fourier series:

$$q_{sk} = \sum_{p=-\infty}^{\infty} \phi_{pN}^{(k)} e^{ipN\psi}$$

for the body motion, and similarly for the drive train degrees of freedom.

The rotor gimbal motion (if present) is in the nonrotating frame, but it is most convenient to solve an equation in the rotating frame for the gimbal motion, along with the other rotor blade equations. Dividing by $(\frac{1}{2}NI_b)$ and substituting for the hub moments, the gimbal equations of motion are

$$-\frac{1}{N} \sum_{m=1}^N 2 \cos \psi_m \frac{\gamma}{\sigma a} C_{m_x} + C_{GC}^* \dot{\beta}_{GC} + I_0^*(v_{GC}^2 - 1)\beta_{GC} = 0$$

$$-\frac{1}{N} \sum_{m=1}^N 2 \sin \psi_m \frac{\gamma}{\sigma a} C_{m_x} + C_{GS}^* \dot{\beta}_{GS} + I_0^*(v_{GS}^2 - 1)\beta_{GS} = 0$$

where C_{m_x} is the flap moment at the blade root. All harmonics of the longitudinal and lateral hub moments cancel within the hub, except those at multiples of N/rev . Similarly, the equation for the teeter motion of a two-bladed rotor is

$$-\frac{1}{2} \sum_{m=1}^2 (-1)^m \frac{\gamma}{\sigma a} C_{m_x} + C_T^* \dot{\beta}_T + I_0^*(v_T^2 - 1)\beta_T = 0.$$

All the even harmonics of the root flap moments cancel within the rotor hub. It can be shown [3] that the gimbal or teeter motion can be obtained by solving the following equation in the rotating frame:

$$-\frac{\gamma}{\sigma a} C_{m_x} + C_G^* \dot{\beta}_G + I_0^*(v_G^2 - 1)\beta_G = 0$$

for just the $pN \pm 1$ harmonics of the rigid flap motion β_G (except for the effects of unsymmetric gimbal springs or dampers, and the fact that the damping is in the

nonrotat

or the har

In the l
blade rigi
written as
 $p_0 = p_r +$
harmonic
equations
duces terr
A harn
solving d.

where β is
matrices,
are time-in
the natura
this equat

Where C
used shou
structural,
not have t
actual dar
so the vis
evaluated
and $\Delta\psi =$

where

With $K_n =$
While it m
error if the
gives a poc
In particul
above valu
number of
By truncati
corners of
the numbe
interest. Th
from the h
to multiply
in the forci

nonrotating frame). Then the harmonics of the gimbal motion are

$$\begin{aligned}(\beta_{GC})_{pN} &= (\beta_G)_{pN-1} + (\beta_G)_{pN+1} \\ (\beta_{GS})_{pN} &= -i(\beta_G)_{pN-1} + i(\beta_G)_{pN+1}\end{aligned}$$

or the harmonics of the teetering motion are $(\beta_T)_n = (\beta_G)_n$, for n odd.

In the limit of infinite control stiffness, the solution of the equation of motion for the blade rigid pitch degree of freedom reduces to $p_0 = p_r$. The total root pitch motion p_0 is written as the sum of p_r and the motion due to elastic distortion of the control system: $p_0 = p_r + p_d$. Substituting for p_0 , the rotor equations of motion will be solved for the harmonics of p_d . The case of infinite control system stiffness then requires only that the equations for p_d be dropped from the solution procedure. Writing $p_0 = p_r + p_d$ introduces terms due to p_r , \dot{p}_r , and \ddot{p}_r in the equations of motion.

A harmonic analysis method is used to integrate the differential equations of motion, solving directly for the harmonics of the motion. Consider equations of the form

$$M\ddot{\beta} + K\beta = g(\dot{\beta}, \beta, \psi)$$

where β is the degree of freedom vector, K and M are the appropriate stiffness and mass matrices, and g is the forcing function (usually nonlinear). It is assumed that K and M are time-invariant. To avoid the singularity of the resonant response at harmonics near the natural frequency, it is necessary to include the damping terms of the left-hand-side of this equation. Thus the term $C\dot{\beta}$ is added to both sides, giving

$$M\ddot{\beta} + C\dot{\beta} + K\beta = g + C\dot{\beta} = F$$

Where C is a constant damping matrix. For good convergence the damping coefficient used should be close to the actual damping of the particular degree of freedom, including structural, mechanical, and aerodynamic damping sources. The damping estimate does not have to be exact however, since it is added to both sides of the equation. In fact the actual damping in the forcing function g will often be time varying and even nonlinear, so the viscous damping coefficient has to be an approximation. Now the function F is evaluated at J points around the rotor azimuth: $F_j = F(\psi_j)$, where $\psi_j = j\Delta\psi$ ($j = 1$ to J and $\Delta\psi = 2\pi/J$). Then the harmonics of a complex Fourier series representation of F are

$$F_n = \frac{1}{J} \sum_{j=1}^J F_j e^{-in\psi_j} K_n$$

where

$$K_n = \left(\frac{J}{\pi n} \sin \frac{\pi n}{J} \right)^2.$$

With $K_n = 1$ these harmonics would give a Fourier interpolation representation of $F(\psi)$. While it matches the function exactly at the known points $F(\psi_j)$ (or with least squared-error if the number of harmonics used is less than $(J-1)/2$), the Fourier interpolation gives a poor representation elsewhere, with large excursions due to the higher harmonics. In particular, poor estimates of the derivatives of the function F are obtained. With the above values for K_n (which reduce the magnitude of the higher harmonics) and an infinite number of harmonics, a linear interpolation between the known points $F(\psi_j)$ is obtained. By truncating the Fourier series ($n = -L$ to L) the representation of F is smoothed, the corners of the linear interpolation being rounded off. Usually $L = J/3$ is satisfactory, so the number of azimuth stations should be about three times the maximum harmonic of interest. Then the solution of the equation of motion for the harmonics of β is obtained from the harmonics of F by $\beta_n = H_n^{-1} F_n$, where $H_n = K - Mn^2 + Cin$. (It is necessary to multiply C by K_n when evaluating H_n , to be consistent with the Fourier analysis of C in the forcing function F .) The iterative solution, required because the nonlinear forcing

function F depends on β and $\dot{\beta}$, proceeds as follows. At a given azimuth ψ_j , the blade motion is calculated using the current estimates of the harmonics. The forcing function F_j is evaluated next. The estimates of the motion harmonics are then updated to account for the difference between the current value of F_j and that found in the last revolution:

$$\Delta\beta_n = H_n^{-1} [F_j - (F_j)_{\text{last rev}}] \frac{1}{J} K_n e^{-in\psi_j}.$$

After adding $\Delta\beta_n$ to the harmonics β_n , the azimuth angle is incremented to ψ_{j+1} . This procedure thus provides an update to the motion at ψ_{j+1} from the revised calculation of the forcing function at ψ_j , based on the assumption that the solution is periodic:

$$\Delta\beta_{j+1} = \sum_n \Delta\beta_n e^{in(\psi_j + \Delta\psi)} = \left[\frac{1}{J} \sum_n H_n^{-1} K_n e^{in\Delta\psi} \right] \Delta F_j.$$

The calculation proceeds around the azimuth in this fashion until the solution converges. The test for convergence is performed typically once each revolution. Requiring that the root-mean-squared change in the blade motion from one revolution to the next be below a specified tolerance, the criterion is $(\Delta\beta)_{rms} < \epsilon$ for all degrees of freedom, where here $\Delta\beta$ is the difference between the motion at the current and the previous revolutions.

To begin the solution at a new azimuth station, the deflection, velocity, and acceleration of each degree of freedom are evaluated from the harmonics. So for the rotor blade bending, q_k , \dot{q}_k and \ddot{q}_k are evaluated at ψ from the harmonics $\beta_n^{(k)}$; the pitch/torsion and gimbal/teeter motion are also evaluated as required. For the second rotor these time derivatives are based on Ω_2 . The rigid body and elastic airframe motion of the aircraft is evaluated from the harmonics $\phi_n^{(k)}$ (for n a multiple of N). In addition, the steady state or slowly varying rigid body motion contributes static velocity terms $(\dot{q}_{s_k})_{\text{static}}$ for $k \leq 6$; and the static elastic airframe gives $(q_{s_k})_{\text{static}}$ for $k \geq 7$. The rotor hub motion is then

$$\alpha = (x_h \ y_h \ z_h \ \alpha_x \ \alpha_y \ \alpha_z)^T = c(q_{s_k}) = c \mathbf{x}_s$$

where c is defined in section 1.2. Recall that in the evaluation of α_x , α_y and α_z (for the aerodynamic analysis) the contributions of the rigid body Euler angles are not included; also, the linear hub displacements are not used in the rotor analysis. Hence α is evaluated due to the elastic airframe modes only ($k \geq 7$). The corresponding velocity and acceleration of the hub are $\dot{\alpha} = c\dot{\mathbf{x}}_s$ and $\ddot{\alpha} = c\ddot{\mathbf{x}}_s + \dot{c}\dot{\mathbf{x}}_s$. For the second rotor, $\dot{\alpha}$ and $\ddot{\alpha}$ are multiplied by Ω_1/Ω_2 and $(\Omega_1/\Omega_2)^2$ respectively. Also for the second rotor, the aircraft motion harmonics are at $n = pN\Omega_2/\Omega_1$ (relative to the time scale of the nonrotating frame, which is based on Ω_1). The net result is that by evaluating the hub motion as a sum of harmonics at $n = pN$, with the azimuth angle of the second rotor, the time scale will be automatically accounted for [3], except that a factor of Ω_1/Ω_2 is still required in the second term of $\ddot{\alpha}$, to account for the scaling of the aircraft velocity in \dot{c} . The acceleration due to gravity is also included in $\ddot{\alpha}$, as an equivalent linear acceleration (with a factor $(\Omega^2 R)_1/(\Omega^2 R)_2$ for the second rotor). Hence the harmonics of the rotor hub motion are obtained from the harmonics of the aircraft degrees of freedom by the following expressions:

$$\begin{aligned} \alpha_n &= c(\phi_n^{(k)}) \\ \dot{\alpha}_n &= inc(\phi_n^{(k)}) \\ \ddot{\alpha}_n &= -n^2.c(\phi_n^{(k)}) + in\dot{c}(\phi_n^{(k)}) \end{aligned}$$

for n a nonzero multiple of N ; and the static components are

$$\begin{aligned} \alpha_{\text{static}} &= c(q_{s_k})_{\text{static}} \\ \dot{\alpha}_{\text{static}} &= \dot{c}(\dot{q}_{s_k})_{\text{static}} \\ \ddot{\alpha}_{\text{static}} &= \ddot{c}(\dot{q}_{s_k})_{\text{static}} + \begin{pmatrix} -gR_{SF}k_E \\ 0 \end{pmatrix} \end{aligned}$$

Factors a and it ma two rotor The harm bending, degrees c The dii ing form

where $\theta_n^{(d)}$ nics for g and dam namic de deflection. F is evalu aerodyna cluded in due to th each azin harmonic The gei

The rotor blades, as to the bla terms. Th frequenc terms by aerodyna evaluate t The diff ing form l the two r

with H_{ne} a

The hub r solved. Th

for n a nor separately. rotor, so $n = (\Omega_2/\Omega$

Factors accounting for the normalization of the second rotor are included as required; and it may also be necessary to account for an azimuthal phase difference between the two rotors. The harmonics of the drive train motion are obtained by a similar procedure. The harmonics of the blade pitch increments due to the governor and the rotor mast bending, required for p_r , are obtained from the harmonics of the drive train and airframe degrees of freedom respectively.

The differential equations of motion for the rotor degrees of freedom take the following form for the n -th harmonic

$$H_n(\beta_n^{(1)} \dots \beta_n^{(i)} \theta_n^{(d)} \theta_n^{(1)} \dots \theta_n^{(i)} \beta_{G_n})^T = F_n$$

where $\theta_n^{(d)}$ is the n -th harmonic of p_d and β_{G_n} is only present for the $n = pN \pm 1$ harmonics for gimbaled or teetering rotors. The matrix H_n is calculated from the mass, spring, and damping matrices discussed in Ref. [2] section 2.2, plus an estimate of the aerodynamic damping and spring forces (some terms in H_n depend on the mean bending deflection therefore, and must be updated as the solution proceeds). The forcing function F is evaluated in the time domain. It consists (as discussed in Ref. [2] section 2.2) of the aerodynamic forces (minus the corresponding estimate of the aerodynamic forces included in H_n); the inertial forces due to the hub, drive train, and control motion (p_r terms, due to the use of p_d as a degree of freedom); and the nonlinear lag damper moment. At each azimuth step ψ_j , the forcing function F_j is evaluated, and then the blade motion harmonics are updated as described above.

The generalized aircraft forces due to the rotor hub reactions are $Q = c^T F$, where here

$$F^T = \frac{\gamma^2}{\sigma a} (C_H C_Y C_T C_{M_x} C_{M_y} - C_Q).$$

The rotor hub reactions are obtained by summing the blade root reactions over all the blades, as discussed in Ref. [2] section 2.2. The root reactions contain inertial terms due to the blade bending and gimbal motion and the shaft angular motion; and aerodynamic terms. The operation of summing over all N blades is equivalent to filtering out all frequencies except multiples of N/rev . This may be accomplished directly in the inertial terms by only using the appropriate harmonics of the rotor degrees of freedom. For the aerodynamic terms, an equivalent approach is to omit the summation operator and only evaluate those harmonics at multiples of N/rev .

The differential equations of motion for the aircraft degrees of freedom take the following form for the n -th harmonic: $H_n(\phi_n^{(k)}) = Q_n$, where here the forcing function is due to the two rotors ($Q = c^T F$) and the transfer function matrix (from section 1.2) is

$$H_n = \begin{bmatrix} -R_c^T I^* R_e n^2 & 0 & 0 \\ -M^*(V \times) R_e i n + G & -M^* n^2 & 0 \\ 0 & 0 & H_{ne} \end{bmatrix}$$

with H_{ne} a diagonal matrix for the aircraft elastic motion:

$$H_{ne} = \left[-M_k^* n^2 + \left(M_k^* g_s \omega_k + \frac{\gamma V}{\sigma a A} F_{q_k \dot{q}_k} \right) i n + M_k^* \omega_k^2 \right].$$

The hub reactions are evaluated at azimuth stations ψ_j as the rotor equations are being solved. Then the airframe vibratory motion is obtained from

$$(\phi_n^{(k)}) = H_n^{-1} c^T F_n = H_n^{-1} c^T \sum_{j=1}^J F_j \frac{1}{J} K_n e^{-i n \psi_j}$$

for n a nonzero multiple of N . The aircraft response to each of the two rotors is evaluated separately. The time scale of the aircraft equations is the rotational speed of the first rotor, so the harmonics of the motion due to the second rotor are at multiples of $n = (\Omega_2/\Omega_1)N_2$. It may be necessary to account for an azimuthal phase difference

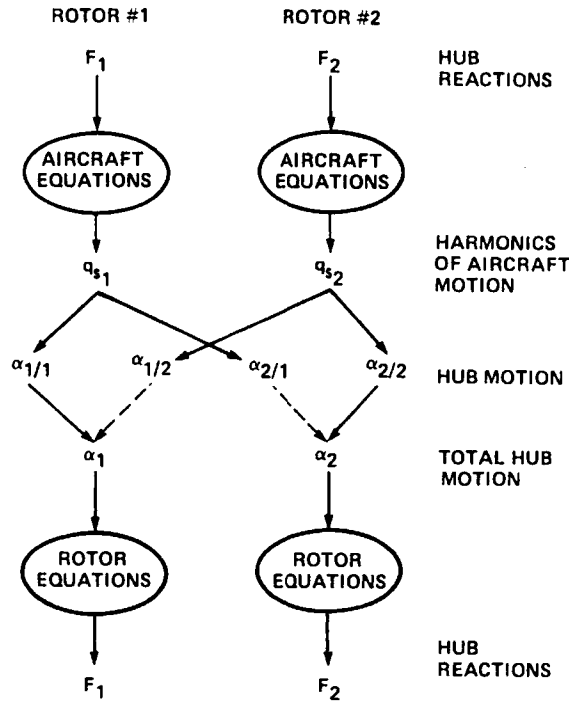


Fig. 1. Outline of dynamic interaction of the two rotors.

between the two rotors. Similarly the equations of motion for the drive train are solved for the harmonics of the rotor and engine speed perturbations and the governor degrees of freedom, as excited by the rotor torques. The corresponding equations for $n = 0$ are solved for the static elastic airframe and drive train deflection due to the mean rotor hub reactions.

In the present model, the two rotors of a helicopter can influence each other through excitation of vibratory airframe motion (Fig. 1). The hub reactions are calculated for each of the two rotors. From these hub reactions, the aircraft equations of motion are solved for the harmonics of the airframe rigid body and elastic motion. Then the hub motion can be evaluated at each rotor, due to the forces of each rotor. The motion at each hub due to the two rotors is summed. Then the rotor equations are solved for the rotor motion and for the hub reactions again. It is useful to be able to suppress the feedback of the nonrotating frame vibration to either or both rotors. The cross coupling can be suppressed by omitting the summation of the two hub motion components at one or both hubs (the dotted line in Fig. 1). The entire vibratory hub motion can be decoupled from the rotor by setting it to zero at one or both hubs (the static or low frequency hub motion and the acceleration due to gravity should be retained however). Decoupling the vibratory hub motion is equivalent to dropping the aircraft degrees of freedom as far as the rotor analysis is concerned, but it still may be useful to evaluate the aircraft vibration due to the hub reactions. The solution procedure described here is based on the assumption that the entire system is periodic, which in fact is true only if both rotors have the same rotational speed. When the two rotors do not turn at the same speed, the motion in the nonrotating frame is not periodic even in steady flight. In order to analyze a periodic system still, it is necessary to neglect the mutual interference of the two rotors. The analysis proceeds as described above, except that the hub motion of one rotor due to the vibratory airframe motion produced by the other rotor is always suppressed. Effectively the helicopter is then being analyzed as two single rotor systems, except for the coupling through the aircraft steady state motion.

The blade motion is calculated for a given induced velocity distribution over the rotor disk. When the converged solution for the motion is obtained, the rotor loading (thrust or bound circulation) is re-evaluated. Then the induced velocity estimate can be updated, and the motion solution repeated. The procedure continues until the root-mean-squared

change in
tolerance le

where Γ_j is
When unif

To improv
calculate λ_i

where $C_{T_{old}}$
calculated
thrust lift c

(see section
ior. Similar
circulation
tion occurs
 $C = 0$. In
 $C_T = -\delta$, v
iteration at
be approach
procedure fo
iteration (th
possible to
achieve C_T

2.2 Rotor pe

Once the
performance
include the
blade radial
rotor hub r
oscillatory r
From the ro
using one of

The rotor
the thrust, p
tip-path pla
to the type c
performance
ideal power

The rotor
inertial forc
integrating t
(really Galer
and it is effi
the blade se

change in the bound circulation from one iteration to the next is less than a specified tolerance level:

$$\frac{1}{J} \sum_{j=1}^J (\Delta \Gamma_j)^2 < (\epsilon 2\pi\sigma/N)^2$$

where Γ_j is the maximum bound circulation and the summation is over the azimuth. When uniform inflow is used, the criterion is

$$(\Delta C_T)^2 + 8(\Delta C_{M_y}^2 + \Delta C_{M_z}^2) < (\epsilon\sigma)^2.$$

To improve the convergence, a lag is introduced in the thrust coefficient used to calculate λ_i :

$$C_T = fC_{T_{\text{new}}} + (1 - f)C_{T_{\text{old}}}$$

where $C_{T_{\text{old}}}$ is the thrust used to calculate λ_i in the last iteration, and $C_{T_{\text{new}}}$ is the thrust calculated using the value of λ_i . Ideally, the factor f should have a value equal to the thrust lift deficiency function [3]

$$C = \left(1 + \frac{\sigma a}{4} \frac{\partial \lambda}{\partial T}\right)^{-1}$$

(see section 3.1), but an even smaller value may be necessary for good numerical behavior. Similarly, for a nonuniform inflow calculation a lag is introduced in the blade bound circulation used to evaluate the induced velocity. A difficulty with the circulation iteration occurs for a hovering rotor at zero blade pitch, for which the lift deficiency function $C = 0$. In this case, the solution converges to an oscillation between $C_T = \delta$ and $C_T = -\delta$, where δ approaches zero as f approaches zero. For $f = 0$ there would be no iteration at all however. Hence the solution $C_T = 0$ cannot be reached exactly, but can be approached as closely as desired, at the cost of many iterations (for small f). A better procedure for this case is to choose f so that the exact solution is achieved on the second iteration (the required value of f depends on the initial conditions). It would even be possible to use f rather than collective pitch as the variable in the trim iteration to achieve $C_T = 0$.

2.2 Rotor performance, loads and noise

Once the solution for the periodic motion of the helicopter has been obtained, the performance, loads and noise of the rotor can be evaluated. The rotor loads of interest include the tension and shear forces, bending moments and torsion moment at various blade radial stations; the control loads; the blade root forces and moments; and the net rotor hub reactions. The rotor-induced vibration can be evaluated from the airframe oscillatory motion, in terms of the inertial acceleration at various points in the aircraft. From the rotor aerodynamic loading and thickness the rotational noise can be calculated using one of the existing rotor acoustic theories.

The rotor performance is described primarily by the mean hub reactions, particularly the thrust, propulsive force, and torque. The hub reactions can be evaluated in shaft axes, tip-path plane axes and wind axes. It is conventional to split the rotor power according to the type of energy loss: induced, interference, profile, parasite, or climb power. Various performance indices of the rotor can be evaluated, including the figure of merit (ratio of ideal power loss to actual power) and rotor lift-to-drag ratio.

The rotor loads at radial station r are calculated by integrating the aerodynamic and inertial forces acting on the blade outboard of r . The root loads are calculated by integrating the forces over the entire blade. This approach is consistent with the modal (really Galerkin) derivation of the blade equations of motion used in the present analysis; and it is efficient, requiring few blade modes. The total tension and shear forces acting on the blade section at r , in coefficient form, are

$$\mathbf{F}_{\text{shear}} = \frac{\mathbf{F}}{I_b \Omega^2 / R} = \frac{\gamma}{\sigma a} (C_{f_s} \mathbf{i}_B + C_{f_r} \mathbf{j}_B + C_{f_t} \mathbf{k}_B).$$

The bending moment acting on the blade section at r is

$$\mathbf{M}_{\text{bend}} = \frac{\mathbf{M}}{I_b \Omega^2} = \frac{\gamma}{\sigma a} (C_{m_x} \mathbf{i}_B - C_{m_z} \mathbf{k}_B)$$

These section loads are obtained in the blade principal axes by a coordinate rotation. The forces and moment at the blade root (\mathbf{F}_{root} and \mathbf{M}_{root}) are defined in a similar fashion. The torsion moment on the blade section at r is $M_{\text{tors}} = M_r / (I_b \Omega^2) = (\gamma / \sigma a) C_{m_r}$. The control load is obtained from the moment about the pitch axis at the blade root: $M_{\text{con}} = M_{FA} / (I_b \Omega^2) = (\gamma / \sigma a) C_{m_c}$. The definition of the force and moment coefficients is

$$\frac{C_f}{\sigma} = \frac{F}{\rho(\Omega R)^2 R c_m} = \frac{F}{\rho(\Omega R)^2 A \sigma / N}$$

$$\frac{C_m}{\sigma} = \frac{M}{\rho(\Omega R)^2 R^2 c_m} = \frac{M}{\rho(\Omega R)^2 R A \sigma / N}$$

where c_m is the blade mean chord, $\sigma = N c_m / \pi R$ the rotor solidity, and A the rotor disk area. All of these loads have aerodynamic and inertial terms, for example

$$\mathbf{F}_{\text{shear}} = (\gamma / a c) \mathbf{F}_A - \mathbf{F}_I / I_b$$

where

$$F_I = \int_r^1 a m d\rho$$

$$F_A = \int_r^1 (F_x \mathbf{i}_B + \tilde{\mathbf{F}}_r \mathbf{j}_B + F_z \mathbf{k}_B) d\rho.$$

Similarly the section bending and torsion moments are obtained from \mathbf{M}_2 and M_r , as defined in Ref. [2] section 2.2. The pitch axis moment M_{FA} and the root reactions are also defined in Ref. [2] section 2.2. The inertia terms are evaluated by a procedure similar to that used for the equations of motion: the expression for the acceleration in terms of the degrees of freedom is substituted, and the integrals of the inertial properties over the span are evaluated. Hence the inertial terms are expressed as linear functions of the rotor degrees of freedom and shaft motion, with some of the coefficients depending on the mean bending deflections (as for the equations of motion). The aerodynamic terms are evaluated by integrating the section aerodynamic forces over the blade span. The total force and moment acting on the rotor hub are obtained from the root forces and moments by resolving the rotating reactions into the nonrotating frame and summing over all N blades, as described in Ref. [2] section 2.2. Here it is not just the mean hub reactions that are required, but the vibratory components as well.

2.3 Steady state or slowly varying aircraft motion

The equations of motion for the aircraft rigid body degrees of freedom are

$$J^*(\ddot{\phi}_F \mathbf{i}_F + \ddot{\theta}_F \mathbf{j}_F + \ddot{\psi}_F \mathbf{k}_F) = \mathbf{Q}_{\text{moment}}$$

$$M^*(\ddot{x}_F \mathbf{i}_F + \ddot{y}_F \mathbf{j}_F + \ddot{z}_F \mathbf{k}_F) - M^*(\mathbf{V} \times) R_c (\dot{\phi}_F \mathbf{i}_F + \dot{\theta}_F \mathbf{j}_F + \dot{\psi}_F \mathbf{k}_F)$$

$$= \mathbf{Q}_{\text{force}} + M^* g \mathbf{k}_E - G(\phi_F \mathbf{i}_F + \theta_F \mathbf{j}_F + \psi_F \mathbf{k}_F).$$

The rotor mass is included in the aircraft gross weight and moments of inertia; the matrix J also includes contributions from the rotor rotational moment of inertia. Note that $M^* g = \gamma 2 C_W / \sigma a$; hence if these equations are divided by $2\gamma/a$, they will be in the form of rotor coefficients divided by solidity, with components in the body coordinate system. The generalized forces \mathbf{Q} include contributions from both rotors and the airframe

aerodynamic
 dynamics an:
 In the ti
 flight cond
 also be tri
 rotor rotat
 zero, so th
 aircraft are

These six a
 the specific
 controls an
 positions a
 and corres
 flight path
 the climb c
 specified o
 with collec
 longitudina
 the helicop
 The trim
 technique.
 of certain t
 $\mathbf{M}(\mathbf{v})$ requi
 gives

or

for the n -th
 introduced
 overshoot c
 minimized.
 although fe
 simply give
 D is calcula
 value of \mathbf{v} :

The partial
 to improve
 net force an
 $\epsilon: C_F / \sigma < \epsilon$
 options.
 In the tra
 integrated i

aerodynamic loads. These equations are the basis for the trim, transient and flight dynamics analysis.

In the trim analysis, the equations are solved for the case of steady state flight. The flight condition is defined by the aircraft speed and flight path angles. The helicopter can also be trimmed in a steady turn by prescribing the yaw rate $\dot{\psi}_F$. It is assumed that the rotor rotational speed is constant. For steady flight the perturbation rigid body motion is zero, so the equations of motion simply state that the net force and moment on the aircraft are zero (except possibly for the inertial term due to the turn rate):

$$\frac{a}{2\gamma} (\mathbf{Q}_{\text{moment}}) = 0$$

$$\frac{C_W}{\sigma} \mathbf{k}_E + \frac{1}{g} \frac{C_W}{\sigma} (\mathbf{V} \times) R_e \mathbf{k}_F \dot{\psi}_F + \frac{a}{2\gamma} (\mathbf{Q}_{\text{force}}) = 0$$

These six algebraic equations are to be solved for the trim variables required to achieve the specified operating condition. The six trim variables in this case are the four pilot's controls and the two aircraft Euler angles. The individual rotor and aircraft control positions are obtained from $\mathbf{v} = T_C \mathbf{v}_P + \mathbf{v}_0$. Additional or alternative trim constraints and corresponding trim variables are readily formulated. For example, in free flight the flight path angle can be adjusted for a specified power available, rather than prescribing the climb or descent rate. In a wind tunnel case, typically the rotor itself is trimmed to a specified operating condition. For example, the rotor thrust or power can be trimmed with collective pitch; and the rotor tip-path plane tilt can be trimmed with lateral and longitudinal cyclic pitch control. The trim iteration can also be omitted, in which case the helicopter or rotor performance is evaluated for a specified control setting.

The trim problem is solved in the present analysis using a modified Newton-Raphson technique. The task is to find the values of the trim variables \mathbf{v} such that the target values of certain trim criteria \mathbf{M} are achieved. The complex, nonlinear form of the equations $\mathbf{M}(\mathbf{v})$ requires an iterative solution procedure. The first-order Taylor expansion of \mathbf{M} gives

$$\mathbf{M}_{\text{target}} = \mathbf{M}_{n+1} \cong \mathbf{M}_n + \frac{\partial \mathbf{M}}{\partial \mathbf{v}} (\mathbf{v}_{n+1} - \mathbf{v}_n)$$

$$\mathbf{v}_{n+1} = \mathbf{v}_n + D^{-1} (\mathbf{M}_{\text{target}} - \mathbf{M}_n) f$$

for the n -th iteration. With $f = 1$ this is the Newton-Raphson method. The factor $f < 1$ is introduced to improve the convergence. By reducing the trim variable increment the overshoot oscillations frequently encountered in the Newton-Raphson technique can be minimized. There are other techniques for solving such nonlinear algebraic equation, although few have been used in helicopter analyses. Some of these other techniques simply give an automatic procedure for evaluating f as the iteration proceeds. The matrix D is calculated by making finite increments in the trim variables v_i around some initial value of \mathbf{v} :

$$D = \frac{\partial \mathbf{M}}{\partial \mathbf{v}} = \left[\dots \frac{\mathbf{M}(v_i) - \mathbf{M}(v_i - \Delta v)}{\Delta v} \dots \right]$$

The partial derivative matrix may be recalculated occasionally as the iteration proceeds to improve convergence. The criterion for convergence in the free flight cases is that the net force and moment be less than a certain tolerance level as specified by the parameter ϵ : $C_F/\sigma < \epsilon C_W/\sigma$ and $C_M/\sigma < \epsilon(0.05 C_W/\sigma)$. Similar criteria are used for the other trim options.

In the transient analysis, the helicopter rigid body equations of motion are numerically integrated in time. A non-equilibrium flight path is produced by a prescribed control or

gust input. In the present analysis it is assumed that the aircraft motion is slow compared to the rotor speed, which allows the periodic rotor motion solution to be used with the transient analysis. It is also assumed that the perturbed rigid body motion is small, because in the rotor analysis it was assumed that the hub motion is small. It is consistent therefore to integrate the linearized equations for the rigid body motion. Subtracting the trim terms, the equations to be integrated are

$$J^*(\ddot{\phi}_F \mathbf{i}_F + \ddot{\theta}_F \mathbf{j}_F + \ddot{\psi}_F \mathbf{k}_F) = \Delta \mathbf{Q}_{\text{moment}}$$

$$M^*(\ddot{x}_F \mathbf{i}_F + \ddot{y}_F \mathbf{j}_F + \ddot{z}_F \mathbf{k}_F) = \Delta \mathbf{Q}_{\text{force}} + M^*(\mathbf{V} \times) R_e(\dot{\phi}_F \mathbf{i}_F + \dot{\theta}_F \mathbf{j}_F + \dot{\psi}_F \mathbf{k}_F) - G(\phi_F \mathbf{i}_F + \theta_F \mathbf{j}_F + \psi_F \mathbf{k}_F)$$

where $\Delta \mathbf{Q}$ is the generalized force less the trim value. These equations are used in the form of increments from trim because the trim solution (obtained by numerical procedures, to within a certain prescribed tolerance) is probably not exact. So there will be small residual forces and moments on the aircraft in the trim state, that if retained would produce spurious transient motions. The initial conditions are zero motion (except for ψ_F when the helicopter is trimmed in a turn). Any of these degrees of freedom can be held constant; if all six are constrained, the analysis produces the quasistatic rotor response to the control and gust inputs. With the input quantities defined as a function of time, the equations take the form $\ddot{y} = f(t, y, \dot{y})$, which is to be integrated for $t > 0$. A fourth-order Runge-Kutta method is used to perform the numerical integration [3].

In the flight dynamics analysis the helicopter stability derivatives are calculated, and the resulting linear differential equations are analyzed. The use of stability derivatives implies again that the body motion is slow compared to the rotor rotational speed, so the quasistatic rotor solution can be used. The assumption that the perturbation body motion is small is also consistent with the stability derivative representation. The equations of motion are used in the same form as for the transient analysis. Here a linear expansion of the generalized forces $\Delta \mathbf{Q}$ is obtained by making successive finite perturbations of the rigid body degrees of freedom, the rotor and airframe controls, and the gust velocity components (the gusts must be uniform throughout space in this case). The coefficients in this expansion are the stability derivatives, which have contributions from each rotor and from the airframe aerodynamics. Combined with the inertial and gravitational terms, the result is a set of time-invariant linear differential equations of the form

$$A_2 \ddot{\mathbf{x}} + A_1 \dot{\mathbf{x}} + A_0 \mathbf{x} = B \mathbf{v} + B_p \mathbf{v}_p + B_G \mathbf{g}$$

describing the flight dynamics of the aircraft. The state vector \mathbf{x} consists of the six rigid-body degrees of freedom; \mathbf{v} is the vector of the individual rotor and airframe controls; \mathbf{v}_p is the vector of the pilot's controls; and \mathbf{g} is the vector of gust velocity components. Using these equations the helicopter flying qualities can be examined, in terms of the eigenvalues and eigenvectors. The transfer function (pole-zero set or frequency response) or the transient response to a prescribed control or gust input can also be obtained.

3. AEROELASTIC STABILITY

The objective of the aeroelastic analysis is to derive a set of linear differential equations describing the perturbed motion of the helicopter from the trim flight condition. The stability of the system is defined by the eigenvalues of these equations. To construct the equations it is necessary to derive a perturbation form of the rotor and airframe models described in the previous sections, by linearizing the aerodynamic and inertial forces about the trim solution. For the most general case, the linear differential equations describing the helicopter motion have periodic coefficients, and must be analyzed by the methods of Floquet-Liapunov theory. With axial flow aerodynamics (and usually other restrictions if the rotor has two blades) the equations have constant coefficients, and the more powerful techniques for analyzing time-invariant systems are applicable. For low

and moderate set of constraints to three cases: and a constant

3.1 Rotor motion

The rotor elastic torsion are written are the degrees of freedom coordinate for q_i , the degrees of freedom

The rotor of freedom responds as dynamic gusts, this behavior the understanding frame is of used in the there have to Consider a (where $\Delta \psi$ = dimensionless the m -th blade degrees of freedom

here β_0 is a mode. The in

which gives to $(N - 1)/2$ freedom applications for the be accompanied to the nonrot

low compared with the advance ratio is small, it is consistent in subtracting the

$\Delta\psi_F k_F$

used in the numerical procedure there will be retained would (except for ψ_F) can be held or response to of time, the fourth-order

calculated, and by derivatives speed, so the perturbation body on. The equation. Here a linear finite perturbation and the gust is case). The contributions from al and gravities of the form

the six rigid controls: v_P components. terms of the icy response) obtained.

al equations addition. The onstruct the frame model ertial forces il equations yzed by the sually other nts, and the le. For low

and moderate advance ratios, it is often possible to describe the helicopter dynamics by a set of constant coefficient differential equations that represent an adequate approximation to the true dynamics for many applications. The present analysis can treat all three cases: periodic coefficient equations, constant coefficient equations in axial flow, and a constant coefficient approximation.

1. Rotor model

The rotor blade motion is described by coupled flap-lag bending, rigid pitch and elastic torsion, and optionally the gimbal or teeter motion. The blade degrees of freedom are written as the sum of trim terms and perturbation terms. The perturbation motions are the degrees of freedom for the aeroelastic analysis. In particular, the generalized coordinate of the i -th blade bending mode is written $q_i = q_{i,trim} + \delta q_i$. After substituting for q_i , the delta notation indicating the perturbed motion is omitted.

The rotor equations of motion have been obtained in the rotating frame, with degrees of freedom describing the motion of each blade separately. In fact, however, the rotor responds as a whole to excitation from the nonrotating frame—shaft motion, aerodynamic gusts, or control inputs. It is desirable to work with degrees of freedom that reflect this behavior. Such a representation of the rotor motion simplifies both the analysis and the understanding of the behavior. The appropriate transformation to the nonrotating frame is of the Fourier type [4]. The Fourier coordinate transformation has been widely used in the classical literature, although often with only a heuristic basis. More recently, there have been applications of the transformation with a sounder mathematical basis. Consider a rotor with N blades equally spaced around the azimuth, at $\psi_m = \psi + m\Delta\psi$ where $\Delta\psi = 2\pi/N$ and the blade index m ranges from 1 to N). Here $\psi = \Omega t$ is the dimensionless time variable. Let $q^{(m)}$ be the degree of freedom in the rotating frame for the m -th blade. The Fourier coordinate transformation is a linear transform of the degrees of freedom to the nonrotating frame, introducing the following new variables:

$$\beta_0 = \frac{1}{N} \sum_{m=1}^N q^{(m)}$$

$$\beta_{nc} = \frac{2}{N} \sum_{m=1}^N q^{(m)} \cos n\psi_m$$

$$\beta_{ns} = \frac{2}{N} \sum_{m=1}^N q^{(m)} \sin n\psi_m$$

$$\beta_{N/2} = \frac{1}{N} \sum_{m=1}^N q^{(m)} (-1)^m$$

where β_0 is a collective mode, β_{1c} and β_{1s} are cyclic modes, and $\beta_{N/2}$ is a reactionless mode. The inverse transformation is

$$q^{(m)} = \beta_0 + \sum_n (\beta_{nc} \cos n\psi_m + \beta_{ns} \sin n\psi_m) + \beta_{N/2} (-1)^m$$

which gives the motion of the individual blades again. The summation over n goes from 1 to $(N-1)/2$ for N odd, and from 1 to $(N-2)/2$ for N even. The $\beta_{N/2}$ degree of freedom appears in the transformation only if N is even. The corresponding transformations for the velocity and acceleration follow directly [3]. The Coordinate transform must be accompanied by a conversion of the equations of motion from the rotating to the nonrotating frame, which is accomplished by operating on the equations as follows:

$$\frac{1}{N} \sum_m (\dots), \frac{2}{N} \sum_m (\dots) \cos n\psi_m, \frac{2}{N} \sum_m (\dots) \sin n\psi_m, \frac{1}{N} \sum_m (\dots) (-1)^m.$$

Note that these are the same operations as are involved in transforming the degrees of freedom. Since the operators are linear, constants may be factored out. Thus with constant coefficients in the equations of motion, the operators act only on the degrees of freedom. By making use of the definition of the degrees of freedom in the nonrotating frame, and the corresponding results for the time derivatives, the conversion of the equations is then straight-forward. Complexities arise when it is necessary to consider periodic coefficients, such as due to the aerodynamics of the rotor in nonaxial flow. The expressions for the total force and moment on the hub in the nonrotating frame involve operators exactly of the form above, acting on the root reactions of the individual blades in the rotating frame.

For the present analysis, the degrees of freedom to be transformed to the nonrotating frame are blade bending, blade pitch and the gimbal motion. The collective and cyclic modes are particularly important because of their fundamental role in the coupled motion of the rotor and the nonrotating components. When the transformation of the equations is accomplished, for axial flow there is a complete decoupling of the variables into the following sets: (a) the collective and cyclic (0, 1c, 1s) rotor degrees of freedom together with the gimbal tilt and rotor speed degrees of freedom and the rotor shaft motion; and (b) the 2c, 2s, . . . , nc, ns and $N/2$ rotor degrees of freedom (as present). Thus the rotor motion in the first set is coupled with the fixed system, while the second set consists of purely internal rotor motion. Nonaxial flow couples, to some extent, all the rotor degrees of freedom and the fixed system variables, primarily due to the aerodynamic terms; still the above separation of the degrees of freedom remains a dominant feature of the rotor dynamics behavior.

The equations of motion for the rotor degrees of freedom and the expressions for the hub reactions are given in Ref. [2] section 2.2. The form of the inertial forces is a linear dependence on the rotor and shaft motion, with the coefficients depending on the mean bending deflection. Hence the inertial terms can be directly linearized. The aerodynamic forces are defined in Ref. [2] section 2.4 in terms of integrals of the section forces over the blade span. A linearized form of the aerodynamic forces is obtained as follows: the velocity and blade pitch are written as a trim term plus a perturbation term; the angle of attack and Mach number perturbations are defined in terms of the velocity perturbations; and the derivatives of the section aerodynamic coefficients with respect to angle of attack and Mach number are evaluated (by making finite increments in α and M). Hence the section loading is expressed in terms of the perturbation of the pitch and velocity components. The velocity components, as discussed in Ref. [2] section 2.4, are linear functions of the rotor degrees of freedom, shaft motion, and gust velocity, with the coefficients depending on the rotor mean velocity and the blade azimuth angle. A perturbation induced velocity is included in the normal velocity u_p , for use with a dynamic inflow model (described below). Combining the expansion for the section loads in terms of the velocity perturbations, and the velocity in terms of the motion of the rotor, the linearized form of the integrated aerodynamic forces is obtained. The aerodynamic coefficients are constant in axial flow, but for nonaxial flow they are periodic functions of ψ_m .

The aerodynamic forces on the rotor result in wake-induced inflow velocities at the disk, for both the trim and transient loadings. The wake-induced velocity perturbation can be a significant factor in the rotor aeroelastic behavior; an extreme case is the influence of the shed wake on rotor blade flutter. The rotor inflow dynamics should therefore be included in the aeroelastic analysis. However, the relationship between the inflow perturbations and the transient loading is likely more complex even than for the steady problem, and models for the inflow dynamics are still under development. In the present analysis, an elementary representation of the inflow dynamics is used. The basic assumption is that the rotor total forces vary slowly enough (compared to the wake response) that the classical actuator disk results are applicable to the perturbation as well as the trim velocities. A contribution to the velocity normal to the rotor disk of the following form is included: $\delta\lambda = \lambda_u + \lambda_x r \cos \psi_m + \lambda_y \sin \psi_m$. The inflow dynamics model relates these inflow components to the transient aerodynamic forces on the rotor, and to

the transient

where

and moment
and λ_y per
inflow moc
relations fo

A time lag
time consta
perturbatio
 $\partial i / \partial z$ can b
the trim in
decrease in
against the
inflow dyna
velocity mo

The line
structed at
and torsion
frame. The
hub forces f
rotor. For t
the rotating
are also the
operates on
factor out c
nonrotating
When the r
blade force
namics of
described b
express the
then to obt
However, t
the coeffic
of the rotor
form is also
with three
two-bladed

the transient rotor velocity perturbations, as follows [3]

$$\begin{pmatrix} \tau_L \dot{\lambda}_u \\ \tau_M \dot{\lambda}_x \\ \tau_M \dot{\lambda}_y \end{pmatrix} + \begin{pmatrix} \lambda_u \\ \lambda_x \\ \lambda_y \end{pmatrix} = \begin{bmatrix} \frac{\partial \lambda}{\partial T} & 0 & 0 \\ \kappa_x \frac{\partial \lambda}{\partial T} & \frac{\partial \lambda}{\partial M} & 0 \\ \kappa_y \frac{\partial \lambda}{\partial T} & 0 & \frac{\partial \lambda}{\partial M} \end{bmatrix} \begin{pmatrix} \tilde{C}_T \\ -C_{M_y} \\ C_{M_x} \end{pmatrix}$$

where

$$\tilde{C}_T = C_T - \frac{C_{T \text{ trim}}}{\mu^2/\kappa_f^2 + \lambda^2/\kappa_h^4} \left(\frac{\mu_x}{\kappa_f^2} \delta\mu_x + \frac{\mu_y}{\kappa_f^2} \delta\mu_y + \frac{\lambda}{\kappa_h^4} \delta\mu_z \right)$$

and momentum theory results give expressions for $\partial\lambda/\partial T$ and $\partial\lambda/\partial M$ [3]. Here the λ_x and λ_y perturbations due to the thrust have been included, consistent with the trim inflow model (Ref. [3] section 2.4 gives expressions for the constants κ_x and κ_y). These relations for the inflow perturbations imply the following lift deficiency functions [4]:

$$C = \begin{cases} (1 + \sigma a/8\mu)^{-1} & \text{forward flight} \\ (1 + \sigma a/8\lambda)^{-1} & \text{moments in hover} \\ (1 + \sigma a/16\lambda)^{-1} & \text{thrust in hover} \end{cases}$$

A time lag in the inflow response to loading changes has been included, defined by the time constants τ_L and τ_M [3]. The effect of the ground on the inflow dynamics is to add a perturbation due to changes in the rotor height above the ground: $\delta\lambda = (\partial\lambda/\partial z)\delta z$, where $\partial\lambda/\partial z$ can be evaluated using the expression for the induced velocity in ground effect from the trim inflow model. A decrease in the rotor height above the ground produces a decrease in the induced velocity, hence a rotor thrust increase that acts as a spring against the vertical height change. Finally, the rotor-rotor interference is included in the inflow dynamics, using the same interference factors κ_{12} and κ_{21} as for the trim induced velocity model.

The linear differential equations for the rotor motion and hub reactions can be constructed at this point. The Fourier coordinate transformation is applied to the bending and torsion degrees of freedom of the blade, so the equations are in the nonrotating frame. The introduction of the Fourier coordinate transformation, and evaluating the hub forces from the blade root reactions, produces a summation over all N blades of the rotor. For the case of a rotor operating in axial flow, the coefficients of the blade forces in the rotating frame are constants, independent of the blade azimuth angle. The coefficients are also then entirely independent of the blade index, so the summation over the blades operates only on the system degrees of freedom, not on the coefficients themselves (which factor out of the summation). As a result, the coefficient matrices of the equations in the nonrotating frame are constants for a rotor in axial flow (and with three or more blades). When the rotor is operating in nonaxial flow, the aerodynamic coefficients of the rotating blade forces are periodic functions of ψ_m because of the periodically varying aerodynamics of the edgewise moving rotor. It follows that the rotor in nonaxial flight is described by a system of differential equations with periodic coefficients. It is possible to express the aerodynamic coefficients of the rotating blade forces as Fourier series, and then to obtain the coefficients of the nonrotating equations in terms of these harmonics. However, the simplest approach for numerical work with large-order systems is to leave the coefficients of the nonrotating equations in terms of the summation over the N blades of the rotor. The summation is easily performed numerically, and it is found that this form is also appropriate for a constant coefficient approximation to the system. Rotors with three or more blades may be analyzed within the same general framework, but the two-bladed rotor is a special case. The rotor with $N \geq 3$ has axi-symmetric inertial and

structural properties and hence the nonrotating frame equations have constant coefficients in axial flow. In contrast, the lack of axi-symmetry with two blades leads to periodic coefficient differential equations, even in the inertial terms and in axial flow. Only in special cases are the dynamics of a two-bladed rotor described by constant coefficient equations.

A constant coefficient approximation for the rotor dynamics in nonaxial flow is desirable (if it is demonstrated to be accurate enough), because the calculation required to analyze the dynamic behavior is reduced considerably compared to that for the periodic coefficient equations, and because the powerful techniques for analyzing time-invariant linear differential equations are then applicable. However, such a model is only an approximation to the correct aeroelastic behavior. The accuracy of the approximation must be determined by comparison with the correct periodic coefficient solutions. The constant coefficient approximation derived here uses the mean values of the periodic coefficients of the equations in the nonrotating frame. To find the mean value of the coefficients, the operator

$$\frac{1}{2\pi} \int_0^{2\pi} (\dots) d\psi$$

is applied to the coefficient matrices, which involve the summation over all the blades. It is found [3] that the constant coefficient approximation is obtained from the periodic coefficient expressions by the simple transformation

$$\frac{1}{N} \sum_{m=1}^N (\dots) M(\psi_m) \longrightarrow \frac{1}{J} \sum_{j=1}^J (\dots) M(\psi_j).$$

The summation over N blades ($\psi_m = \psi + m\Delta\psi$, $\Delta\psi = 2\pi/N$) for a periodic coefficient is replaced by a summation over the rotor azimuth ($\psi_j = j\Delta\psi$, $\Delta\psi = 2\pi/J$) for the constant coefficient approximation. This is quite convenient since the same numerical procedure may be used to evaluate the coefficients for the two cases, with simply a change in the azimuth increment. The periodic coefficients must be evaluated throughout the period, while the constant coefficient approximation (mean values only) is evaluated only once. The constant coefficient approximation is not as useful or as accurate for a two-bladed rotor as for $N \geq 3$. With three or more blades, the source of the periodic coefficients is nonaxial flow, hence the periodicity is of the order of the advance ratio. At low advance ratio then (less than about 0.5), the constant coefficient approximation may be expected to be a good representation of the correct dynamics. The two-bladed rotor has in addition periodic coefficients due to the inherent lack of axi-symmetry of the rotor. This periodicity is large even for axial flow, and neglecting it in the constant coefficient approximation may be a poor representation of the dynamics. In particular, it is not possible to use the approximation as formulated here for the flight dynamics analysis of a two-bladed rotor helicopter, since this averaging eliminates the coupling between the rotor and the shaft motion.

3.2 Aircraft model

The aircraft motion is described by the rigid body and elastic airframe degrees of freedom, as defined in section 1.2. The aircraft controls consist of flaperon, elevator, aileron and rudder deflections. The rotor hub motion is obtained from $\alpha = c\mathbf{x}_s$, where c is defined in section 1.2. In addition there is a linear acceleration due to the rotation of the velocity vector in body axes by the Euler angular velocities, written $\Delta\ddot{\alpha} = \bar{c}\dot{\mathbf{x}}_s$.

The equations of motion for the aircraft rigid body and elastic degrees of freedom are given in section 1.2. The generalized forces due to the rotor hub reactions are $\mathbf{Q} = c^T \mathbf{F}$. The generalized forces due to the aircraft aerodynamics are linearized by making successive, finite perturbations of the variables (as for the calculation of the stability derivatives). A perturbation form of the model described in section 1.2 for the rotor induced interfer-

ence velocities are defined

3.3 Coupling

The equations are of the form

the rotor equations of motion, given in section 1.2, are of the form $\mathbf{M}\ddot{\mathbf{x}}_r + \mathbf{C}\dot{\mathbf{x}}_r + \mathbf{K}\mathbf{x}_r = \mathbf{F}$, where \mathbf{x}_r is the rotor displacement vector, \mathbf{M} is the rotor inertia matrix, \mathbf{C} is the rotor damping matrix, \mathbf{K} is the rotor stiffness matrix, and \mathbf{F} is the rotor force vector. The rotor equations are written in terms of the rotor hub displacements \mathbf{x}_r and the rotor hub velocities $\dot{\mathbf{x}}_r$. The rotor hub displacements \mathbf{x}_r are written in terms of the rotor hub displacements \mathbf{x}_r and the rotor hub velocities $\dot{\mathbf{x}}_r$. The rotor hub velocities $\dot{\mathbf{x}}_r$ are written in terms of the rotor hub displacements \mathbf{x}_r and the rotor hub velocities $\dot{\mathbf{x}}_r$.

$$a_2 \ddot{\mathbf{x}}_s$$

The vector \mathbf{v}_s consists of

The equations of motion for the aircraft rigid body and elastic degrees of freedom are given in section 1.2. The generalized forces due to the rotor hub reactions are $\mathbf{Q} = c^T \mathbf{F}$. The generalized forces due to the aircraft aerodynamics are linearized by making successive, finite perturbations of the variables (as for the calculation of the stability derivatives). A perturbation form of the model described in section 1.2 for the rotor induced interfer-

The vector \mathbf{v}_s consists of the drive train motion, engine thrust, The coupling between the rotor equations and the aircraft equations that accounts for the rotor induced inflow effect, rotor motion. The two rotor equations are bending of the rotor hub, modelled to account for the rotor induced inflow effect, rotor motion. The two rotor equations are bending of the rotor hub, modelled to account for the rotor induced inflow effect, rotor motion. The two rotor equations are bending of the rotor hub, modelled to account for the rotor induced inflow effect, rotor motion.

It is frequently assumed that the rotorcraft equations of motion are quasistatic, which consists of

ence velocities at the wing and tail is also included. The drive train degrees of freedom are defined, and the linearized equations of motion are discussed, in section 1.3.

3.3 Coupled rotor and aircraft

The equations of motion for the rotor, and the expressions for the hub reactions, take the form

$$A_2 \ddot{x}_R + A_1 \dot{x}_R + A_0 x_R + \tilde{A}_2 \ddot{\alpha} + \tilde{A}_1 \dot{\alpha} + \tilde{A}_0 \alpha = B v_R + B_G g_s$$

$$F = C_2 \ddot{x}_R + C_1 \dot{x}_R + C_0 x_R + \tilde{C}_2 \ddot{\alpha} + \tilde{C}_1 \dot{\alpha} + \tilde{C}_0 \alpha + D_G g_s$$

the rotor degrees of freedom vector x_R consists of flap-lag bending, rigid pitch and elastic torsion, gimbal or teeter motion, rotational speed, and inflow perturbations. The degrees of freedom used for the inflow dynamics model are λ_u , λ_x and λ_y , defined by $\dot{\lambda} = \lambda$ (so that the highest derivatives are second order). The rotor control vector v_R consists of the blade pitch control. The gust vector in shaft axes is related to the gust vector in velocity axes by $g_s = R_G g$. The vector F consists of the six components of the hub forces and moments, in the nonrotating frame. The vector α consists of the six components of the linear and angular shaft motion. The hub motion is related to the aircraft degrees of freedom by $\alpha = c x_s$, $\dot{\alpha} = c \dot{x}_s$ and $\ddot{\alpha} = c \ddot{x}_s + \tilde{c} \dot{x}_s$. For rotor No. 2 it is necessary to change the time scale to the rotational speed of rotor No. 1; so the matrices with subscript 1 are multiplied by (Ω_1/Ω_2) ; and the matrices with subscript 2 are multiplied by $(\Omega_1/\Omega_2)^2$. The aircraft equations of motion take the form

$$a_2 \ddot{x}_s + a_1 \dot{x}_s + a_0 x_s = b v_s + b_G g + b_\lambda (\lambda_{u1} (\Omega_1/\Omega_2) \lambda_{u2})^T + c_{R1}^T F_{R1} + c_{R2}^T F_{R2}$$

The vector x_s consists of the aircraft rigid body and elastic airframe degrees of freedom; v_s consists of the aircraft controls; and g is the gust velocity, in wind axes.

The equations for the rotor and aircraft can now be combined to construct the set of linear differential equations that describes the dynamics of the complete system. These equations take the following form:

$$A_2 \ddot{x} + A_1 \dot{x} + A_0 x = B v + B_P v_P + B_G g$$

The vector x consists of the degree of freedom of the two rotors, the airframe, and the drive train. The vector v consists of the controls of the two rotors, the airframe and the engine throttle. The pilot's controls are related to the individual controls by $v = T_C v_P$. The coupled equations of motion are obtained by substituting the hub motion into the rotor equations and hub reactions, and then substituting the hub reactions into the body equations of motion. By this means the terms in the coefficient matrices are constructed that account for the coupling of the rotors and aircraft through the rotor hubs. It remains to account for the coupling that occurs through other paths. The rotor equations are constructed with the aerodynamic thrust and moment terms in place for the dynamic inflow equations. These equations are completed at this stage, including the ground effect, rotor-rotor interference and rotor-airframe interference terms. The rotor equations are constructed with the torque in place for the rotational speed equation of motion. The coupled drive train degrees of freedom are introduced, and the torques of the two rotors are combined as required from the ψ_s and ψ_l equations. Then the equations are completed, including the engine and governor terms. Next the pitch/mast bending coupling terms and the governor feedback terms are introduced. If the rotor is modelled as having a rigid control system, the equations are appropriately restructured to account for the rigid pitch motion becoming a control variable rather than a degree of freedom ($p_0 = p_r$ in this limit).

It is frequently possible to reduce the order of the system of equations describing the rotorcraft dynamics by considering a quasistatic approximation for certain of the degrees of freedom. Assume that the equations of motion have been reordered so that the quasistatic variables (x_0) appear last in the state vector. The quasistatic approximation consists of neglecting the acceleration and velocity terms of these variables. Thus the

equations of motion take the form

$$\begin{bmatrix} A_2^{11} & 0 \\ A_2^{01} & 0 \end{bmatrix} \begin{pmatrix} \ddot{x}_1 \\ \ddot{x}_0 \end{pmatrix} + \begin{bmatrix} A_1^{11} & 0 \\ A_1^{01} & 0 \end{bmatrix} \begin{pmatrix} \dot{x}_1 \\ \dot{x}_0 \end{pmatrix} + \begin{bmatrix} A_0^{11} & A_0^{10} \\ A_0^{01} & A_0^{00} \end{bmatrix} \begin{pmatrix} x_1 \\ x_0 \end{pmatrix} = \begin{pmatrix} B^1 \\ B^0 \end{pmatrix} v.$$

The quasistatic variables now are not described by differential equations but rather by linear algebraic equations. Solving the equations for x_0 and substituting in the x_1 equations of motion gives then the reduced-order equations for the quasistatic approximation. In the present analysis, the quasistatic approximation can be applied as appropriate to the inflow dynamics, to the pitch and torsion degrees of freedom, to all the degrees of freedom for either or both rotors, or even to all the degrees of freedom except the rigid body motions of the aircraft. The quasistatic approximation retains the low-frequency dynamics of the eliminated degrees of freedom. Whether that is a satisfactory representation of the behavior must be established by comparison with the results of the higher order model. The quasistatic approximation as implemented here does not give the low frequency response when applied to a two-bladed rotor. The source of this difficulty is the fact that the teetering equations of motion are still in the rotating frame, so the response of the teetering modes to low frequency inputs from the nonrotating frame is not at low frequency also, but rather at frequencies around 1/rev.

Using these linear differential equations, the aeroelastic stability characteristics of the system can be examined, in terms of the eigenvalues and eigenvectors. When the equations have periodic coefficients, the eigenvalues are obtained by the methods of Floquet-Liapunov theory. For time-invariant equations, the zeros, frequency response, transient response, or rms gust response can be evaluated.

4. SOME APPLICATIONS OF THE ANALYSIS

In Fig. 2 the lateral flapping angle calculated using the present analysis is compared with experimental results. The data were obtained in a test of a model helicopter rotor in a wind tunnel [5]. The four-bladed rotor had a radius of 0.832 m, solidity of 0.0891 and a Lock number equal 5.80. The tip speed was 137 m/sec. For the case shown here, the rotor was operated at $C_T/\sigma = 0.08$, and the shaft angle was adjusted so that the tip-path plane angle of attack was maintained at approximately 1° (tilted aft). The wind tunnel walls may have produced a significant angle of attack change at the lowest speeds shown, but both the theory and the experiment show that the influence of the angle of attack on the lateral flapping is very small at such low speeds. In the analysis, the blade rigid flap motion was the only degree of freedom considered. The lateral tilt angle of the tip-path plane relative to the shaft, positive toward the retreating side of the disk, is β_{1s} . The

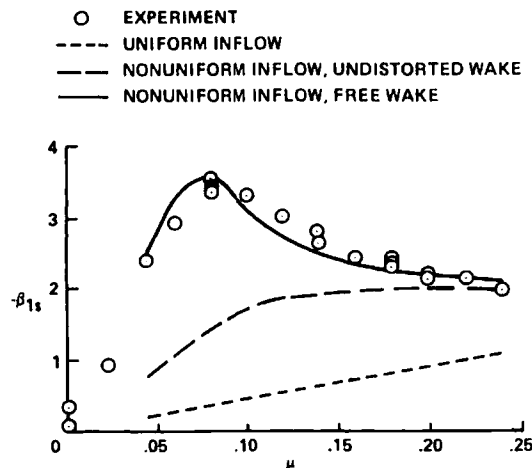


Fig. 2. Comparison of measured and calculated model rotor lateral flapping angles as a function of advance ratio ($C_T/\sigma = 0.08$ and $\alpha_{tip} \cong 1^\circ$).

induced v
concentrated
near wake
points at v
trailed vor
The inboa
with a larg
shed wake
Four revo
geometry
downwar
geometry

The late
gradient c
forward fl
loads at t
rotor resp
advancing
tion prop
predicted
undistorte
to include
flapping.
numerous
blade chor
induced ve
geometry
sensitive to
induced by
core radiu
factors in
vortex-ind
rollup, lift
bursting o
about each
which to a

In Figs
compared
single, gim
radius of 3
using longi
zero. The l
were used
bending m
per blade. l
or zero to
each degre
calculated
calculated
to account
rotor due t

The osci
for three sp
The beam
The oscilla

induced velocity and circulation were evaluated at fifteen stations along the blade, concentrated toward the tip. The trailed vorticity in the wake directly behind the blade (the near wake) was represented by discrete vortex lines positioned midway between the points at which the circulation was calculated. The near wake extended for 30° , then the trailed vorticity was concentrated into a single line, modelling the rolled up tip vortex. The inboard sheet of trailed vorticity was also represented by a single vortex line, but with a large core radius to avoid unrealistically large induced velocity near the line. The shed wake was modelled with radial, discrete vortex lines (again with a large core radius). Four revolutions of the wake behind each blade were modelled. An undistorted wake geometry was obtained by assuming that each element of the velocity is convected downward at a rate equal to the mean induced velocity at the rotor disk. The free wake geometry was also calculated, for two revolutions of the tip vortices only.

The lateral flapping angle of an articulated rotor depends primarily on the longitudinal gradient of the induced velocity distribution over the disk. The induced velocity in forward flight is larger at the rear of the disk than at the front, which produces larger loads at the front, hence an aerodynamic pitch moment on the rotor. An articulated rotor responds to this moment like a gyro, so the tip-path plane tilts laterally, toward the advancing side ($\beta_{1s} < 0$). In forward flight there is also a small lateral flapping contribution proportional to the coning angle. Figure 2 shows that the lateral flapping is under-predicted when uniform inflow is used, and even when nonuniform inflow based on the undistorted wake geometry is used. Below an advance ratio of about 0.16, it is necessary to include the free wake calculation in order to obtain a good estimate of the lateral flapping. There is significant self-induced distortion of the tip vortices, resulting in numerous blade-vortex interactions in which the vertical separation is a fraction of the blade chord. The result of such distortion is a much larger longitudinal gradient of the induced velocity, which produces the observed lateral flapping. In this case the free wake geometry places the tip vortices so close to the blades that the calculated flapping is sensitive to the value of the viscous core radius, which determines the maximum velocity induced by the vortex. With the undistorted wake geometry, there is little influence of the core radius. A value of $0.05R$ was used for the core radius here. There are a number of factors in addition to the core radius that combine to determine the magnitude of the vortex-induced loading, including the tip vortex strength, the extent of the tip vortex rollup, lifting surface effects on the induced blade loading, and possibly even vortex bursting or vortex-induced stall on the blade. In the absence of complete information about each of these phenomena, the vortex core radius is a convenient parameter with which to account for their cumulative influence on the rotor blade loading.

In Figs 3 and 4 the oscillatory loads measured on a full scale tilting proprotor are compared with calculated results. The data were obtained in a wind tunnel test of a single, gimbaled proprotor on a powered test stand [6]. The three-bladed rotor had a radius of 3.81 m, a solidity of 0.089 and a Lock number of 3.67. The rotor was trimmed using longitudinal cyclic control so that the longitudinal flapping relative to the shaft was zero. The lateral cyclic control was zero. In the analysis the following degrees of freedom were used to define the blade motion: gimbal pitch and roll; three coupled flap-lag bending modes per blade; rigid pitch mode for each blade; and one elastic torsion mode per blade. Little influence on the blade loads was found using two to six bending modes, or zero to two elastic torsion modes. Ten harmonics of the motion were calculated for each degree of freedom. Static, two-dimensional airfoil characteristics were used. The calculated inflow varied linearly over the rotor disk. The mean induced velocity was calculated from momentum theory with the ideal value multiplied by a factor of $\kappa_f = 2.0$ to account for nonideal induced power losses, which are expected to be large for this rotor due to its high twist and small number of blades.

The oscillatory beamwise bending moment as a function of thrust is shown in Fig. 3 for three speeds. The rotor shaft is tilted 15° forward from vertical in this case ($\alpha_p = 75^\circ$). The beamwise moment was measured at 35% radius, relative to the blade principal axes. The oscillatory load is one-half the difference between the maximum and minimum

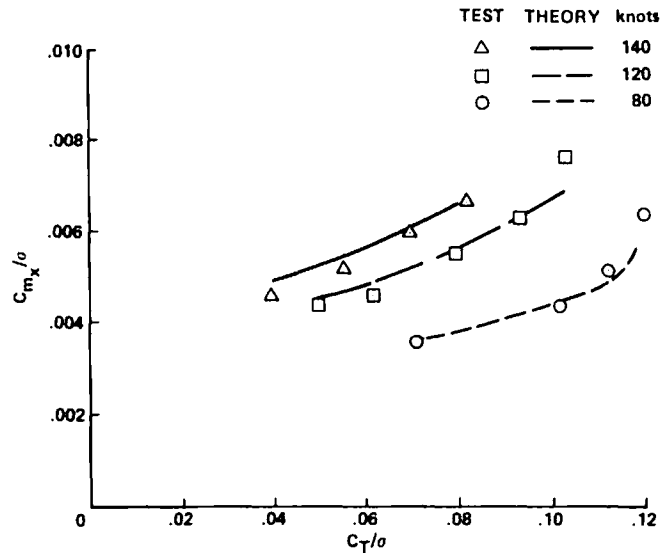


Fig. 3. Oscillatory beamwise bending moment on a tilting proprotor blade as a function of thrust for $\alpha_p = 75^\circ$ and $\Omega = 565$ rpm.

values occurring in a rotor revolution. In Fig. 4 the corresponding results are shown for the oscillatory spindle chord bending moment (which was measured at the blade root, relative to the shaft axes). The oscillatory loads are predicted well in Figs 3 and 4, although the beamwise bending moments increase somewhat faster than predicted at the highest thrust. The use of uniform inflow is generally adequate for the calculation of the oscillatory loads on this rotor. Further discussion and additional results are given in Ref. [7].

In Fig. 5 the bound circulation calculated using the present analysis is compared with experimental results for a model rotor in hover. The data were obtained using a two-component laser velocimeter to measure the circulation around a box enclosing the blade at a specified radial station [8, 9]. The two-bladed rotor had a radius of 1.045 m, a solidity of 0.0464 and a twist of -11° . The data in Fig. 5 are for the blade with a rectangular tip planform. The rotor was operated at a tip speed of 76.6 m/sec, and at a thrust of $C_T/\sigma = 0.10$. In the analysis, the induced velocity and circulation were evalu

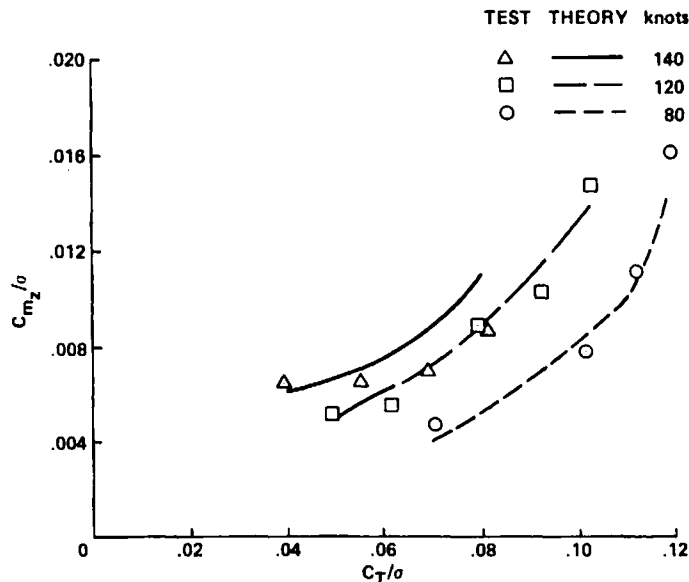


Fig. 4. Oscillatory spindle chord bending moment on a tilting proprotor blade as a function of thrust for $\alpha_p = 75^\circ$ and $\Omega = 565$ rpm.

Fig.

ated at fifth
in the near
points at v
vorticity v
extent of
from ten
vorticity v
increment
were moc
modelled
circumfer
ting the r
approxima
part of the
cantly unc
convection
Recall tha
it encount
and K_2 de
The cor
Fig. 5 is qu
it first pas
 $B = 0.985$
blade trail
wake geon
There wer
under the
and measu
used to co
were slight
lation calc
loading wa
rate after t
chosen bas
was slightl
calculated
loss, which
value, K_2

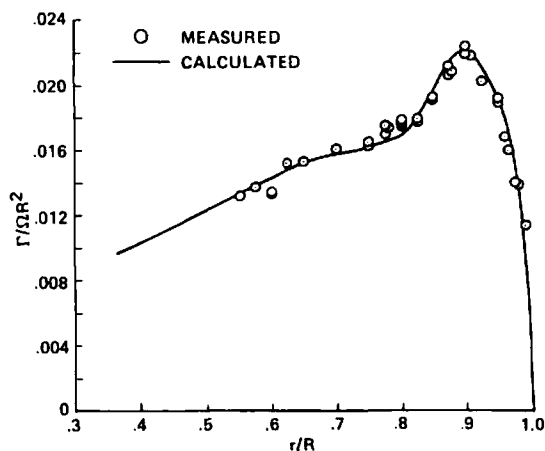


Fig. 5. Comparison of measured and calculated circulation for a two-bladed rotor in hover, with a rectangular tip planform.

of thrust

are shown for the blade root, Figs 3 and 4, predicted at the tip of the blade given in Ref.

compared with using a two-bladed rotor of 1.045 m. diameter with a tip speed of 100 m/sec, and at a tip speed of 100 m/sec were evaluated.

ated at fifteen stations along the blade, concentrated toward the tip. The trailed vorticity in the near wake was represented by discrete vortex lines positioned midway between the points at which the circulation was calculated. After an azimuth extent of 30° , the trailed vorticity was concentrated into a line, to model the rolled up tip vortex. The azimuthal extent of the near wake was varied from 15° to 60° , and the number of radial stations from ten to fifteen, with little effect on the calculated loading. The inboard trailed vorticity was represented by a single vortex line with large core radius. The azimuthal increment in the wake model was 15° . Five revolutions of the wake behind each blade were modelled in this fashion. An additional thirty revolutions of the wake were modelled using rectangular vortex sheet panels to construct a cylinder of axial and circumferential vorticity representing the tip vortices, and an axial line vortex representing the root vortices. By this means the wake far from the rotor blade (extending approximately to ten rotor radii below the disk) was economically accounted for; if this part of the wake were neglected, the induced velocity at the rotor disk would be significantly underestimated. The tip vortex geometry was described by the two-stage vertical convection and exponential radial contraction model defined in Ref. [2] section 3.1. Recall that the parameters K_1 , K_3 and K_4 determine the position of the tip vortex when it encounters the following blade; K_4 determines the contracted radius in the far wake; and K_2 determines the vertical convection after the first blade passage.

The correlation of the calculated and measured circulation distributions shown in Fig. 5 is quite good. The calculations used the measured position of the tip vortex when it first passed under the following blade and a value of 0.055 for K_2 . A tip loss factor of $B = 0.985$ was used, based on the measured position of the rolled up tip vortex at the blade trailing edge. The circulation distribution was also calculated using the prescribed wake geometry models developed by Landgrebe [10], and by Kocurek and Tangler [11]. There were small differences between the position of the vortex when it first passed under the following blade as predicted by these two models, and between the predicted and measured positions. These differences are within the scatter of the data originally used to construct the models. However, although the differences in the vortex positions were slight, the differences in the calculated loading were not negligible [12]. The circulation calculation was definitely improved by using the measured vortex position. The loading was initially calculated using a value of $K_2 = 0.0608$ for the vertical convection rate after the first blade passage. Since this parameter was not measured, its value was chosen based on the prescribed wake models. Using $K_2 = 0.0608$, the calculated loading was slightly lower outboard and higher inboard than measured [12]. In addition, the calculated induced power was only 3% higher than the ideal momentum-theory induced loss, which is much better performance than would be expected. By using a 10% smaller value, $K_2 = 0.0550$, the correlation of the measured and calculated loading was im-

tion of

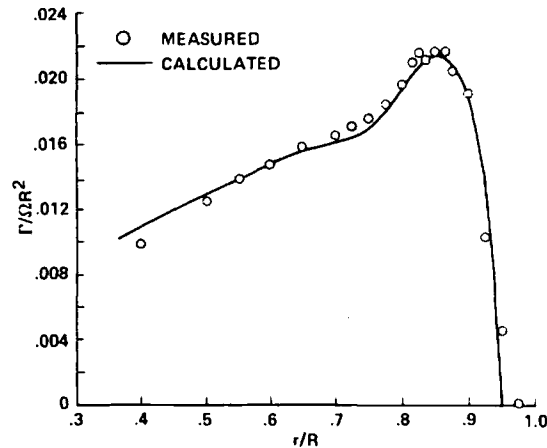


Fig. 6. Comparison of measured and calculated circulation for a two-bladed rotor in hover, with an ogee tip planform.

proved (Fig. 5), and the calculated induced power was 12% higher than ideal, a more reasonable value. The circulation distribution was also measured for this model rotor with an ogee planform extending over the outer 10% of the blade tip [8]. The calculated and measured results are compared in Fig. 6; the correlation is nearly as good as for the rectangular tip blade. The calculations used the measured position of the tip vortex when it first passed under the following blade, and a value of 0.0500 for K_2 . For the ogee tip there are no corresponding prescribed wake models to provide a guide for the choice of K_2 ; the wake convection must be specified on the basis of the peak circulation and the predicted induced power. The measured data showed the tip vortex rollup occurring at $0.94R$ with the ogee planform, so $B = 0.94$ was used. Properly modelling the tip vortex rollup at $0.94R$ was found to be essential for an accurate calculation of the loading distribution [12]. In summary, quite good correlation has been found for the predicted and measured circulation distributions in hover. This correlation was only possible using the measured wake geometry characteristics, including the tip vortex rollup, the radial and vertical position of the vortex when it first encountered the following blade, and the vertical convection rate in the far wake. An accurate wake geometry calculation will be necessary for a completely analytical calculation of hover performance and loading. The wake geometry defined by the available prescribed wake models was found to give the general features of the loading distribution well, although significant changes in the peak loading are produced by geometry differences that are within the scatter of the data from which the prescribed wake models were constructed.

A reasonable prediction of the induced power was not obtained here using the prescribed wake models. The far wake convection parameter K_2 determines the density of the circumferential vorticity in the wake, hence it controls the value of the mean induced velocity at the rotor disk. By reducing K_2 to a value 10% smaller than that given by the prescribed wake geometry models, the induced power was increased to a more appropriate level (and the correlation with the measured circulation distribution was improved). With one exception, this problem has been encountered in all recent investigations of the influence of the wake on hover performance. The exception was the work of Landgrebe [10], who obtained generally acceptable predictions of measured rotor performance using his wake geometry model. Summa and Clark [13] found that their performance calculation using a lifting surface theory was optimistic with the prescribed wake model. Therefore they used a free wake calculation, which produced a 6.5% smaller value of K_2 and a 16% smaller value of K_1 , hence a more reasonable induced power estimate (14% higher than ideal). In initial calculations with a new prescribed wake geometry model and a lifting surface theory, Kocurek and Tangler [11] found the power was about 15% lower than measured (actually less than ideal), although they used only four revolutions of the wake. With eight revolutions the calculated power was about 10%

low. Since spirals, the proposed the expansion disk to r showed g modified boundary proportic vertically seem exc about the the detail geometry tip to fo obtained of these r wake. Th grated effi approach by the ve wake reg data.

Recent theory to interpret cases the entirely d wake moc both liftir halves of theory mu theories i lifting line be genera predictor blade, and at the first and other general cc tions as requireme

In Figs measured model hin of 0.811 m the untwi: cambered The blade pitch-lag and roll sp mode occi resonance flap flexur The rotat:

low. Since their wake geometry model was based on experimental data for the first four spirals, they attributed the discrepancy to the far wake influence. Specifically, they proposed that the problem was due to the additional recirculation resulting from radial expansion of the wake. They accounted for this effect by adding a vortex ring below the disk to represent the diffused vorticity. With this model the performance calculations showed good agreement with the data. In a more recent work [14] the model has been modified to represent the diffusion and entrainment in the far wake by having the wake boundary expand radially at an angle of 15° from vertical, and decreasing K_2 inversely proportional to the cross-sectional area of the wake. Again the wake was truncated vertically, at 1.4 to 1.8R below the rotor disk in this case. These models for the far wake seem excessively complex considering that no deterministic wake actually exists beyond about the first five spirals; and the sensitivity of the induced velocity at the rotor disk to the details of the wake model decreases very rapidly with distance. The prescribed wake geometry models are based on measured data for the tip vortex position from the blade tip to four or five spirals below the disk. In most cases nearly the same results are obtained from the various models available. So there is no reason to suspect the validity of these models near the rotor, but neither is there reason to extrapolate them to the far wake. The near wake determines the details of the loading distribution, while the integrated effect of the far wake determines the mean induced velocity level. The simplest approach is to use an idealized model for the far wake, which can be described primarily by the vertical convection rate. It may be necessary to infer the value of K_2 in this far wake region from the performance measurements rather than from flow visualization data.

Recent developments of hover analyses have involved application of lifting surface theory to the rotary wing [11, 13, 14]. The results of these investigations are difficult to interpret because of the strong involvement of the wake model in this problem. In some cases the comparison of lifting line theory and lifting surface theory has been made with entirely different wake models. Yet the comparison is also misleading if exactly the same wake model is used, for there is no reason to expect the same wake model to be valid for both lifting line and lifting surface theories. The wing model and wake model are two halves of the same problem, so the comparison of lifting line theory and lifting surface theory must be made using a fully consistent theory in each case. The ultimate test of the theories is comparison with experimental data. For the cases shown in Figs 5 and 6, lifting line theory as used in the present analysis is quite adequate. From that it cannot be generally concluded however that lifting surface theory is not needed for accurate predictions of hover loading. The case investigated here involves a high aspect ratio blade, and the combination of high thrust and two blades makes the vertical separation at the first vortex-blade interaction as large as is likely to be encountered. Other rotors and other operating conditions may perhaps go beyond the limits of lifting line theory. A general conclusion of the present work, supported by the results of these other investigations as well, is that a consistent and accurate wake model is the most important requirement for an accurate analysis of the hovering rotor.

In Figs 7 and 10 calculated ground resonance stability results are compared with measured data. The frequency and damping data were obtained in a hover test of a model hingeless rotor supported on a gimbal [15]. The three-bladed rotor had a radius of 0.811 m, a solidity of 0.0494, and a Lock number of 6.1. For the cases considered here, the untwisted blades were operated at zero pitch of the structural axes. However, the cambered airfoil used produced a calculated thrust of $C_T/\sigma = 0.0056$ in this condition. The blades had flap and lag flexures at radial station 0.105R, with no pitch-flap or pitch-lag coupling. The rotor hub was located 0.30R above the gimbal. The gimbal pitch and roll spring rates were such that resonances of the body modes with the regressing lag mode occurred where the lag frequency was below once-per-revolution. Hence a ground resonance instability was possible, depending on the damping in the system. The blade flap flexure produced a rotating natural frequency of about 1.12/rev at high rotor speed. The rotating natural frequency of the lag mode was 0.81/rev at the body pitch mode

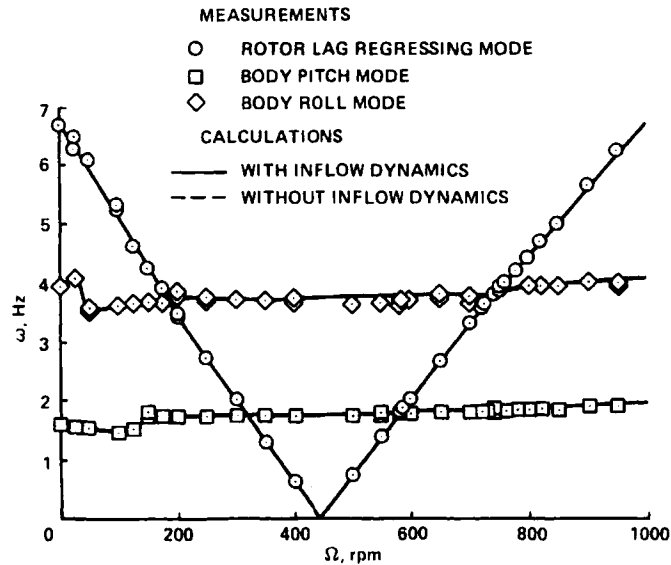


Fig. 7. Comparison of measured and calculated modal frequencies as a function of rotor speed, for a hovering model hingeless rotor on a gimbal.

resonance (585 rpm), and 0.69/rev at the body roll mode resonance (745 rpm). In the analysis, the only blade motion considered was the fundamental flap and lag modes. Higher bending modes and the torsion motion were neglected (the blade was very stiff in torsion). The trim flap and lag deflections of the blade were small for this low thrust operating condition. The degrees of freedom used in the flutter analysis were the flap and lag motion of the blades, the body pitch and roll motions, and the rotor inflow dynamics variables. The coning, collective lag, and uniform inflow degrees of freedom form a separate set that decouples from the ground resonance problem in hover. The inflow dynamics model relates induced velocity components that vary linearly over the rotor disk to the net aerodynamic pitch and roll moments of the rotor, including a time lag (see section 3.1). The inertias, nonrotating frequencies, and nonrotating damping of the rotor and body were set to the measured values.

The measured and calculated frequencies of the regressing lag mode, body pitch mode, and body roll mode are compared in Fig. 7. The damping of these modes as a function of rotor speed is presented in Figs 8 to 10. (The eigenvalues are $\sigma \pm i\omega$, where ω is the frequency and σ the damping.) The correlation is good when the inflow dynamics model is included. The frequencies are predicted well (the shift of the body mode frequencies below 150 rpm is due to resonance with the regressing flap mode). The blade and body mode damping is predicted well, although smaller values of the system structural damping would improve the correlation for the lag mode at the instability. Without the inflow dynamics model, the calculated frequencies of the body modes (not shown) were too low by about 0.1–0.2 Hz for rotor speeds above the resonance. The calculated damping is also in error without the inflow dynamics model. In particular, the body roll mode damping is

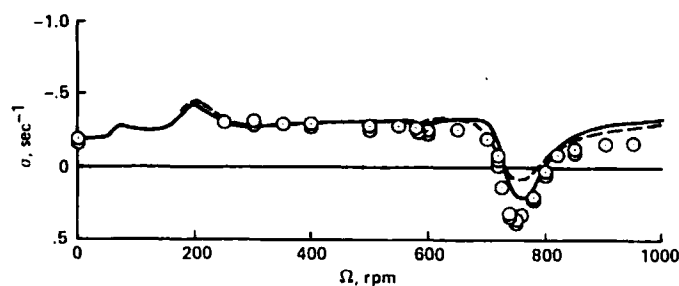


Fig. 8. Measured regressing lag mode damping compared with calculations (with and without inflow dynamics). See Fig. 7 for legend.

Fig. 9.

greatly over-
quasistatic
unsatisfactory
body frequency
regressing lag
occur around
was not predicted
time lag is
evidently is
accurately predicted
The important
the blade flapping
will then predict

The original
been described
appropriate

Fig. 10.

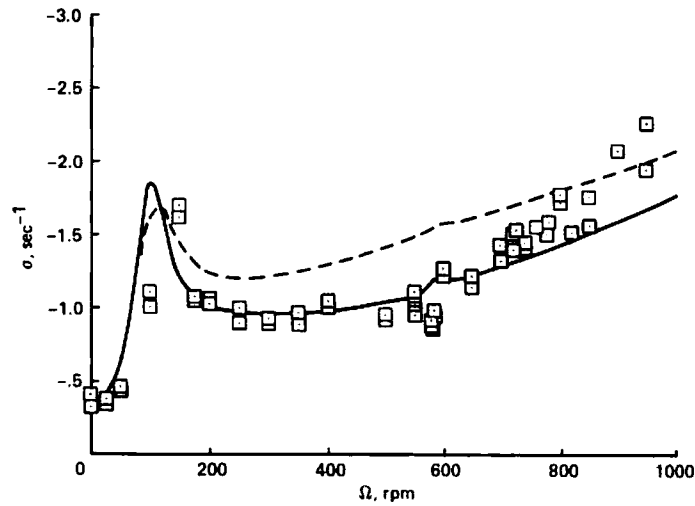


Fig. 9. Measured body pitch mode damping compared with calculations (with and without inflow dynamics). See Fig. 7 for legend.

greatly overpredicted at high rotor speed (Fig. 10). Calculations were also made using a quasistatic inflow dynamics model, in which the time lag was neglected. The results were unsatisfactory, principally due to shift in the body mode frequencies. The nonrotating body frequencies were still predicted well, but for rotor speeds above about 250 rpm the frequencies were 10–20% too high (0.3–0.5 Hz). Consequently the resonances with the regressing lag mode were shifted to higher rotor speeds, with the instability predicted to occur around 800 rpm instead of 750 rpm as measured. Also, the body mode damping was not predicted as well as with the complete inflow dynamics model. The effect of the time lag is to eliminate the influence of the inflow dynamics at high frequencies, which evidently is a crucial aspect of the phenomenon. It is concluded that the present analysis accurately predicts ground resonance stability characteristics involving hingeless rotors. The importance of the inflow dynamics may be attributed to the cantilever restraint of the blade flap motion, which allows the rotor to develop net pitch and roll moments that will then produce induced velocity perturbations.

5. CONCLUDING REMARKS

The origins, development and structure of a comprehensive analysis for rotorcraft have been described. Since the analysis is implemented in a digital computer program, it is appropriate to close with a few rules governing the use of large codes.

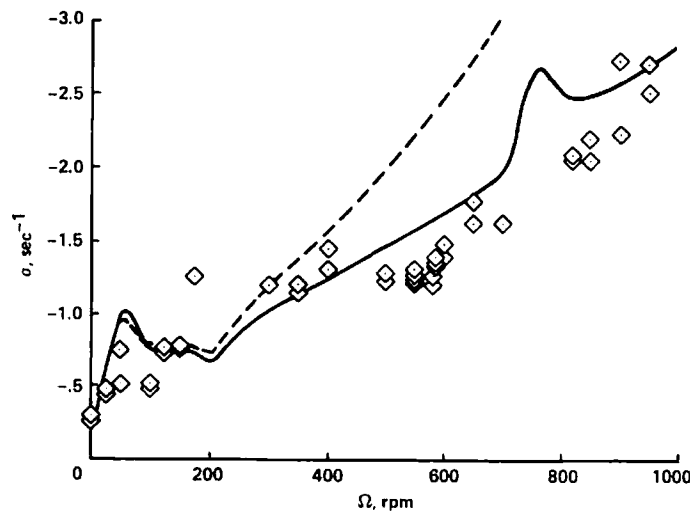


Fig. 10. Measured body roll mode damping compared with calculations (with and without inflow dynamics). See Fig. 7 for legend.

When using a large code, the results should never be accepted without scrutiny. It will usually be possible to establish that the results are satisfactory for the intended purpose. However, by adopting the habit of questioning the code, the user will be more likely to recognize the cases when the results are in fact unreliable, and furthermore in the process the user will develop a better understanding of what the program is doing.

For any new problem, the code probably will not work right the first time, and it may not run at all. A successful calculation will ordinarily be achieved only after some effort, for this kind of analysis is still much an art. Both the mathematical model and the solution procedure frequently require a little help from the engineer.

The code will always be growing, from the day of its initial release to the end of its useful life. The program cannot be expected to be static, for the problems it is intended to solve are not. The important thing is not to avoid changing the code, but rather to maintain control of the process.

The job could always be done better. The hard task is recognizing when it *should* be done better. Any good code will have a range of validity extensive enough to ensure it a long life. Eventually however, problems will begin to overwhelm it and the technology will march beyond it. That is the time to start work on the next generation of codes.

REFERENCES

1. B. Etkin, *Dynamics of Flight*, Wiley, New York (1959).
2. W. Johnson, Development of a Comprehensive Analysis for Rotorcraft—I. Rotor Model and Wake Analysis. *Vertica* 5, 99-129 (1981).
3. W. Johnson, A Comprehensive Analytical Model of Rotorcraft Aerodynamics and Dynamics. *NASA TM 81182* (1980).
4. W. Johnson, *Helicopter Theory*, Princeton University Press, Princeton, New Jersey (1980).
5. F. D. Harris, Articulated Rotor Blade Flapping Motion at Low Advance Ratio. *J. Am. Helicopter Soc.* 17, No. 1 (1972).
6. Bell Helicopter Company, Advancement of Proprotor Technology—Wind Tunnel Test Results. *NASA CR 114363* (1971).
7. W. Johnson, Comparison of Calculated and Measured Blade Loads on a Full-Scale Tilting Proprotor in a Wind Tunnel. *NASA TM 81228* (1980).
8. J. D. Ballard, K. L. Orloff and A. B. Luebs, Effect of Tip Shape of Blade Loading Characteristics for a Two-Bladed Rotor in Hover. *Annual National Forum of the American Helicopter Society*, Washington D.C., May 1979.
9. J. D. Ballard, K. L. Orloff and A. B. Luebs, Effect of Tip Planform on Blade Loading Characteristics for a Two-Bladed Rotor in Hover. *NASA TM 78615* (1979).
10. A. J. Landgrebe, The Wake Geometry of a Hovering Helicopter Rotor and its Influence on Rotor Performance. *J. Am. Helicopter Soc.* 17, No. 4 (1972).
11. J. D. Kocurek and J. L. Tangler, A Prescribed Wake Lifting Surface Hover Performance Analysis. *J. Am. Helicopter Soc.* 22, No. 1 (1977).
12. W. Johnson, Comparison of Calculated and Measured Model Rotor Loading and Wake Geometry. *NASA TM 81189* (1980).
13. J. M. Summa and D. R. Clark, A Lifting-Surface Method for Hover/Climb Airloads. *Annual National Forum of the American Helicopter Society*, Washington, D.C., May 1979.
14. J. D. Kocurek, L. F. Berkowitz and F. D. Harris, Hover Performance Methodology at Bell Helicopter Textron. *Annual National Forum of the American Helicopter Society*, Washington, DC, May 1980.
15. W. D. Bousman, An Experimental Investigation of the Effects of Aeroelastic Couplings on Aeromechanical Stability of a Hingeless Rotor Helicopter. *J. Am. Helicopter Soc.* 26, No. 1 (1981).

Abstract—Du
rate at which
resolution of
magnetic tap
ments which
analysis how
Vertol Compu
based on a la
unmatched in
This paper
current capab

- Calculati
expansion
- Harmoni
- Non-dim
test.
- A data ba
(or progr
flights by

Also summa
extension of th
The paper c
the system to
and Airspeed
discussed will
damage incurr
lives, together

The Boeing
time data s
3100 compu
after the co
should reco
effort betwe
and we shou
whereby ph
merged, trai
computation
attempted to
since the co
mation befor

*Presented a
tember 1980.